

TECHNISCHE UNIVERSITÄT WIEN

DISSERTATION

Curved Planar Reformation for Vessel Visualization

ausgeführt
zum Zwecke der Erlangung des akademischen Grades
eines Doktors der technischen Wissenschaften

unter der Leitung von
Ao.Univ.Prof. Dipl.-Ing. Dr.techn. Eduard Gröller,
Institut 186 für Computergraphik und Algorithmen,

eingereicht
an der Technischen Universität Wien,
Fakultät für Technische Naturwissenschaften und Informatik,

von
Dipl.-Ing. Armin Markus Kanitsar
Matrikelnummer 9625009,
Mühlbreitenstraße 24,
A-8280 Fürstenfeld, Österreich,
geboren am 4. September 1976 in Graz.

Wien, im Jänner 2004.

Deutsche Kurzfassung

Die Einführung hoch auflösender Computer Tomographen erlaubt die Akquisition immer feinerer anatomische Details. Dadurch werden neue Untersuchungsmethoden ermöglicht. Die Erfassung von Gefäßstrukturen mittels Computer Tomographie, genannt Computer Tomographie Angiographie (CTA), ist eine der wichtigsten Anwendungen dieser neuen Verfahren. Die rasante Entwicklung im Bereich der Akquisitionstechniken erlaubt hoch qualitative und nahezu isotropische Daten in sehr kurzer Aufnahmedauer (40–70s). Die anschließende Befundung der Schichtbilder (bis zu 1500 Einzelbilder!) ist jedoch langwierig. Dies bedeutet, dass die Nachbearbeitung der akquirierten Daten zum limitierenden Faktor in der klinischen Routine wurde. Computer unterstützte Nachbearbeitung und Visualisierung wird daher zu einem integralen Bestandteil dieser Anwendungen.

Der Schwerpunkt dieser Arbeit ist die klinisch relevante Visualisierung von kontrastierten Blutgefäßen in Computer-Tomographie-Angiographie-Daten. Verschiedene Methoden zur Darstellung des Gefäßquerschnittes durch Curved Planar Reformation (CPR) werden vorgeschlagen. Ein robustes Verfahren zur Extraktion der Gefäßzentralachse wird erläutert. Des Weiteren werden verschiedene Visualisierungs-Algorithmen anhand eines komplexen Volumensdatensatz untersucht.

Einführend werden Untersuchungsverfahren großer Bildserien aus CTA Untersuchungen der unteren Extremitäten vorgestellt. Zwei verschiedene Ansätze zur Diagnose von Gefäßanomalien peripherer Gefäße (Stenosen, Verschlüsse, Aneurysmen und Verkalkungen) werden vorgestellt. Ein semi-automatisches Verfahren zur Berechnung der Gefäßzentralachse wird präsentiert. Weiters wird eine interaktive Segmentierungsmethode für die Detektion von Knochen vorgeschlagen.

Basierend auf der abgeleiteten Gefäßachse werden verschiedene Visualisierungsansätze vorgeschlagen. Eine Möglichkeit röhrenartige Strukturen darzustellen ist die Extraktion und Darstellung einer längsverlaufenden Schnittebene entlang der Zentralachse. Dadurch werden Durchmesser (z.B. das Gefäßlumen) und mögliche Anomalien (z.B. Verkalkungen) in dieser Schnittebene sichtbar. Dieses Verfahren wird als Curved Planar Reformation (CPR) bezeichnet. Es werden drei CPR-Methoden beschrieben: die Projizierende CPR, die Gestreckte CPR und die Ausgerichtete CPR. Die unterschiedlichen Eigenschaften der Darstellungen werden anhand eines Phantom Datensatzes gezeigt. Schwachpunkte des CPR Verfahrens konnten durch die Einführung von Erweiterungen verbessert werden. Die Schicht CPR erhöht die Toleranz gegenüber ungenauen Gefäßachsen. Mittels rotierbarer CPR kann der gesamte Querschnitt des Gefäßes erfasst werden. Die Multiple Gefäß CPR erlaubt die Darstellung ganzer Gefäßbäume.

Eine weitere Verbesserung des CPR Verfahrens kann durch die Auflösung räumlicher Beziehungen erreicht werden. Es werden zwei neue CPR Methoden vorgestellt, welche dadurch eine effiziente Darstellung von Gefäßen erlauben. Die Spiralförmige CPR stellt das gesamte Gefäßvolumen in einem einzelnen

Bild dar. Die Extraktion der Schnittebene basiert nicht mehr auf einer erzeugenden Geraden sondern auf zwei ineinander verschachtelten Spiralen. Die zweite Methode bietet die Möglichkeit den gesamten Gefäßbaum überschneidungsfrei darzustellen. Dies wird durch geringe Rotationen an den Bifurkationen realisiert. Die benötigte Deformation wird durch ein rekursives Verfahren bestimmt.

Der letzte Teil dieser Arbeit beschäftigt sich mit der generellen Akquisition komplexer Strukturen mittels Computer Tomographie. Im Gegensatz zu herkömmlichen Modellierungs- und Aufnahmeverfahren ist die geometrische Komplexität des untersuchten Gegenstandes irrelevant. Hohlräume, Löcher, verschachtelte Strukturen und Oberflächendetails werden korrekt abgebildet. Lediglich die, sich stetig verbessernde, Auflösung des Computer Tomographen stellt eine natürliche Einschränkung hinsichtlich der Qualität der akquirierten Daten dar. Die Vorteile dieses Modellierungsverfahren werden anhand eines Christbaum Modells demonstriert, welches die Charakteristika eines komplexen Objektes erfüllt. Die Anwendung von bestehenden Volumsvisualisierungstechniken auf diesen Datensatz ist unmittelbar möglich. Unter anderem wird an diesem Datensatz die Robustheit der CPR Darstellungen demonstriert.

Abstract

With the introduction of high-resolution computed tomography modalities the acquisition of fine anatomical details is made possible. This allows new investigation procedures. The coverage of vascular structures using computed tomography, i.e. computed tomography angiography (CTA), is one of the most important applications in this area. Recent developments in the field of acquisition techniques provide high-quality, near isotropic data within small acquisition times (40–70s). The subsequent evaluation of the cross-sectional images (up to 1500 images!) is a time-consuming process. Therefore post-processing of acquired data was found out to be the bottleneck in the clinical routine. Computer aided post-processing and visualization becomes an essential part of this application.

The main focus of this work is the clinical relevant visualization of vascular structures from computed tomography angiography data. Different methods for visualizing the vessel lumen by means of curved planar reformation are proposed. The appropriate center line extraction for the vessel is discussed. In addition to that a complex volumetric data set is presented and evaluated by different visualization algorithms.

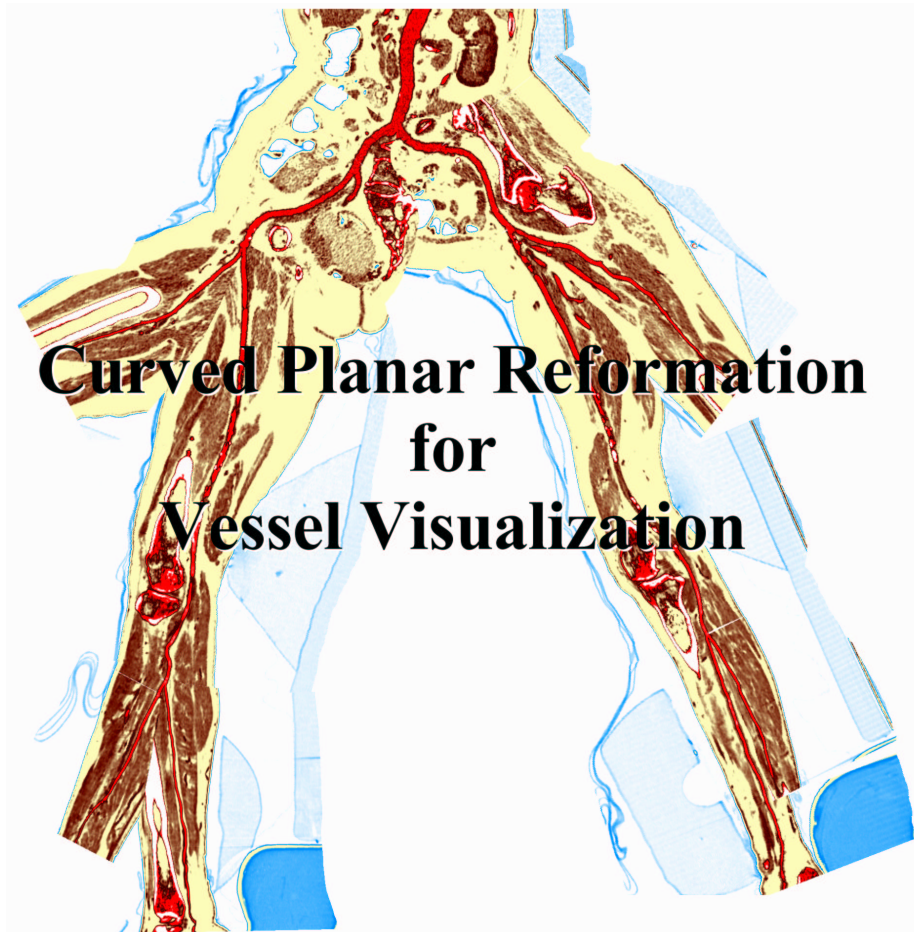
Investigation methods of large image sequences of the lower extremities are discussed. Two different approaches for peripheral vessel diagnosis dealing with stenosis and calcification detection are introduced. A semi-automated vessel-tracking tool for centerline extraction and an interactive segmentation tool for bone removal is discussed.

Based on the deduced central axis different visualization techniques are proposed. One way to display tubular structures for diagnostic purposes is to generate longitudinal cross-sections in order to show their lumen, wall, and surrounding tissue in a curved plane. This process is called curved planar reformation(CPR). Three different methods to generate CPR images are described: Projected CPR, stretched CPR, and straightened CPR. A tube-phantom was scanned with Computed Tomography (CT) to illustrate the properties of the different CPR methods. Targeting the drawbacks of visualizing tubular structures using CPRs three enhancements to the basic methods are introduced. The thick-CPR method improves the tolerance of imprecise vessel centerlines. A rotating-CPR covers the complete vessel cross section. The multi-path-CPR displays entire vascular trees.

A further improvement of CPR techniques is accomplished by the relaxation of spatial coherence. Two advanced methods for efficient vessel visualization, based on the concept of CPR, are introduced. A helical CPR visualizes the interior of a vessel in a single image. The curved plane extraction is no longer based on a generating line, but on two interleaved spirals. Furthermore, a method to display an entire vascular tree without mutually occluding vessels is presented. Minimal rotations at the bifurcations avoid occlusions. For each viewing direction the entire vessel structure is visible. The estimation of the necessary deformation is done in a recursive manner.

The final part of this work reports on using computed tomography as a

model acquisition tool for complex objects in computer graphics. Unlike other modeling and scanning techniques the complexity of the object is irrelevant in CT, which naturally enables to model objects with, for example, concavities, holes, twists or fine surface details. The only limitation of this technique is the steadily increasing resolution of computed tomography modalities. For demonstration purposes a Christmas tree is scanned. It exhibits high complexity which is difficult or even impossible to handle with other techniques. The application of existing volume visualization methods is straight forward. The robustness of CPR techniques is demonstrated on this dataset.



<http://www.cg.tuwien.ac.at/research/vis/adapt>

Der Gegenstand der wissenschaftlichen Forschung soll die Entwicklung und Adaption von Methoden der Computergraphik und insbesondere der 3D Volumenvisualisierung sein. Ziel des Projektes ist, ein Softwaresystem für die tägliche medizinische Praxis in radiologischen Fachbereichen zu entwickeln, welches Schwerpunkte der computerunterstützten Diagnose (Computer Aided Diagnosis) – Diagnose, Analyse und Planung – umfassen soll.

Zielsetzung des Forschungsprojektes ADAPT.

Contents

1	Introduction	13
1.1	X-Rays - A New Kind of Rays	14
1.2	Angiography	14
1.3	Conventional Tomography	17
1.4	Computed Tomography	18
1.5	Computed Tomography Angiography	21
1.5.1	Clinical Requirements of Vessel Visualization	22
1.5.2	'State-of-the-art' in CT-Angiography (CTA)	22
1.6	The Scope of this Work	23
2	Peripheral Vessel Investigation	25
2.1	Introduction	26
2.2	Peripheral vessel investigation	26
2.3	Visualization Methods for CTA	28
2.4	Automated CPR Generation	28
2.4.1	The Cost Function	29
2.4.2	The Implementation of the Path Generation	30
2.4.3	Centering the path	31
2.5	Semi-automatic Bone Segmentation	32
2.6	Results	33
2.7	Clinical Evaluation	39
2.8	Conclusion	40
3	CPR - Curved Planar Reformation	41
3.1	Introduction	42
3.2	Related Work	43
3.3	CPR Methods	44
3.3.1	Projected CPR	45
3.3.2	Stretched CPR	46
3.3.3	Straightened CPR	47
3.4	Evaluation of the CPR methods	48
3.5	CPR Enhancement	49
3.5.1	Thick CPR	51
3.5.2	Rotating CPR	53

3.5.3	Multi-Path CPR	54
3.6	Conclusions and Discussion	60
4	Advanced Curved Planar Reformation: Flattening of Vascular Structures	61
4.1	Introduction	62
4.2	Related Work	63
4.3	Helical CPR	64
4.3.1	Method Description	64
4.3.2	Sampling Strategy	65
4.3.3	Phantom Dataset	66
4.3.4	Results	68
4.4	Untangled CPR	68
4.4.1	Method outline	69
4.4.2	The vessel hull primitive	69
4.4.3	Putting things together	70
4.4.4	Layout definition	74
4.4.5	Image space partitioning	75
4.4.6	Results	76
4.5	Conclusions and Discussion	79
5	Computed Tomography as a Tool for Mastering Complex Real World Objects with Applications in Computer Graphics	80
5.1	Introduction	81
5.2	Related Work	82
5.3	Dataset Acquisition	82
5.4	Visualization algorithms	84
5.5	Conclusions	88
6	Conclusions	90
7	Acknowledgements	97
A	Curriculum Vitae	103

List of Figures

1.1	Radiograph of Anna Bertha Roentgen's hand (Dec. 22 nd , 1895).	15
1.2	First angiogram (Jan. 17 th , 1896).	15
1.3	Digital Subtraction Angiography	16
1.4	Conventional tomography	17
1.5	First prototype of a computed tomograph	18
1.6	First clinical prototype of a computed tomograph	19
1.7	Concept of a computed tomograph	20
2.1	Different arterial diseases	27
2.2	CPR generation principle	29
2.3	User Interaction of vessel tracking	31
2.4	CPR of the anterior tibial artery	34
2.5	Segmentation results I	35
2.6	Segmentation results II	36
2.7	CPR generation result	37
2.8	Non-photorealistic direct Volume Rendering	38
2.9	Evaluation of the results at the AKH-Wien.	39
3.1	Principle of the CPR visualization	44
3.2	Different CPR generation methods	45
3.3	Iso-surface extraction of the 'Tubes Phantom' at -224 HU.	48
3.4	Comparison of CPR methods	50
3.5	Artificial stenosis introduced by imprecise central axis computation.	51
3.6	Resampling strategies of CPR methods	52
3.7	Minimum intensity CPR	52
3.8	Rotating Stretched CPR	53
3.9	Enlargement of Rotating Stretched CPR	53
3.10	MIP compositing of projected CPRs.	54
3.11	Concept of Multi-Path CPR.	55
3.12	Generation of multi-path CPRs.	56
3.13	Projected multi-path CPR	58
3.14	Stretched multi-path CPR	59
4.1	An untangled vascular tree of the peripheral arteries.	62
4.2	Helical CPR generation	64

4.3	Sampling strategies of helical CPR	65
4.4	Phantom dataset for helical CPR generation	66
4.5	Real world example of helical CPR	67
4.6	The vessel hull primitive	70
4.7	Assembling of vessel hulls.	71
4.8	The cases for combining vessel hulls.	72
4.9	Image space partitioning	73
4.10	Undersampled area	74
4.11	Different layout definition	75
4.12	Comparison of introduced distortion	76
4.13	A comparison of multi-path and untangled CPR	77
4.14	A colored sequence of untangled CPR	78
5.1	Christmas Tree rendered with RTVR	81
5.2	A picture of the Christmas tree.	83
5.3	Christmas Tree: SSD	85
5.4	Christmas Tree: raytracing	85
5.5	Christmas Tree: DVR rendering	86
5.6	Christmas Tree: wavelet based visualization	87
5.7	Pre-integration rendering	87
5.8	A Curved Planar Reformation of the XMas-Tree dataset.	88
5.9	Christmas Tree: non-photorealistic rendering	89
5.10	Christmas Tree: arboroscopy	89
6.1	The example dataset	92
6.2	Projected CPR	93
6.3	Stretched CPR	93
6.4	Straightened CPR	94
6.5	Helical CPR	94
6.6	Multi-path projected CPR	95
6.7	Multi-path stretched CPR	95
6.8	Untangled CPR	96
6.9	CPR of the Christmas-Tree dataset	96

List of Tables

1.1	Development of high-end CT modalities (1972–2000)	21
2.1	Parameters of the test datasets.	33
2.2	Investigation time of the datasets.	33
2.3	Results of the evaluation process.	39
3.1	Properties of CPR types	45
6.1	Comparison of CPR methods	91

Chapter 1

Introduction

*History is the version of past events
that people have decided to agree upon.*
— Napoleon Bonaparte (1769 - 1821)

1.1 X-Rays - A New Kind of Rays

In 1895 Wilhelm Conrad Roentgen (1845 – 1923) was studying the phenomena accompanying the passage of electric current through gas of extremely low pressure, which at that time was a very popular research area. On the evening of November, 8th 1895, he found that invisible rays were emitted from the discharge tube. While working in a darkened room he observed that a paper plate covered on one side with barium platinocyanide became fluorescent when placed in the path of the rays. The discharge tube was enclosed in a sealed, thick black carton to exclude all light. The illuminance only depended on the thickness of interposed objects.

After six weeks Roentgen finished his first scientific work on this research including the first radiograph (see Figure 1.1) taken from the hand of his wife Anna Bertha Roentgen (1839 – 1919). On Saturday, 28th of December he submitted his manuscript 'on a new kind of rays' [47] to the secretary of the Physical-Medical Society in Wuerzburg. On Tuesday, 31st December he sent the off-prints together with nine X-rays and New Year greetings to his colleagues.

Among the addressees was Professor Franz Exner (1849 – 1926), the director of the II. Physical-Chemical Institution of the university in Vienna. He presented the X-rays which had been taken by Roentgen to his assistants during a discussion evening on January 4th, 1896. At the very same day the Vienna's daily newspaper 'The Press' was informed of the discovery. On the next day the first article was published in 'The Press' under the headline 'A Sensational Discovery'. The news spread all over the world within days.

The year 1896 played an outstanding role in the discoveries and inventions in radiodiagnosics and the first signs of radiotherapy. In the first year after the discovery of X-rays, a total of 49 books, brochures and 1044 scientific essays were written on the scientific aspects and possible applications of the newly discovered rays [18]. Many of these publications dealt specifically with the possibilities of applications in medicine.

1.2 Angiography

The imaging of blood vessels in a medical context is referred to as *angiography* originating from the Greek word $\alpha\gamma\gamma\epsilon\iota\omicron\nu$ (aggeion – vessel, bucket). Soon after the discovery of the X-rays the first angiogram was produced by Eduard Haschek (1875 – 1947) and Otto Lindenthal (1872 – 1947) at the physical institute in Vienna (see Figure 1.2). On the 17th of January 1896 the hand of a corpse was prepared for the X-ray exposure. As the attenuation of blood vessels does not significantly differ from surrounding tissue, the arterial vessels were filled



Figure 1.1: Radiograph of Anna Bertha Roentgen's hand (Dec. 22nd, 1895).

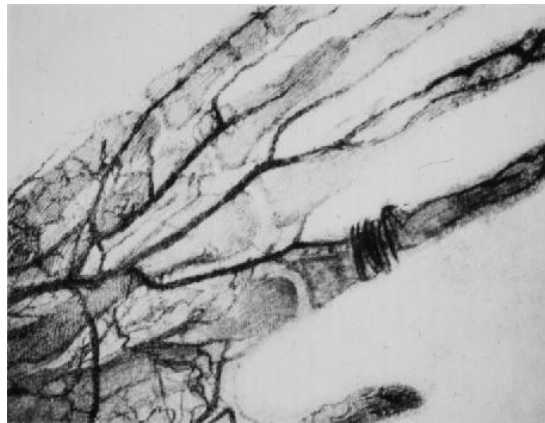


Figure 1.2: First angiogram (Jan. 17th, 1896).

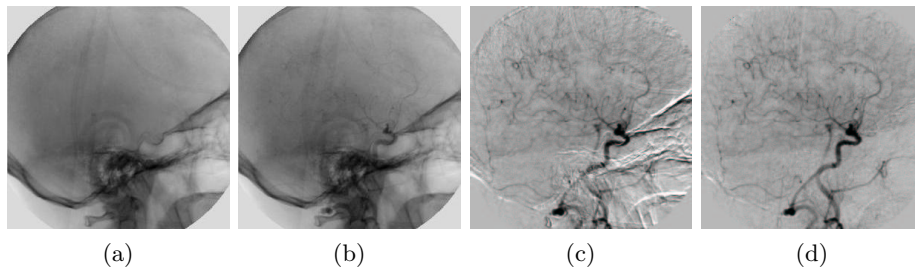


Figure 1.3: Digital Subtraction Angiography: Mask image (a), live image (b), subtracted image including motion artifacts (c) and motion corrected image (d) (from [41]).

with Teichmann's solution. This liquor contains lime, cinnabar (mercury) and petroleum. The exposure time for the first angiogram was 57 minutes.

Roentgen himself observed that salts in liquids cause attenuation of X-rays according to their permeability [47]. In order to enhance blood vessels *in vivo* the applied liquid (*contrast media*, *contrast agent*) must be applicable to the human being without harm and attenuate radiation. In 1923 J. Berberich and S. Hirsch performed the first *in vivo* angiography on a human being and demonstrated the arterial blood supply of the thumb [11]. On June 26th, 1927 Egas Moniz (real name Antonio Caetano de Abreu Freire, 1874 – 1955) obtained the first successful cerebral angiogram *in vivo*. After eight unsuccessful tries he finally succeeded using sodium iodide as contrast medium [62]. Due to the high risk and severe adverse effects, substantial progress in the development of relatively safe contrast agents and radiological equipment was needed before introducing this technique for the purpose of diagnosis and intervention.

The photographic subtraction technique was known since the early 1900s and since then used for instance in astronomy [40]. In 1934 Bernard Ziedses des Plantes (1902 – 1993) introduced image subtraction into the field of X-ray angiography [45]. The *subtraction angiography* was a significant improvement over conventional angiography as the contrast enhanced vessels are made visible without superimposing structures. A *native* X-ray image – taken before the application of a contrast agent – is subtracted from an image with contrast enhanced arteries by photographic means. It is also common to use the terminology *mask image* for the native image and *live image* for images with opacified structures.

In the 1960s the time consuming film subtraction process was replaced by analog video subtraction techniques [25]. The development of powerful computer systems lead to the introduction of *digital subtraction angiography* (DSA) [35]. With this technique DSA is possible at interactive frame rates of 30 fps and thus allows the application during surgical interventions. Patient movements (i.e. cardiac movement) introduce artifacts into the subtracted images as after the movement the mask image need not correspond to the background of

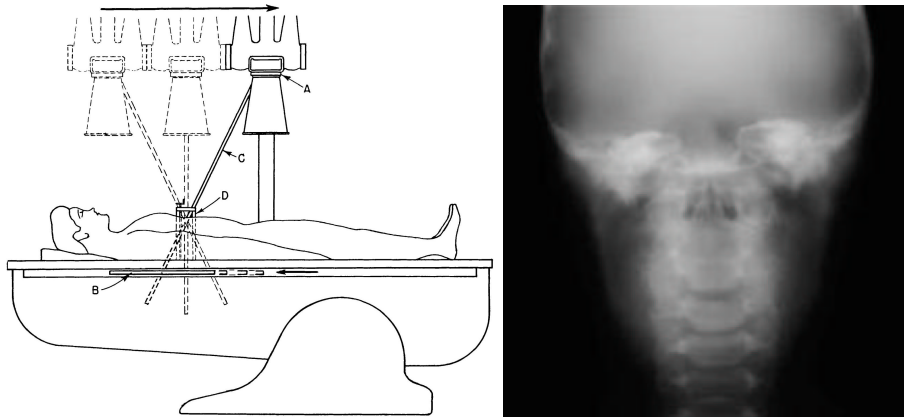


Figure 1.4: Left: Conventional tomography. Diagram shows motion of the tube and film about a fixed pivot point. A = X-ray tube, B = film tray, C = connecting lever rod, D = adjustable fulcrum (from [24]). Right: A pluridirectional tomography (from [4]).

the current live image (see Figure 1.3). Such distortions may be corrected by motion correction algorithms on the fly [41]. Because of its reproducibility and high 2D resolution this acquisition technique is up to now regarded as the 'Gold Standard' in angiography by most radiologists. However this invasive method – it requires catheterization – implies a certain risk for the patient.

1.3 Conventional Tomography

The term *tomography* is derived from the Greek words $\tau\omicron\mu\omicron\varsigma$ (tome – a cutting, section) and $\gamma\rho\alpha\phi\epsilon\iota\nu$ (graphein – to write). It stands for mapping a two dimensional section from a three dimensional object.

In the early 1900s a lot of effort was done in improving X-ray imaging. As the different anatomical levels accumulate to undesired shadows in the final X-ray image a method to acquire sectional X-ray images was of high interest. Despite some predecessors of *conventional tomography* it lasted until 1934 when Bernard Ziedses des Plantes proposed this technique together with subtraction angiography in his thesis [24]. The proposed method – originally named *planigraphy* – was the first comprising the homothetic movement of two elements of the triad (tube, patient and film), which is a requirement for true tomography [59]. The basic principle of the method is as follows. Tube and film move around a common pivot point during irradiation. The movement applied may be linear, oval, elliptic, or spiral. By this movement structures in plane with the pivot point are displayed sharply and structures above and below this plane are displayed blurred (see Figure 1.4). This is because during the trajectory of tube and film in relation to the patient, each point on the section is projected

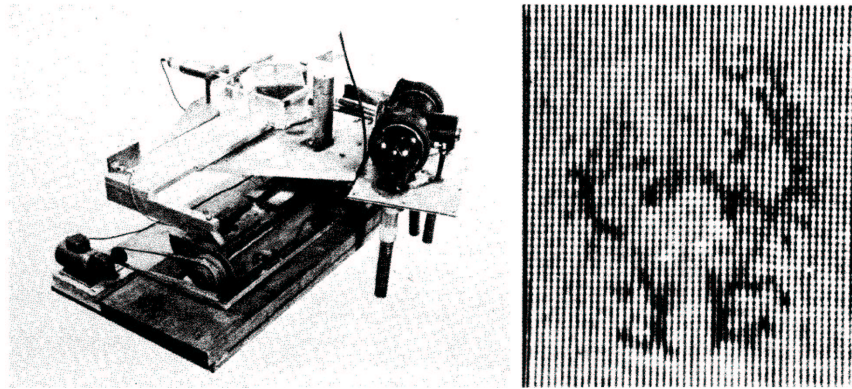


Figure 1.5: Left: Hounsfield's prototype showing the X-ray tube and a mounted human brain. Right: First scan of a specimen of a human brain. (from [27]).

on the same image area. Consequently they have a more significant influence on the resulting attenuation than other areas. However, a major limiting factor with planigraphy was its failure to obscure or 'blur' shadows of linear structures that lay in the same direction as the tube-film excursion [24].

1.4 Computed Tomography

In 1917 the Austrian mathematician Johann Radon (1887 – 1956) proved that any function f in \mathbb{R}^2 is well defined by all line integrals of the function f [46]. This purely theoretical approach provided the mathematical foundations for further research towards computed tomography. Nearly half a century later Allan Cormack (1924 – 1998) did first experiments with X-rays absorption on phantoms made of material like wood or aluminum. In 1963 he published his work on calculating radiation absorption distribution in the human body based on transmission measurements [9]. At that time Cormack was not aware of Radon's work, which could have saved him a lot of time, as he mentioned [28]. However this publication remained unnoticed for years.

Based on Cormack's work Godfrey Hounsfield (*1919) successfully implemented a prototype of *computed tomography* (CT) in 1968 (see Figure 1.5). After first experiments with gamma rays – which took 9 days per scan – Hounsfield used X-rays for scanning the probes. Thereby scanning was reduced to 9 hours per sample. The image reconstruction took at least 2 hours. Even though the image quality of the first images was comparably poor, the main objective – differentiating grey and white matter of the human brain – was achieved (see Figure 1.5). Further improvements lead to the first clinical prototype in 1972 with an image acquisition time of about 18 seconds (see Figure 1.6). In the same year the first patient was scanned. The patient was a woman who had a

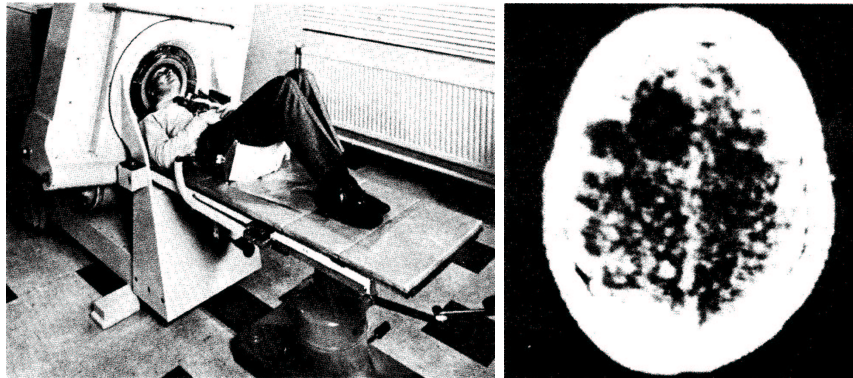


Figure 1.6: Left: First clinical prototype. Right: First clinical image from prototype machine. (from [27]).

suspected brain lesion, and the picture showed clearly in detail a dark circular cyst in the brain (see Figure 1.6). Since then Hounsfield is generally recognized as the inventor of computed tomography [26].

The basic principle of computed tomography consists of measuring the spatial distribution of a physical quantity to be examined from different directions. From the measured data a superposition free image is calculated. Traversing an object, the X-ray beam is attenuated according to the attenuation coefficient μ of each spatial point on the ray (see Figure 1.7). The total attenuation I of a ray with length d can therefore be calculated by the following equation:

$$I = I_0 \cdot e^{-\int_0^d \mu ds} \quad (1.1)$$

In the case of computed tomography the attenuation coefficient $\mu(x, y)$ at position x, y is unknown. However, according to Radon's theorem the unknown distribution $\mu(x, y)$ is well defined by an infinite number of line integrals of $\mu(x, y)$. As shown previously the total attenuation I represents an integral of the function $\mu(x, y)$. In practice only a finite number of measurements are acquired by measuring the X-ray attenuation while rotating the X-ray tube and the *collimator* (detector) around the scanned object (see Figure 1.7). Thus the computed reconstruction is an approximation of the true distribution of $\mu(x, y)$ and consequently only an approximation of the objects represented by $\mu(x, y)$.

As the measured physical quantity μ depends on the used spectral energy, a quantitative statement is difficult. Comparisons of images from different CT scanners with different voltage and filtration based on μ are limited. Therefore a unit relative to the attenuation coefficient of water μ_{water} for CT images was introduced. CT numbers or *intensity values* are specified in *Hounsfield Units* (HU). For an arbitrary tissue T with attenuation coefficient μ_T the CT value is defined as [28]:

$$CT \text{ value} = (\mu_T - \mu_{water}) / \mu_{water} \times 1000 \text{ HU} \quad (1.2)$$

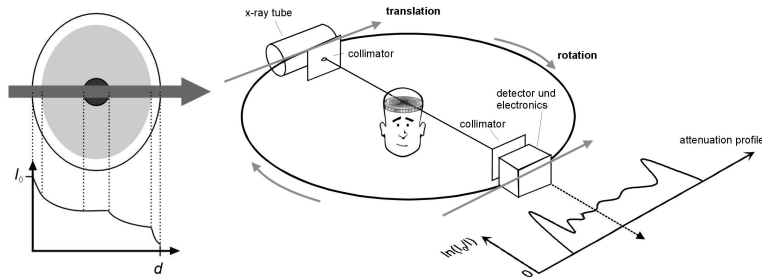


Figure 1.7: Left: Attenuation along a X-ray. Right: Principal setup of a computed tomography modality. (from [28]).

From 1972 on the computed tomography techniques steadily improved image quality and acquisition speed (see Table 1.1). The development is categorized in *four generations*. The first two generations are only of historical importance. CT modalities of the *3rd generation* comprise of a rotating X-ray source and an – as well rotating – opposite detector arc. During acquisition these two components – also referred to as *gantry* – rotate around the patient in a symmetric manner. Modalities of the *4th generation* are composed of a stationary detector ring and a rotational X-ray source. However modalities of the *3rd generation* have prevailed.

Besides these well established techniques alternative scanner concepts were developed. The *electron beam CT* (EBT) performs data acquisition without mechanical motion. The electron beam is generated from a fixed mounted electron gun and re-directed electromagnetically to a ring-like target enclosing the patient. From the targeted position X-ray radiation is emitted which is measured by an opposite detector ring. This technique allows extremely short acquisition times (50–100 ms per image) which are useful for cardiac imaging for instance. In contrast to conventional CT modalities a *cone beam CT* performs a 3D reconstruction by measuring the X-ray attenuation on a 2D detector array. The *Dynamic Spatial Reconstructor* (DSR) is conceptually an extension to cone beam CT. Fourteen X-ray tubes and fluorescent screens – which are captured by video or CCD cameras – rotate continuously around the patient. Only a fraction of a full revolution is needed to acquire 240 slices at 0.9 mm width [48].

A significant improvement of acquisition techniques was the development of *spiral CT* modalities in the late 1980s [42]. In contrast to previously mentioned techniques the patient position is no longer fixed in relation to the X-ray tube and detector units. During the acquisition process the patient is continuously moved through the gantry. The acquired data are no more in plane but describe helical or spiral (hence the name spiral CT) cuts through the patient. During the reconstruction process the true sections are interpolated from the acquired data along the direction of the table movement. Thus images may be reconstructed at arbitrary positions. This technique leads to higher data resolution

	1972	1980	1990	2000
Minimum scan time	300s	5–10s	1–2s	0.3–1s
Data per 360° scan	57.6 kB	1 MB	2 MB	42 MB
Image matrix	80 x 80	256 x 256	512 x 512	512 x 512
Power consumption	2 kW	10 kW	40 kW	60 kW
Slice thickness	13 mm	2–10 mm	1–10 mm	0.5–5 mm

Table 1.1: Performance development of high-end CT modalities from 1972 to 2000 (from [28]).

and new clinical applications. A further advancement was the introduction of the *multi-slice CT* (MSCT) technique. Using multiple row detectors allows the acquisition of interleaved helical sections. Thus the reconstructed image sections are of higher resolution and the acquisition duration is reduced. This is because the *table feed* – the movement of the patient in mm per 360° rotation – can be increased. Especially these two developments significantly influenced the research in volume visualization. This is mainly because of the numerous near isotropic images at high resolution. They result in large data and which are therefore tedious to inspect image by image.

1.5 Computed Tomography Angiography

Non-invasive vascular imaging is a challenging field of scientific research in clinical medicine and in medical imaging sciences alike. The goal of non-invasive vascular imaging is to visualize vascular anatomy and pathology using modern non-invasive cross-sectional imaging modalities. Thereby obviating the need for intra-arterial digital subtraction angiography (DSA) [6], which is an invasive and costly procedure requiring arterial catheterization.

With the introduction of latest multi-detector array computed tomography (CT) systems (multi-slice CT), acquisition speed, temporal, and spatial resolution have been improved dramatically compared to single-detector array CT. With this technology further improvements (e.g. eight or more channels compared to currently available four-channel systems) can be expected in the near future [28]. Due to its increased anatomic coverage, multi-slice CT has enabled the investigation of new vascular territories – such as the entire arterial system of the lower extremities [51]. Multi-slice CT thus has become a potential non-invasive imaging modality for peripheral arterial occlusive diseases (PAOD), which is a significant health problem in the industrialized world [15].

The accuracy and clinical usefulness of this promising new technique is still unknown and needs to be evaluated in the future. Compared to other vascular territories, visualization of PAOD is demanding. First of all, because the anatomic range to be scanned is large. Second, because not only atherosclerotic plaque, vessel wall calcifications and luminal stenoses, but also long segments of complete vascular occlusions need to be visualized [6]. The acquisition (CT

scanning) of high-resolution volumetric CT-Angiography (CTA) datasets of the peripheral arteries with powerful CT equipment is readily at hand. The pure acquisition time requires no more than 40 to 70 seconds. However the scientific evaluation of its potential benefits for vascular diagnosis and treatment is substantially hampered due to long post-processing time.

Most currently available post-processing techniques are unsuited to effectively extract and visualize the diagnostically relevant information from large CTA datasets within a reasonable time-frame. Using segmentation and visualization tools provided by the state-of-the-art clinical workstations requires up to four hours of manual editing and image manipulation to visualize the presence and distribution of peripheral arterial disease in a single patient’s dataset. This is unsuitably long for conducting a clinical trial that compares CTA with DSA in a large number of patients. For a potential routine clinical use, post-processing time should not exceed 30 minutes.

1.5.1 Clinical Requirements of Vessel Visualization

For visualizing vascular pathology with CTA it is necessary to provide a representative angiography-like overview of the vessels of interest, together with images from which the flow-lumen (with its stenoses and wall abnormalities) can be assessed. The former requirement can be conveniently accomplished with maximum intensity projection (MIP) images, shaded-surface display (SSD), or volume rendering (VR) techniques. The latter requirement (assessing the vascular flow channel) can be best accomplished with curved planar reformations (CPR) along the central axis of the vessel. CPRs are not limited by the occurrence of vessel wall calcifications, which obscure the vessel lumen when the former techniques are used.

1.5.2 ‘State-of-the-art’ in CT-Angiography (CTA)

All of the earlier mentioned methods are widely available on state-of-the-art medical visualization workstations. They have been successfully used in clinical practice for visualizing a wide variety of vascular territories. MIP, SSD and VR techniques, however, require substantial manual image editing and manipulation. In order to obtain an unobstructed view on the vessels, bony elements have to be identified and removed from the datasets first. State-of-the-art clinical workstations provide a number of manual editing tools for this purpose, all of which are – depending on the size of the datasets – time consuming. CPR generation requires manual tracing of the vessel centerline, which is user-dependent and time consuming as well. With the recent introduction of multi-slice CT technology CTA of the peripheral arteries has become possible. However, all of the above methods are therefore prohibitively impractical for visualizing peripheral arterial occlusive disease.

Numerous sophisticated image segmentation and processing tools have been developed and described in the technical literature: overviews [19, 49], shape and deformable models [58, 38], classification [36], enhancement [52, 17]. A

detailed overview of vessel detection and visualization can be found in [7]. Such techniques, however, have not been introduced into clinical practice because with few exceptions they are not available on medical imaging workstations.

1.6 The Scope of this Work

The main focus of this work is the clinical relevant visualization of vascular structures from computed tomography angiography data. Different methods for visualizing the vessel lumen by means of curved planar reformation are proposed. The appropriate center line extraction for the vessel is discussed. In addition to that a complex volumetric data set is presented and evaluated by different visualization algorithms.

Chapter 2 deals with vessel exploration based on computed tomography angiography. Large image sequences of the lower extremities are investigated in a clinical environment. Two different approaches for peripheral vessel diagnosis dealing with stenosis and calcification detection are introduced. The Chapter presents an automated vessel-tracking tool for curved planar reformation. An interactive segmentation tool for bone removal is proposed.

Visualization of tubular structures such as blood vessels is an important topic in medical imaging. One way to display tubular structures for diagnostic purposes is to generate longitudinal cross-sections in order to show their lumen, wall, and surrounding tissue in a curved plane. This process is called *Curved Planar Reformation* (CPR). Chapter 3 presents three different methods to generate CPR images. A tube-phantom was scanned with computed tomography (CT) to illustrate the properties of the different CPR methods. Furthermore enhancements to these methods are introduced: thick-CPR, rotating-CPR and multi-path-CPR.

Traditional volume visualization techniques may provide incomplete clinical information needed for applications in medical visualization. In the area of vascular visualization important features such as the lumen of a diseased vessel segment may not be visible. Curved Planar Reformation (CPR) has proven to be an acceptable practical solution. Existing CPR techniques, however, still have diagnostically relevant limitations. Chapter 4 introduces two advanced methods for efficient vessel visualization, based on the concept of CPR. Both methods benefit from relaxation of spatial coherence in favor of improved feature perception. A new technique is presented to visualize the interior of a vessel in a single image. A vessel is re-sampled along a spiral around its central axis. The helical spiral depicts the vessel volume. Furthermore, a method to display an entire vascular tree without mutually occluding vessels is presented. Minimal rotations at the bifurcations avoid occlusions. For each viewing direction the entire vessel structure is visible.

Chapter 5 reports on using computed tomography (CT) as a model acquisition tool for complex objects in computer graphics. Unlike other modeling and scanning techniques the complexity of the object is irrelevant in CT, which naturally enables to model objects with, for example, concavities, holes, twists

or fine surface details. Once the data is scanned, one can apply post-processing techniques for data enhancement, modification or presentation. For demonstration purposes a Christmas tree is scanned. It exhibits high complexity which is difficult or even impossible to handle with other techniques. However, care has to be taken to achieve good scanning results with CT. Further, Chapter 5 illustrates post-processing by means of data segmentation and photorealistic as well as non-photorealistic surface and volume rendering techniques.

In Chapter 6 a comparison of the introduced methods is presented.

Chapter 2

Peripheral Vessel Investigation

This chapter is based on following publications:

Kanitsar, A., Wegenkittl, R., Felkel, P., Fleischmann, D., Sandner, D., Gröller, E.: Peripheral Vessel Investigation for Routine Clinical Use. *In Proceedings of IEEE Visualization 2001*, pages 477-480, October 2001.

Kanitsar, A., Wegenkittl, R., Felkel, P., Sandner, D., Gröller, E., Fleischmann, D.: Automated Vessel Detection at Lower Extremity Multislice CTA (Abstract), *European Congress of Radiology 2001 (ECR 2001) Supplement 1 to Vol. 11*, page 236, Vienna.

Kanitsar, A., Wegenkittl, R., Felkel, P., Fleischmann, D., Sandner, D., Gröller, E.: Peripheral Vessel Investigation for Routine Clinical Use. Technical Report TR-186-2-01-13, Institute of Computer Graphics and Algorithms, Vienna University of Technology. March 2001.

*Do not go where the path may lead,
go instead where there is no path
and leave a trail.*
— *Ralph Waldo Emerson (1803 - 1882)*

2.1 Introduction

Lower extremity arterial disease is a significant health problem in the industrial world. The prevalence of symptomatic disease (intermittent claudication) in patients between 55 and 74 years of age is 4.6% [15]. Nowadays, intra-arterial digital subtraction angiography (iaDSA) is the pretherapeutic imaging technique of choice. iaDSA, however, is an invasive and costly procedure, which requires arterial catheterisation. A non-invasive technique for imaging the entire inflow vessels and run-off vessels is therefore desirable.

Latest technical developments in computed tomography (CT) – notably multi-slice helical CT – allow an unprecedented volumetric resolution and a widespread anatomic coverage. A multi-slice helical CT thus has the potential to accurately show the entirety of the lower extremity vessels with a single intravenous contrast-medium injection at a high, near isotropic spatial resolution.

The *data acquisition* time for a dataset of the lower limbs is in the range of minutes. On the other hand, the *post processing* time using conventional techniques takes up to four hours. However this step is necessary in order to extract useful information from the huge amount of acquired data. In order to make this investigation method applicable in the daily clinical use, the post processing time has to be shortened.

2.2 Peripheral vessel investigation

Computed tomography angiography (CTA) datasets of the peripheral vessel structures belong to the largest datasets in medical imaging. Current resolution is up to 1500 slices, each slice containing 512^2 pixels with a depth of 16 bit. Therefore for the practicability of CTA of the lower limbs it is crucial to provide an appropriate visualization tool for vessel investigation. It turned out that this tool should have the following properties:

- *Easy and fast to handle*, as the tool should be used in a clinical environment for routine purposes.
- *Adequate quality of the results*, which means the results should be diagnosable.
- *Robust algorithms* are required as the anatomic variations are quite large due to different vessel diseases.

Stenoses, calcifications and occlusions are the main arterial diseases that shall be investigated with CTA. A *stenosis* is a narrowing of the arterial flow lumen.

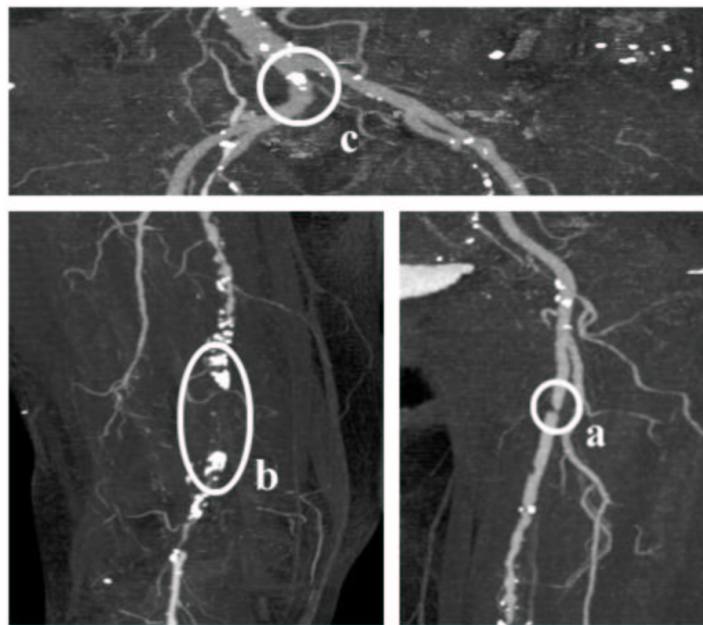


Figure 2.1: Different arterial diseases: Stenosis (a), Occlusion caused by calcification (b) and Calcification (c).

Arterial stenoses are caused by atherosclerotic plaque (Figure 2.1a). A complete obstruction of a vessel is referred to as an *occlusion* (Figure 2.1b). The blood flow is redirected through secondary vessels (*collateral vessels*), which circumvent the occluded vascular segment. The vessel wall of diseased arteries, as well as atherosclerotic plaque may calcify. With CT, calcified tissue is of high attenuation. In Figure 2.1, several areas of *calcification* can be seen (e.g., Figure 2.1c).

2.3 Visualization Methods for CTA

Basically two different approaches were taken in order to provide a feasible tool for investigating CTA datasets [29]. The first is to generate a curved planar reformation (CPR). This method is already used in medical environments. Therefore, it is a visualization technique that is very likely to be accepted for daily clinical use by the medical staff in hospitals. One of the biggest disadvantages of this technique is an extremely time-consuming and error prone manual generation process. For this reason, a semi-automatic generation method is desirable, which can handle most of the anatomical cases. This approach is described in Section 2.4.

The second approach is dealing with bone segmentation and removal. As the vessel tree in the lower extremity areas consists of a huge number of blood vessels of all sizes it is very difficult to identify every single vessel. Nevertheless, these small vessel structures are important to a radiologist. For instance the lumen of the small collateral arteries may allow a deduction of the spatial extent of a stenosis of the main artery. The basic idea is to hide structures of less or no importance (i.e., bones), which are easier to identify. This allows to emphasize the structures of interest. The entire vessel tree is made visible with a *maximum intensity projection* (MIP) by first removing the bones from the dataset. This method is described in more detail in Section 2.5.

It turned out that both visualization techniques are needed in order to produce results with diagnostical value. An overview of the whole vessel tree is provided by MIP visualization. Additionally the extent of a calcification can be determined, as every calcified area will be visualized in its entirety. Precise information concerning the vessel lumen and the extents of the stenoses are made available by the CPR visualization.

2.4 Automated CPR Generation

Planar cross-sections through volume data are often used for investigating CTA datasets in medical imaging. This is a rather tedious method for vessel investigation as only small parts of the vessels are visible within one planar cross-section. For this reason we want to compute a cross-section through the centerline of a vessel.

The centerline of a vessel is a 3D curve. A line, which is parallel to the

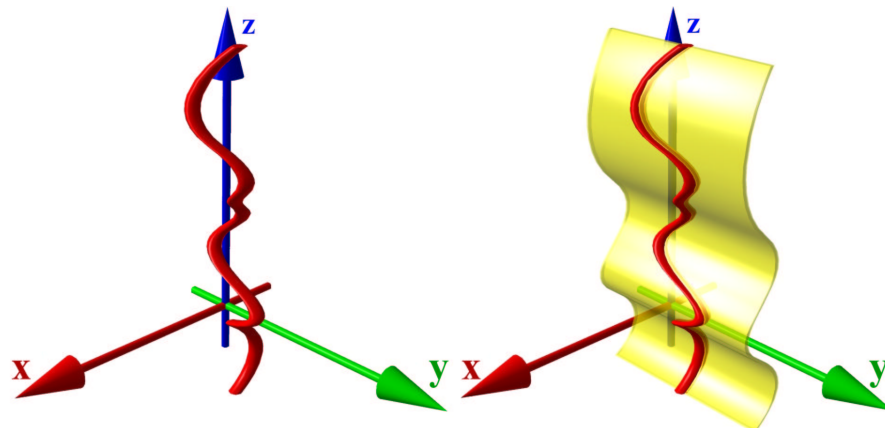


Figure 2.2: Left: Vessel centerline (3D curve). Right: Curved plane in 3D space.

horizontal axis of the viewing plane, is specified through each point of this curve. This line is swept along the 3D curve, generating a curved surface (see Figure 2.2). The voxels in the close neighborhood of the surface are resampled. Finally the surface is flattened and displayed in 2D. This process is called *curved planar reformation* (CPR). Taking the vessel centerline as curved line for the CPR prevents the vessel from being covered by bony structures. Furthermore, the correct vessel lumen can be determined in this representation even if calcified vessel walls are present. Finding the vessel centerline is a graph theoretical problem where voxels of the dataset are vertices and adjacent voxels are connected by edges. Each edge is weighted by a cost function indicating the likeliness of being part of a contrast enhanced artery. The cost function should introduce a low penalty if the edge is very likely to be within a vessel structure. Finding the path (from a user defined starting point to an endpoint) with the lowest accumulated cost within this weighted graph is known as *the shortest path problem* [5]. With high probability the resulting path is inside the arterial structure. The path is not necessarily the centerline of the vessel. This is, however, crucial for correct results, as deviations of the path from the central axis produce falsely simulated lesions. Therefore, the path has to be centered within the vessel before applying a curved planar reformation. First we explain the path search.

2.4.1 The Cost Function

The local cost function $f_C(x, y)$ for stepping from voxel x to the adjacent voxel y is defined as:

$$f_C(x, y) = c_{step} + f_I(y) + f_G(x, y) + f_L(y) \quad (2.1)$$

where a constant penalty c_{step} keeps the number of voxels in a path low and thus prefers smooth paths. The second component $f_I(y)$ punishes paths entering regions that are beyond the intensity interval typical for contrast enhanced arteries. In the following equations $f(y)$ is the intensity value of voxel y . The thresholds $c_{lowerBorder}$ and $c_{upperBorder}$ define the valid interval of artery density values. Within the smaller interval from c_{lower} to c_{upper} no penalty is given, as this area is regarded as optimal. With this definitions $f_I(y)$ is:

$$f_I(y) = \begin{cases} \infty & f(y) < c_{lowerBorder} \\ (c_{lower} - f(y)) \cdot \omega_{lower} & c_{lowerBorder} \leq f(y) < c_{lower} \\ 0 & c_{lower} \leq f(y) \leq c_{upper} \\ (f(y) - c_{upper}) \cdot \omega_{upper} & c_{upper} < f(y) \leq c_{upperBorder} \\ \infty & c_{upperBorder} < f(y) \end{cases} \quad (2.2)$$

The third component $f_G(x, y)$ assumes that in the direction of the central vessel axis the gradient magnitude is lower than in the direction of the vessel boundary:

$$f_G(x, y) = |f(x) - f(y)| \quad (2.3)$$

Finally, the fourth component $f_L(y)$ prevents the algorithm from tracking along and into bones. A convolution with the Laplacian edge detector L is done and resulting values above a threshold $c_{Laplace}$ are identified as unwanted transitions to bony structures:

$$f_L(y) = \begin{cases} \infty & (L \otimes f)(y) > c_{Laplace} \\ 0 & else \end{cases} \quad (2.4)$$

The parameters turned out to be quite invariant for several different datasets. However a feature, similar to grayscale windowing, has been introduced to alter these parameters. A color coded overlay in the image visualizes the current parameter settings. Taking advantage of this information a proper set of parameters can be found easily.

2.4.2 The Implementation of the Path Generation

First, the user defines a starting point at the root of the vessel tree (i.e. the aorta) and an arbitrary number of endpoints marking the ends of the peripheral arteries (see Figure 2.3).

According to Dijkstra's algorithm [5], all possible optimal paths from a given starting point are calculated. A snap shot of this process, showing the current search space, can be seen in Figure 2.3b. Because of the enormous size of the datasets two main performance improvements have to be done:

- *Caching temporary data*: The whole dataset is subdivided into independent cache blocks. For each cache block temporary data structures as direction information and accumulated costs are allocated only if needed. Thus the memory requirements are reduced.

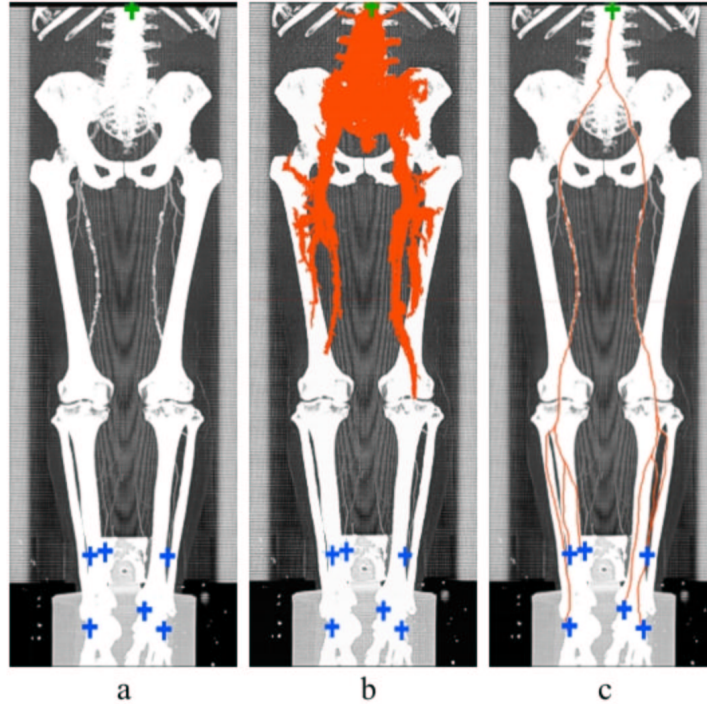


Figure 2.3: User Interaction of vessel tracking: User-defined starting point (top) and endpoints (bottom) (a), path generation process (b) and calculated centered paths (c).

- *Discretizing the cost function*: This method avoids the bottleneck of explicitly sorting the nodes according to their accumulated cost [12]. The resulting complexity is linear to the number of voxels in the search space. Therefore, acceptable computation times can be achieved even on large datasets.

The resulting path is taken as input to a vessel-center approximation-algorithm as described in the following section.

2.4.3 Centering the path

For each point of the computed path a cross-sectional plane of the vessel is computed. Within this plane a good approximation of the center point is calculated. The algorithm consists of four main steps:

1. *Tangent computation*: This step approximates the tangent at each voxel of the original path. A B-spline curve is used in order to smoothen the tangent.

2. *Plane construction*: A 2D cross section is extracted from the 3D dataset according to the current point of the original path. Its normal vector is calculated from the B-spline curve (tangent vector).
3. *Center approximation*: The vessel center within the 2D plane is approximated. Radial rays from the original point are intersected with the border of the vessel resulting in a set of points. Averaging these points, weighted according to their arc length, an approximation of the center point is computed. Afterwards, the retransformation into 3D space is done.
4. *Path reconstruction*: The new path consists of holes and loops because the points were moved in 3D space during step 3. These artifacts are removed using a B-spline curve again.

The centered paths can be seen in Figure 2.3c.

2.5 Semi-automatic Bone Segmentation

Because of the large datasets the segmentation process is kept quite simple. The user may alter the parameter settings according to the varying anatomy of different parts of the body. Together with the capability of user intervention regarding the type and the spatial connection of identified objects, the method provides a useful tool for the segmentation of bones. This approach produces results which are of diagnostic value.

Basically the algorithm is working on so called slabs. A slab consists of several adjacent volume slices. Typically 30 to 50 slices are combined into one slab. The algorithm is applied independently for each slab. The basic idea is to classify major parts of the objects with high accuracy and then inflate the identified areas to avoid partial volume artifacts and to cover fine details.

The algorithm consists of three steps. First a rough distinction between the different objects (bones, vessels) is done. The classification is done using t_{class} for a relatively safe object separation. Secondly the objects are labeled. In the final step the correct shape is computed. These steps are done without user intervention. A predefined set of parameters is used for each slab. The user can change this set of parameters during the segmentation process. For each slab the set of parameters consists of:

- t_{class} : This threshold is used to distinguish different objects.
- t_{expand} : Threshold to enhance already identified objects. This threshold handles partial volume effects and marrow inside the bones.
- t_{label} : Threshold, which separates between objects considered as bones or vessels. The threshold t_{label} operates on the average density of objects.

First, all slices are classified using a high threshold t_{class} in order to distinguish different objects. The classification process is based on the intensity value and on the gradient magnitude of the voxels. The connected regions are merged

Name	Spatial resolution in voxels	Size [MB]	Volume size [mm]
Pat1.dat	512 x 512 x 988	494,5	257 x 257 x 1070
Pat2.dat	512 x 512 x 550	275,5	240 x 240 x 1102
Pat3.dat	512 x 512 x 1000	500	260 x 260 x 1100

Table 2.1: Parameters of the test datasets.

Name	CPR	CPR	CPR	Segmentation
	computation	user interaction	center finding	
Pat1.dat	16 min 20 s	1 min 30 s	1 min 14 s	25 min 41 s
Pat2.dat	8 min 10 s	2 min 10 s	28 s	31 min 25 s
Pat3.dat	15 min 40 s	1 min 20 s	29 s	18 min 11 s

Table 2.2: Investigation time of the datasets.

and finally labeled with t_{label} according to their properties as average density and size. The second iteration of the whole process (except of labeling) is done with a lower threshold t_{expand} . This step improves the quality of the segmented dataset by reducing noise caused by partial volume effects and bone marrow. As the merging of different object types is prevented, bones and vessels remain separated. After this step a user defined labeling of objects is possible. This allows eventually occurring segmentation errors to be corrected manually. Finally the objects labeled as bone are removed.

2.6 Results

The test environment consists of a PII 350 MHz system with 704 MB main memory, running Windows NT 4.0 SR 5. The volume rendering was done on the commercial medical image processing system JVision/Space-Vision [39]. Table 2.1 and Table 2.2 summarize the dataset properties and the computation times for each of the three sample datasets. Figure 2.4 presents the CPR of the anterior tibial artery of the dataset in Figure 2.3. Note the stent in the topmost enlargement. Figure 2.5 presents a comparison between the MIP of a dataset without and with a segmentation post-processing. In contrast to the original dataset the segmented dataset provides a clear overview of the vascular structures. In Figures 2.6, 2.7 and 2.8 the results of investigating another dataset are shown. In contrast to iaDSA the heavy calcifications are clearly visible. Figure 2.8 shows non-photorealistic images created by direct volume rendering. For additional information we refer to www.cg.tuwien.ac.at/research/vis/angiovis.

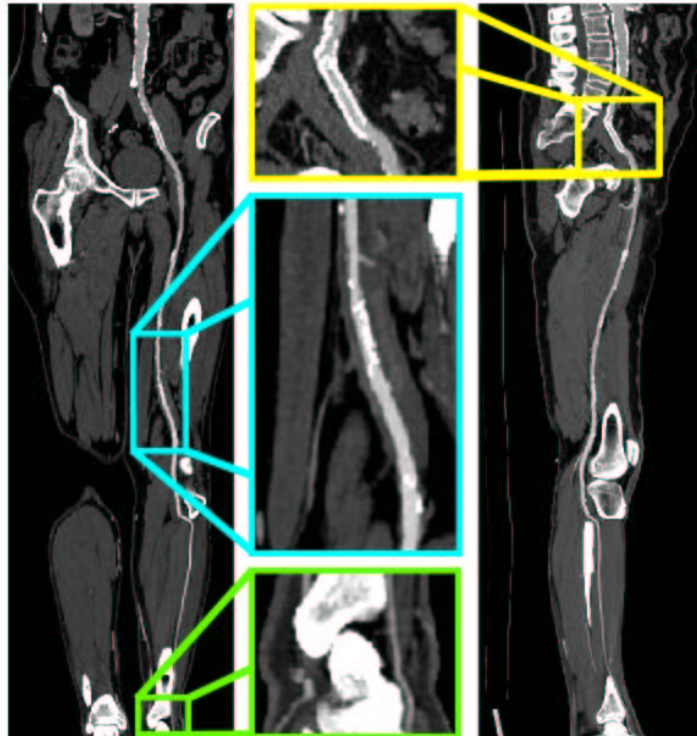


Figure 2.4: Coronar CPR (left side) and sagittal CPR (right side) of the anterior tibial artery from the dataset in Figure 2.3.

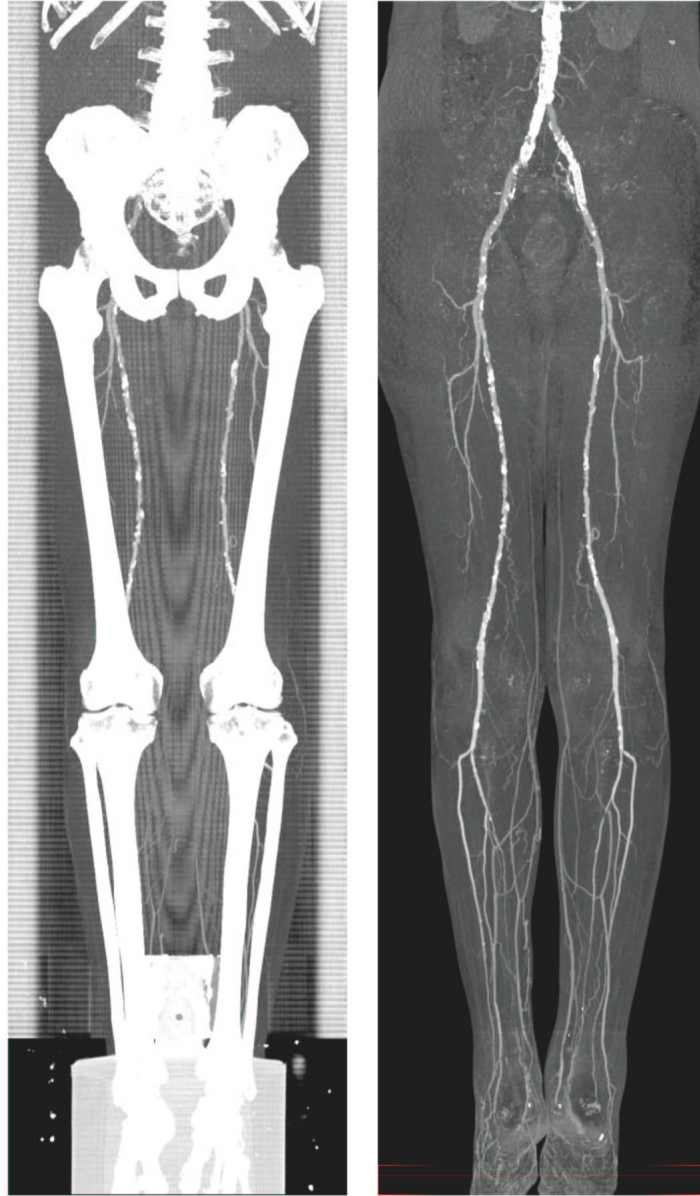


Figure 2.5: Segmentation results I: A MIP of a segmented dataset on the right side and a MIP of the corresponding dataset on the left side.

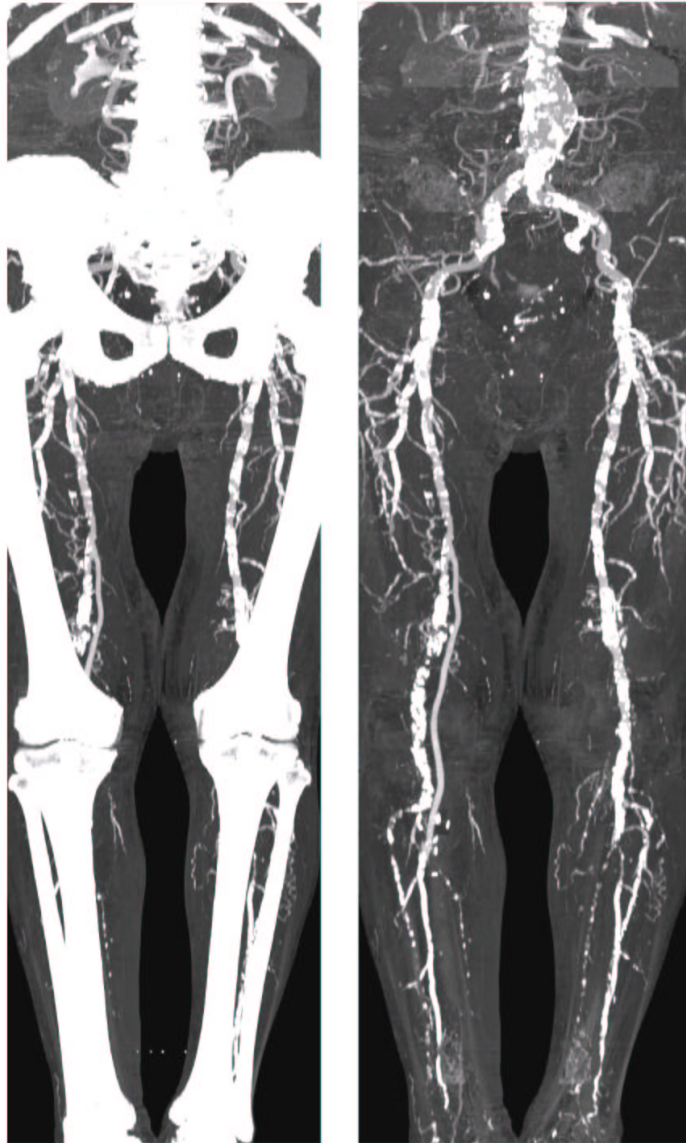


Figure 2.6: Segmentation results II: A sample dataset with heavy calcifications. MIPs of the original dataset (left) and the segmented dataset (right).

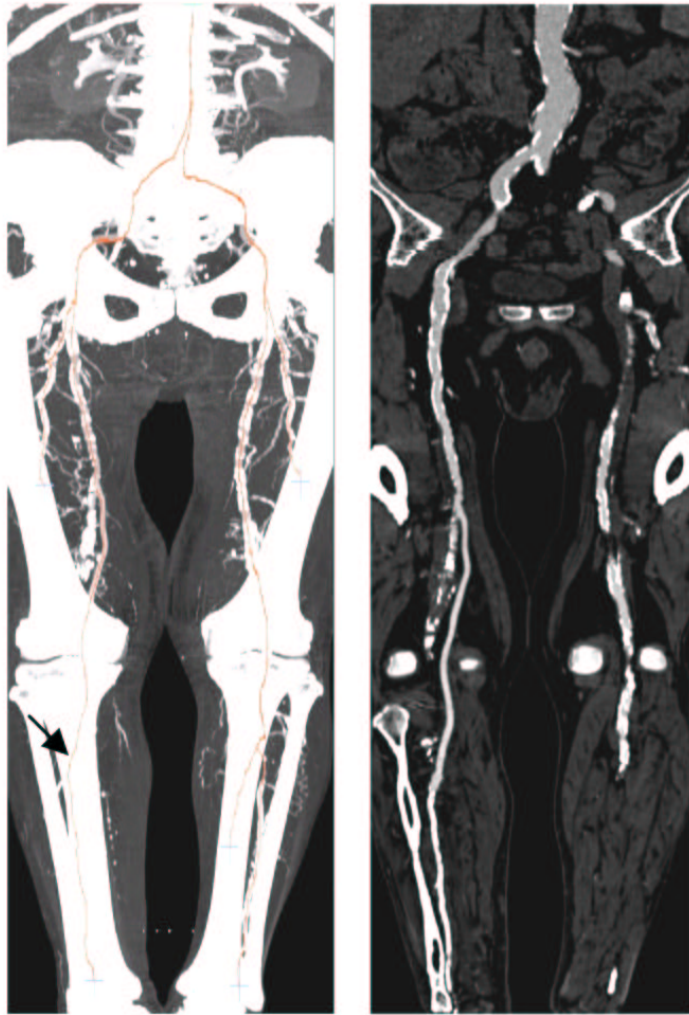


Figure 2.7: CPR generation result: Computed paths (left) with a CPR (right) corresponding to the path marked with an arrow.

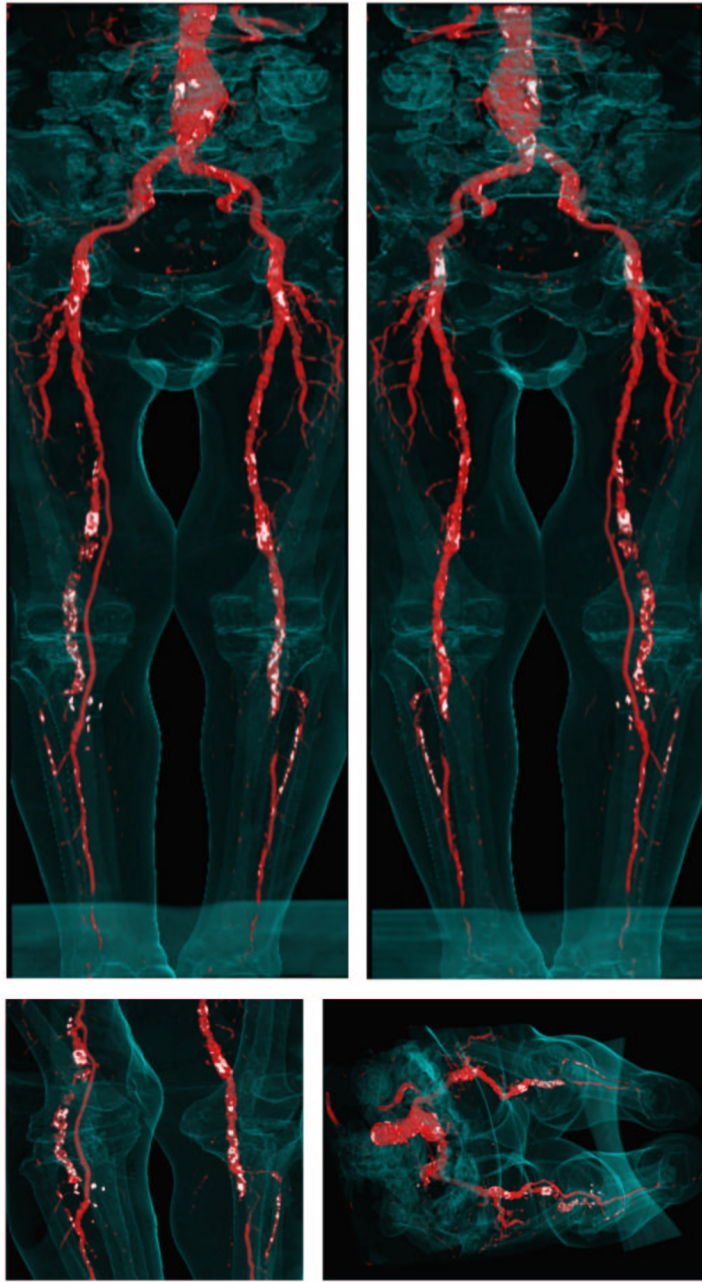


Figure 2.8: Non-photorealistic direct volume rendered images of the sample dataset. Calcifications and arteries are colored white and red. The outline of the body is visualized as guidance for the surgeon.



Figure 2.9: Evaluation of the results at the AKH-Wien.

	Automated		Manual	
	MIP	CPR	MIP	CPR
Completely removed arteries	–	–	3	–
Partially removed arteries	3	–	1	1
Investigation time	30 – 45 min		3 1/2 – 4 h	

Table 2.3: Results of the evaluation process.

2.7 Clinical Evaluation

For clinical evaluation three datasets with 988 to 1202 slices were manually post-processed by an experienced radiologist [32]. The same datasets were also investigated with the methods described in this work. The results were printed on laser film and a vascular radiologist compared the results vessel by vessel for searching lesions. iaDSA was taken as a reference standard for this purpose (see Figure 2.9). Completely removed arteries are clearly visible errors, as whole pieces of the artery are missing. Partially removed arteries are hard to identify as errors as they look very much like stenoses. Table 2.3 shows that automated post-processing produces results which are comparable to manually generated results. They are, however, generated in a much shorter time. The three totally removed parts of the arteries in the manual process corresponds to those which are partially removed by the semi-automatic method.

2.8 Conclusion

In this work post-processing and visualization tools are proposed, supporting CTA, which reduce the investigation time from 4 hours to 45 minutes. The results were of diagnostical quality and comparable to those manually generated. This could be accomplished by introducing a new cost model for vessel tracking. A tool for removing bones before visualization was implemented according to the special workflow of the diagnosis of peripheral arterial diseases.

Possible further work includes the enhancement of the reliability of the algorithms. One approach might be applying more sophisticated filter techniques [53]. Another possibility is to introduce segmentation techniques like boundary based segmentation methods in order to be able to address the non-uniform intensity values of bony structures.

Chapter 3

CPR - Curved Planar Reformation

This chapter is based on the following publications:

Kanitsar A., Fleischmann D., Wegenkittl R., Felkel P., Gröller M. E.: CPR - Curved Planar Reformation. *In Proceedings of IEEE Visualization 2002*, pages 37-44, October 2002.

Kanitsar, A., Fleischmann, D., Wegenkittl, R., Felkel, P., Gröller, M. E.: Multi-Path Curved Planar Reformation: Visualization of a Vascular Tree (Abstract), *European Congress of Radiology 2003* (ECR 2003), B-0204, Vienna.

Kanitsar A., Fleischmann D., Wegenkittl R., Felkel P., Gröller M. E.: CPR - Curved Planar Reformation. Technical Report TR-186-2-02-06, Institute of Computer Graphics and Algorithms, Vienna University of Technology. March 2002.

*Make visible what, without you,
might perhaps never have been seen.*
— Robert Bresson

3.1 Introduction

In medical imaging the assessment of tubular structures (i.e., blood vessels, bronchi, and colon) is a topic of high interest. Computed tomography (CT) and magnetic resonance imaging (MRI) provide three-dimensional volumetric data sets of the human body, which contain these objects of interest. The data gained from CT and MRI, however, include many objects of less or no interest. This makes volume-rendering (i.e., maximum intensity projection (MIP), ray casting, shaded surface display) without preprocessing often impossible or inaccurate. Furthermore the objects of interest are hardly located entirely within a single plane. In order to investigate these objects their central axis is derived from the data set. In this respect several algorithms [31, 61, 64] have been developed with different properties concerning reliability, speed and accuracy. The central axis as an output of these algorithms, can be used as a camera path (i.e., for virtual endoscopy) [60]. As vascular structures have a relatively small diameter, the central axis is often taken as input for further vessel analysis. Different properties (i.e., minimal and maximal vessel diameter, average attenuation) can be displayed.

Another way to visualize structures with small diameter is to re-sample and visualize the data set according to the high level information gained from the centerline detection process. This process is called *CPR - Curved Planar Reformation*. This technique displays the whole tubular structure within a single image. Vascular abnormalities i.e., stenoses, occlusions, aneurysms and vessel wall calcifications, are then investigated by physicians. This process is sometimes referred to as *multi planar reformation* (MPR). However the term MPR is not precise enough, as it is commonly used for planar cross-sections re-sampled from volumetric data.

Even though CPR is an established technique in the medical community, the visual properties, the advantages, and the problems of different types of CPRs have not been specifically addressed in the literature. Understanding the problems is essential for the accurate interpretation of the resulting images. Typically medical workstations contain some type of CPR, however important properties like length preservation are often not known to the user. This paper thus focuses on the generation, properties, and enhancements of different CPR methods. A comparison of this technique with conventional volume visualization techniques is not the topic of this paper, as such comparisons are already available [2].

Section 3.2 describes related work in this area. In Section 3.3 different CPR methods are introduced and their technical details are described. A short evaluation of the proposed methods on a dedicated tube-phantom is presented in Section 3.4. Section 3.5 proposes some extensions and variants of the previously

introduced CPR methods. Notably a new method for compositing multiple CPRs is proposed. Possible improvements and conclusions are discussed in Section 3.6.

3.2 Related Work

Latest CT technology, such as multiple detector-array CT, provide high resolution volumetric data sets. Due to the large size of these data sets (up to 1500 transverse cross-sectional images of the abdomen and entire legs), the investigation of the original images is no longer an option. Therefore volume visualization and data reformation play an important role in medical imaging. As accuracy is an important aspect of medical imaging, most of the literature in this area is written from a medical point of view. There is little literature available on the technical aspects and on issues relevant for implementation of CPR.

Avants and Williams present a vessel tracking method consisting of two parts [3]. From user defined seed points a surface expansion is computed based on the eikonal partial differential equation. A minimal cost path is calculated from these regions. From this path a cross-sectional area/radius profile is generated.

He et al. [23] proposed a path extraction method based on a two-dimensional region-growing algorithm with a subsequent shortest path algorithm. The resulting path was refined using the multi-scale medial response. The vascular tree is flattened in a semi-automatic method called *Medial Axis Reformation*.

Some authors take the central axis as an input for the generation of an abstract vessel model. Abstract vessel-models allow fast rendering, as polygonal meshes of low complexity are generated [14]. Furthermore non-photorealistic rendering provides the possibility to emphasize global properties of the vascular tree [22]. Bullitt and Aylward [8] exploit central axis information for speeding up conventional MIP. In a first step the surrounding of the vascular structures are projected to a modified z-buffer. In a subsequent step only non-empty areas are rendered according to the z-buffer values. For non tubular vascular structures (i.e., cardiac vessels) a lot of model representations exist. A systematic overview of models for cardiac function analysis is provided by Frangi et al. [16].

A comparison of MPR, MIP, shaded surface display (SSD), and direct volume rendering (DVR) with respect to accuracy is given by Addis et al. [2]. According to this comparison all rendering techniques accurately display vessels of a diameter greater than 4 mm. Except DVR the error in all visualization methods increases for smaller structures. The problem of finding an appropriate transfer-function, respectively iso-value, is not addressed by this paper.

Further information about the clinical relevance of the CPR visualization technique can be found in [1], [31], and [50].

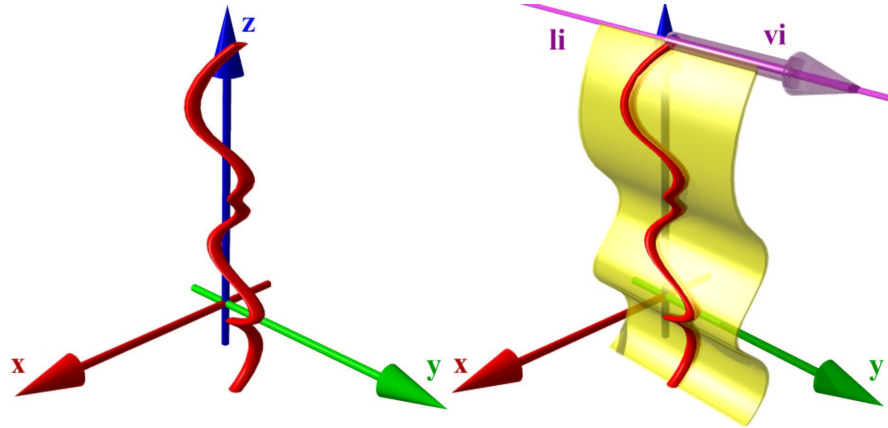


Figure 3.1: Principle of the CPR visualization: The vector-of-interest (vi) and the line-of-interest (li) defining the re-sampled plane.

3.3 CPR Methods

The goal of CPR visualization is to make a tubular structure visible in its entire length within one single image. To accomplish this goal a-priori information about the tubular structure, notably the object's central axis, is required. Without loss of generality the object's central axis is assumed to be a sequence of points at sub voxel resolution.

In general the spatial position and shape of the central axis determines which parts of the 3D space are visualized. On the left side of Figure 3.1 the central axis is shown. The re-sampled surface is shown on the right side of Figure 3.1. As the surface is not well defined by just one curve in 3D, an additional vector vi (*vector-of-interest*) is introduced. In some cases it is possible to define the vector-of-interest to be parallel to the xy-plane, which increases the performance of the generation process. Together with a point from the central axis, the vector-of-interest defines a straight line li (*line-of-interest*). All voxels touched by this line are taken to re-sample the volume along the line-of-interest.

The following subsections describe different methods for CPR generation with their respective geometric properties pointed out in detail. These properties are summarized in table 3.1.

Figure 3.2 illustrates the different CPR methods. The horizontal plane represents the image and the image y-axis as horizontal blue arrow. Corresponding to this axis, the curve in the volumetric data set is sketched by the vertical blue arrow.

CPR Method	Spatial perception	Isometry	Occlusion
Projected CPR	high	no	possible
Stretched CPR	medium	yes	no
Straightened CPR	low	yes	no

Table 3.1: Properties of CPR types

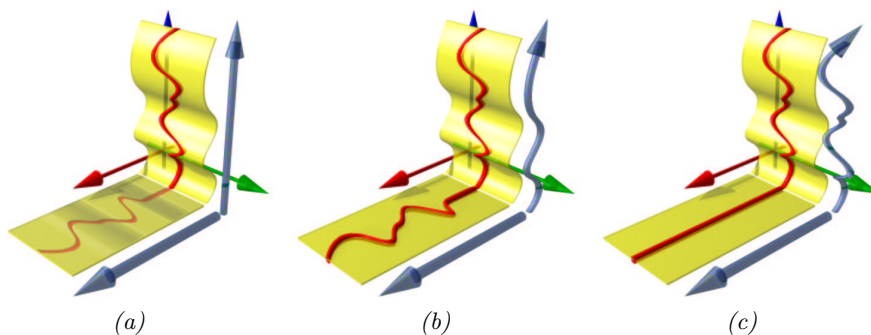


Figure 3.2: Different CPR generation methods: a) Projected CPR, b) Stretched CPR, c) Straightened CPR

3.3.1 Projected CPR

The projected CPR can be seen as a parallel projection of a data set, taking into account only a thin slice of voxels (see Figure 3.2). This slice is defined by the central axis of the tubular structures and the vector-of-interest. We assume the vector-of-interest to be colinear with the y-axis and apply a parallel projection to a free-form surface along the x-axis.

In particular, for each point of the central axis the line-of-interest is projected to the corresponding line of the image. This relationship is defined by the camera's coordinate system (i.e., the up-vector). If the up-vector of the camera is parallel to the z-axis, the z-coordinate of the line-of-interest is mapped directly to the image. The resulting image size only depends on the size of the data set.

For this camera coordinate system (the up-vector being parallel to the z-axis), a monotonously increasing central axis with respect to the z-axis is the most simple case. Each line in the image buffer may be overwritten without considering the contained values. However this restriction normally does not hold with real-world data sets. Therefore voxel compositing is done using *maximum intensity projection* (MIP), *minimum intensity projection* (MinIP), or *averaging* (AVG).

Due to parallel projection the spatial relations are maintained by this method. This helps the observer to perceive the spatial arrangement of the vessels.

The first disadvantage of this method is that structures of higher intensity (i.e., bony structures) still may obscure the structures of interest (i.e., vessels). This situation arises, if parts of the line-of-interest associated with a certain point of the central axis contains bony structures and this parts are projected to an image region containing vascular structures from a previous or following line-of-interest. The occurrence of such situations heavily depends on the application area. In the case of peripheral vascular structures this case hardly ever arises. However, the visualization of the carotid artery at the level of the skull-base, for example, often leads to such situations.

Another disadvantage of the projected CPR method is the distortion of the central axis' length due to parallel projection. Therefore isometry is not preserved.

3.3.2 Stretched CPR

The surface defined by the vessel central axis and the vector-of-interest is curved in one dimension and planar in the other one. Stretching the curved dimension results in a plane showing the tubular structure in its entirety without overlapping objects (see Figure 3.2). This type of CPR is referred to as *Stretched CPR*.

Processing all points of the central axis successively, the corresponding lines-of-interest are mapped to the image. This is done by rotating the consecutive point of the central axis around the current line-of-interest. The point is rotated in a way that the resulting plane is coplanar to the viewing plane. Isometry is maintained as the distance between the two consecutive points is preserved in image space by this operation. Thus the image size does not only depend on the length of the path, but also on the vector-of-interest. This fact is easy to see as the image height is small, if the path is highly curved in the resulting image.

Especially we are only interested in the image y-coordinates of the lines-of-interest. Let's assume point P_i to be the last processed point and point P_{i+1} the currently processed point of the central axis. The vector $\vec{d}_i = \overrightarrow{P_i P_{i+1}}$ represents the path direction at position i . Furthermore \vec{l} is the normalized direction of the line-of-interest. According to formula (3.1) the offset Δ_i in image space is.

$$\Delta_i = \sqrt{|\vec{d}_i|^2 - (\vec{l} \cdot \vec{d}_i)^2} \quad (3.1)$$

The image position y_{i+1} of the line-of-interest related to point P_{i+1} is given by $y_{i+1} = y_i + \Delta_i$ where $y_0 = 0$.

The central axis is assumed to be sampled with sub-voxel resolution. Therefore all rows of the image are filled. Introducing a zooming capability requires to interpolate between the lines-of-interest, if necessary.

The generation process of a stretched CPR ensures that other objects do not cover vascular structures. This is one of the key requirements in vessel visualization. The curvature of the tubular structure is still largely maintained by this kind of visualization, thus spatial orientation is still possible for the user.

The main advantage of this CPR type is the preserved isometry. This is important for accurate preoperative planning of endovascular stent-graft treatment of aortic aneurysms. The lengths of normal and abnormal vascular segments need to be determined accurately for sizing the endovascular prosthesis. This is possible in the case of a stretched CPR, but not in the case of a projected CPR.

3.3.3 Straightened CPR

The third type of curved planar reformation fully straightens the tubular structure (see Figure 3.2). This CPR method generates a linear representation of the vessel with varying diameter. The height of the resulting image corresponds to the length of the central axis.

In contrast to the above mentioned methods, the line-of-interest is no longer necessarily parallel to the axial slices. At each point P_i of the central axis the tangent vector t_i is calculated. The plane ε_i (*cross-section*) is defined by P_i and t_i . A local coordinate system is defined by two generating vectors of the plane ε_i : \vec{u}_i and \vec{v}_i whereby $\vec{u}_i \perp \vec{v}_i$. The line-of-interest is defined within the plane ε_i by an angle within the unit circle: the angle-of-interest φ .

As either \vec{u} or \vec{v} is mapped to the local coordinate system's x-axis, excessive rotation along the central axis may cause undesired artifacts. Methods exist to minimize this effect [34].

In particular it is not necessary to re-sample the entire cross-section from the data set. It is more efficient to do a transformation from the local coordinate system to the global coordinate system. The direction of the line-of-interest \vec{l}_i is given by formula (3.2):

$$\vec{l}_i = \cos \varphi \cdot \vec{u}_i + \sin \varphi \cdot \vec{v}_i \quad (3.2)$$

The image offset Δ_i for the line-of-interest corresponding to point P_{i+1} equals the distance from point P_i to P_{i+1} :

$$\Delta_i = |\overrightarrow{P_i P_{i+1}}| \quad (3.3)$$

The most obvious disadvantage is the lack of spatial orientation. Only short segments of visible side branches of the parent vessels indicate the topographic position of a given arterial segment.

One advantage of this method is the preserved isometry. Furthermore the direct relation between image height and central axis length makes it easy to create linked displays. Whenever the user points at a certain position of the image, the corresponding cross-section is displayed in a separate view. This feature eases the lack of spatial orientation.

Another advantage is the easy perception of variances of the diameter. Due to the elimination of curvature of the central axis the only varying property along the central axis is the diameter.

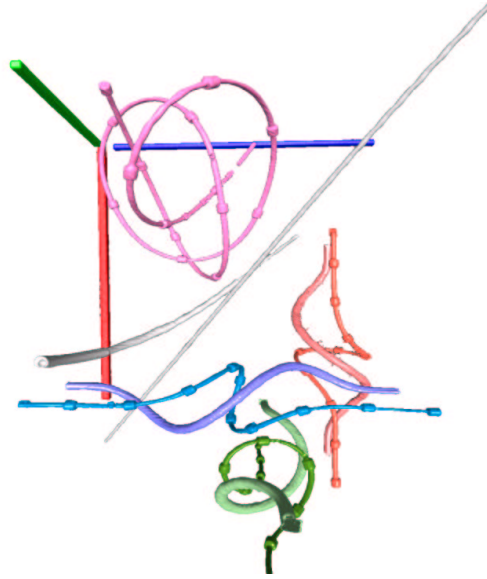


Figure 3.3: Iso-surface extraction of the ‘*Tubes Phantom*’ at -224 HU.

3.4 Evaluation of the CPR methods

To evaluate the different CPR methods a phantom (*Tubes Phantom*) simulating vascular structures in predefined spatial positions was assembled. The phantom was scanned with CT at a resolution of 512x512x509 voxels. The real world size of the phantom was 382 mm in transversal and 509 mm in longitudinal direction. The display window of the CPR images is centered at -251 HU (Hounsfield Units) at a width of 1452 HU.

Apart from different objects for evaluating measurement accuracy, the phantom contained water-filled tubes simulating blood vessels wrapped around three cardboard cylinders of 6 cm diameter oriented in the three main directions (see Figure 3.3). Each thin tube was 50 cm long and was scaled each 5 cm by a marker. Furthermore a 1.5 m long tube in arbitrary position, also filled with water, was included. The distance between each marker of 1 cm width was 9 cm. The diameter of the thin tubes was 4.6 mm, which is comparable to the arteries distal of the knees. In the case of the projected CPR the voxels are composited using MIP. The first row of Figure 3.4 shows the MIP of the phantom data set. The visualized tubes are highlighted, by showing their central axis in blue color.

Comparing the projected CPR to the corresponding MIP, the similarity proposed in chapter 3.3 is quite obvious. Whenever the central axis is orthogonal to the camera coordinate system’s up-vector, the visible diameter of a vessel may degenerate. At the inflection point in image space of the projected central axis at most half of the true diameter is displayed in case of a perfect central

axis. The diameter may degenerate to a line if the critical section is not covered by a point of the central axis prior or afterwards. These artifacts (red markers) can be seen in the second row of Figure 3.4.

The stretched CPR method was found out to produce highly reliable results. However any deviation of the central axis from the optimal central position increases the displayed length of the tubular structure. As the difference is quite small compared to the length of the structure the error is usually negligible. In rare situations not the length of the object, but it's diameter may appear larger than real. This occurs, if the tangent vector of the central axis is nearly parallel to the vector-of-interest.

The straightened CPR is highly sensitive to inaccuracies of the underlying central axis. Any deviation of the computed path from the true central axis results in a shift of the object in image space.

3.5 CPR Enhancement

All of the above CPR methods have some limitations in common. In this section different enhancements of traditional CPR techniques are proposed to overcome these limitations. The main disadvantages from a clinical point of view turned out to be the following three points.

First, all CPRs depend on the quality of the computed central axis. This is an important constraint, as the central axis computation at branching points as well as at highly calcified vessel parts is not trivial.

Second, only those parts of the vascular structures are visible in the image, which are touched by the re-sampled plane. For diagnostic purpose, however, it is important to inspect the entire vessel lumen. This is necessary to make sure that no calcified parts or stenosis are missed during the investigation.

Third, only one tubular structure of an entire vascular tree can be visualized simultaneously. Thus for the inspection of a vascular tree i.e., the peripheral arterial tree, a large set of images have to be investigated.

Despite of these visualization related limitations orientation and navigation is an additional issue. As surrounding tissue may be distorted in the image, it can be difficult to immediately recognize portions of a vessel tree actually displayed. In the context of a medical workstation it is easy to overcome this limitation of CPR methods. Taking advantage of the linked view concept, the position pointed at with the input device – in general a mouse – is shown in the original data. Thus the corresponding axial slice is displayed.

The enhancements of the CPR methods are demonstrated on a real-world data set with a scanned resolution of 512x512x988 voxels. The patient suffers from high graded stenoses in both femoral arteries. Calcifications are visible in both popliteal arteries and a complete occlusion in the left popliteal artery is present.

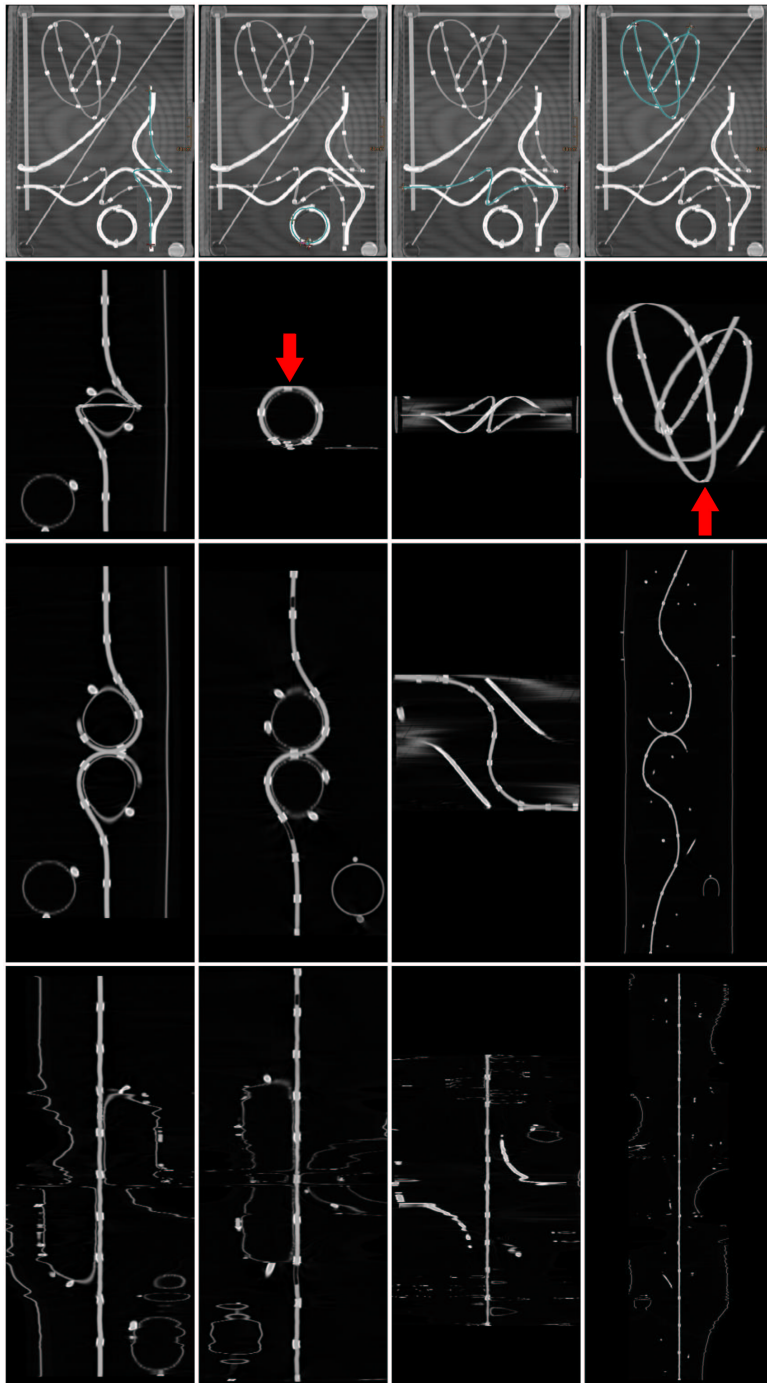


Figure 3.4: Top to bottom: MIP, Projected CPR, Stretched CPR, Straightened CPR. Left to right: Major central axis direction parallel to z-axis, parallel to y-axis, parallel to x-axis, in arbitrary direction.

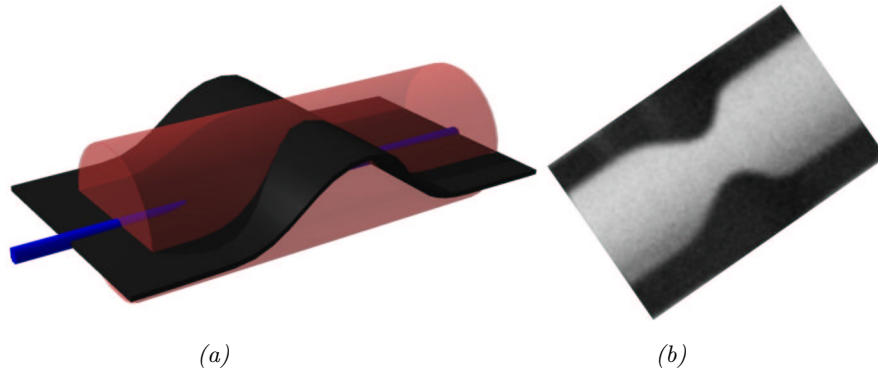


Figure 3.5: Artificial stenosis introduced by imprecise central axis computation.

3.5.1 Thick CPR

Up to now only a thin surface was taken into consideration to be re-sampled from the data set. Especially in the case of arteries with a small diameter an inaccurate central axis (see Figure 3.5a) immediately results in an artificial stenosis (see Figure 3.5b). In order to make this visualization method less sensitive to imprecise central paths a slab of a certain thickness is re-sampled from the data set. The voxels in a predefined distance from the longitudinal section are also taken into account. The computed sub-volume is displayed according to one of the following re-sampling strategies.

Averaging the voxels projected to one pixel in image space naturally results in blurred images (see top row of Figure 3.6). Especially tiny structures tend to fade out as well as calcified parts may decrease in attenuation. However especially for data with low signal to noise ratio this kind of re-sampling improves the image quality.

Using maximum intensity projection for re-sampling basically gives the maximum extent of high attenuation objects within the slab from the current viewing direction. Thus no artificial stenosis are possible as long as the true central axis is within the range of the re-sampled slab. Another advantage of MIP re-sampling is an increase of spatial orientation, as side branches and bifurcations of the main arteries become visible (see second row of Figure 3.6). However, depending on the viewing direction, vascular structures might be obscured by adjacent bones.

Analogously the minimum intensity re-sampling method is intended to emphasize structures of low attenuation (i.e., bronchi). A comparison between MIP and MinIP on a thoracic data set is shown in Figure 3.7.

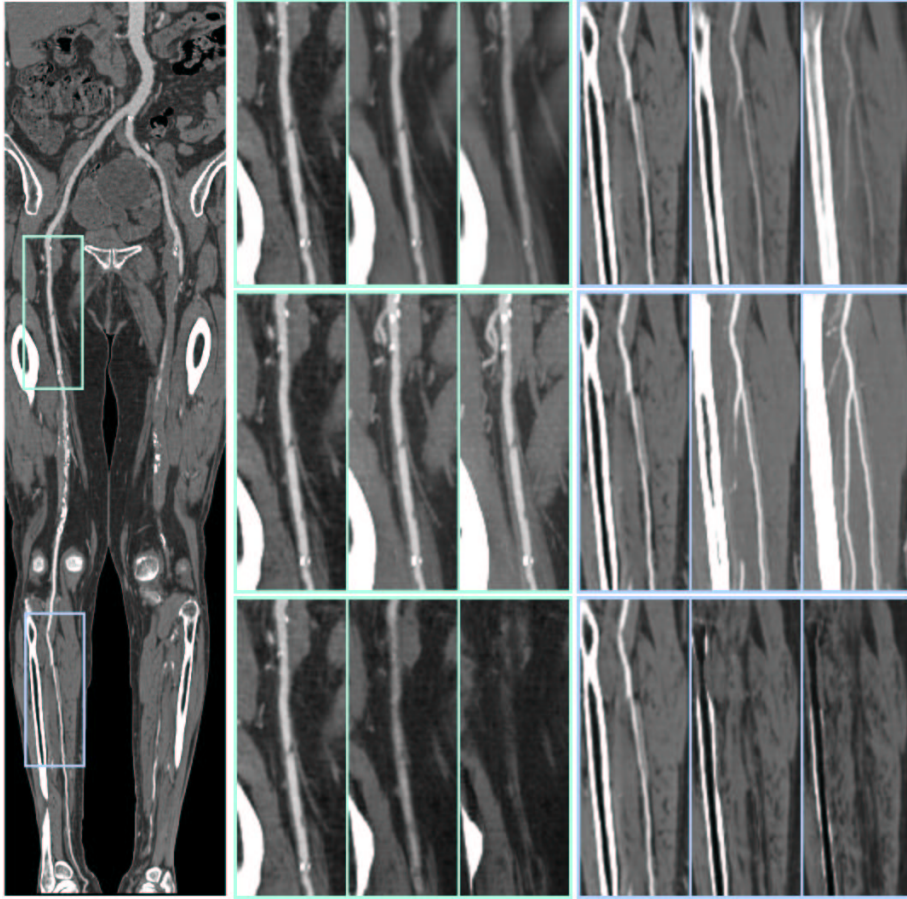


Figure 3.6: Left side: A stretched CPR of the entire data set. Middle and right side: Enlargement of the upper and lower sector. Top row to bottom row: Averaging, MIP, and MinIP with resampling of 0 mm, 5 mm and 10 mm thickness.

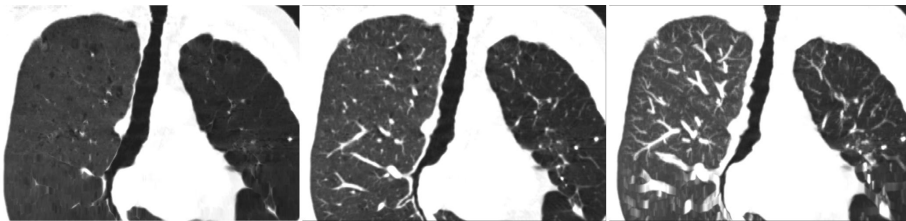


Figure 3.7: Left to Right: MinIP of 5 mm thick slab, MIP of 0 mm thick slab, MIP of 5 mm thick slab.

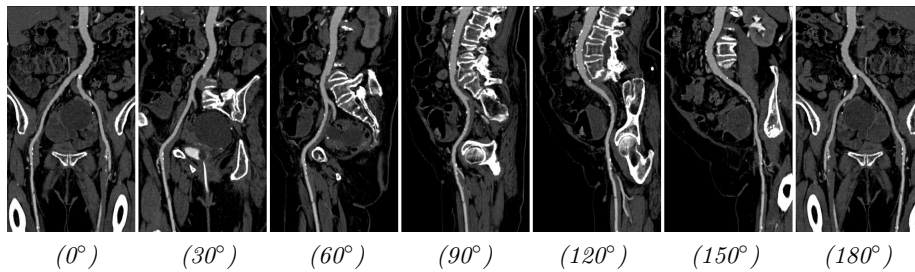


Figure 3.8: Rotating Stretched CPR

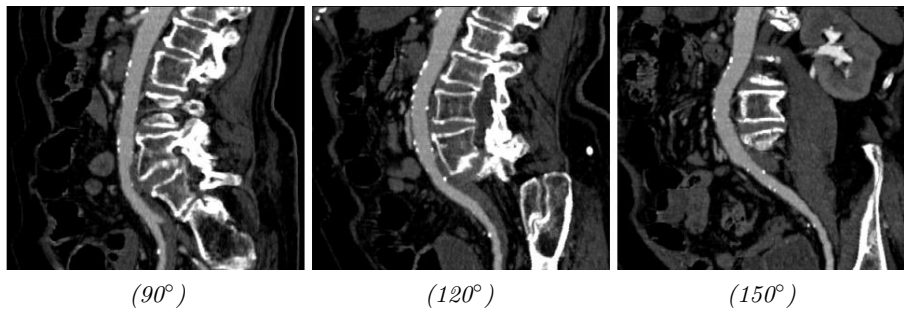


Figure 3.9: Enlargement of semi-circumferential vessel wall calcification

3.5.2 Rotating CPR

Visualizing the lumen of the vessel hides features, which are not touched by the displayed longitudinal section. Rotating the longitudinal section around the central axis provides the possibility to inspect the entire vessel. This technique is referred to as *rotating CPR*.

A stretched or projected CPR is generated by rotating the vector-of-interest around a predefined axis. This results in a continuous movement of the vascular structure within the generated image. Semi-circumferential vessel wall calcification becomes visible at certain viewing angles.

The straightened CPR is rotated by changing the angle-of-interest accordingly. As the vessel central axis is centered in the image space any deviation of the vessel diameter is immediately perceived by the investigating radiologist.

In Figure 3.8 a stretched CPR from seven different viewing directions is shown. The rotation axis is parallel to the head-feet axis of the patient and centered within the axial slices. The deviation of the current view from anterior view is the rotation angle of the CPR. Vessel wall calcifications become visible at 90° , 120° and 150° (see Figure 3.9).



Figure 3.10: MIP compositing of projected CPRs.

3.5.3 Multi-Path CPR

One substantial disadvantage of CPR visualization for diagnostic purposes is the restriction to only one tubular element. Most clinically relevant 'tubes' are part of a branching, anatomic structure. For instance the peripheral arterial tree begins at the abdominal aorta and branches into the left and right common iliac artery which again branches into internal and external iliac arteries. The latter is in continuity with the common femoral artery, which branches into a deep and into a superficial femoral artery, which becomes the popliteal artery and diverges into the anterior tibial, the posterior tibial, and the peroneal arteries. A comprehensive display of all clinically relevant vessels in one image is highly desirable.

The straight forward approach of simply compositing all calculated CPRs does not produce the desired result. No matter which re-sampling strategy is applied artifacts are always introduced in the generated image. In Figure 3.10 vascular structures are obscured by bones from different layers (see red marker). Therefore we propose a new image space driven method for compositing projected or stretched CPRs from multiple central axes.

The investigation of a vascular tree using traditional CPR methods results in a set of CPR images for each main vessel. Each image displays a different vessel segment from the same viewing angle. A comparison of the different CPR images shows that areas in image space exist which are redundant or of no diagnostic relevance. These image areas can be discarded without influencing the diagnostic value of the image (see Figure 3.11). The basic idea is to fill these image regions with information of another vessel segment.

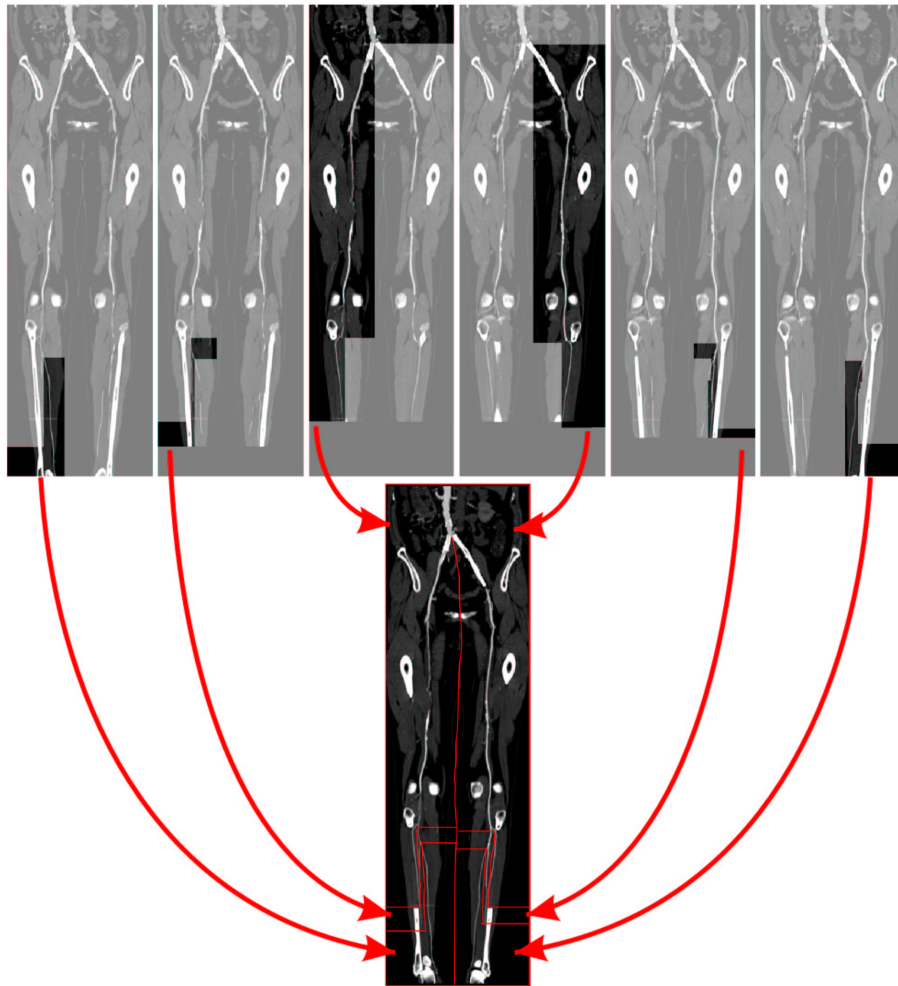


Figure 3.11: Concept of Multi-Path CPR.

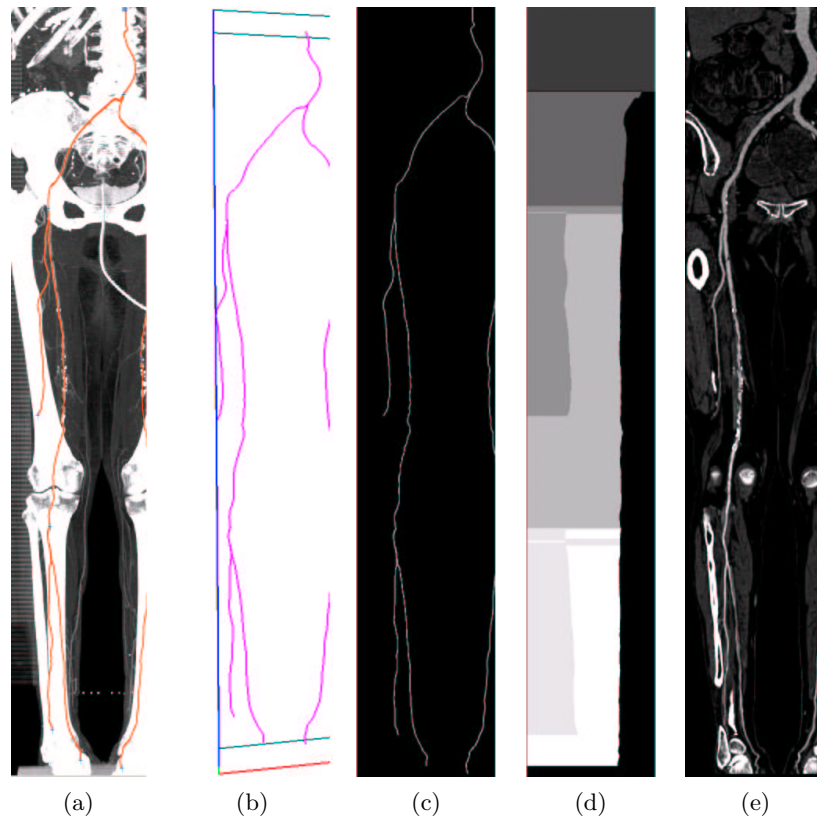


Figure 3.12: Generation of multi-path CPRs.

The tree of central axes and the volumetric data set is taken as input for the algorithm (Figure 3.12a). An enhanced z-buffer b of the same size as the image provides space for information entries containing a reference to a path, a reference to a point of this path (*point*), and depth information. Furthermore each entry contains information about an associated span *begin* and *end*. A span represents the part of an image scan line belonging to a certain path segment. Before each rendering pass these information entries are reset to initial values.

Tree projection. The tree (3.12b) is mapped to the buffer b according to the applied CPR method. This can be done using either projected CPR method or stretched CPR method. Figure 3.12c shows the entries of the buffer after the CPR generation process. If points of different paths are mapped to the same image position, the one spatially closer to the observer is taken by taking advantage of the depth information.

Buffer traversal. In a second step two buffer traversals are needed to determine the length of the spans. A span is computed so that the space between neighboring paths within a line is equally divided. The scan line at the border of the image is assigned to the leftmost or rightmost path segment respectively (see Figure 3.12d).

Data re-sampling. In the final step the buffer is traversed again. Each filled entry $b[x, y]$ is processed so that the image line y is filled from position $b[x, y].begin$ to $b[x, y].end$ with the data values associated with point $b[x, y].point$. This results in a composited CPR through multiple vessel center paths without overlapping structures, as each tree segment is drawn in a separate image region (see Figure 3.12e).

A projected multi-path CPR is presented in Figure 3.13. The projected multi-path CPR on the left provides an overview of the processed data set. A close-up of the upper image region is shown from different viewing directions. The CPR can still be rotated and the thick CPR enhancement is achieved by re-sampling the voxels adjacent to the extracted fragment of the longitudinal section.

If the vessel tree is mapped into the image space according to the stretched CPR method a combination of isometry preserving vessel segments is displayed. In Figure 3.14 the corresponding area was processed using the stretched multi-path CPR method.

As the vessel course in the straightened CPR is fixed to the center of the image, all CPRs would be mapped to the same image position. Therefore we propose a tree-like arrangement of the CPRs from the tree segments.

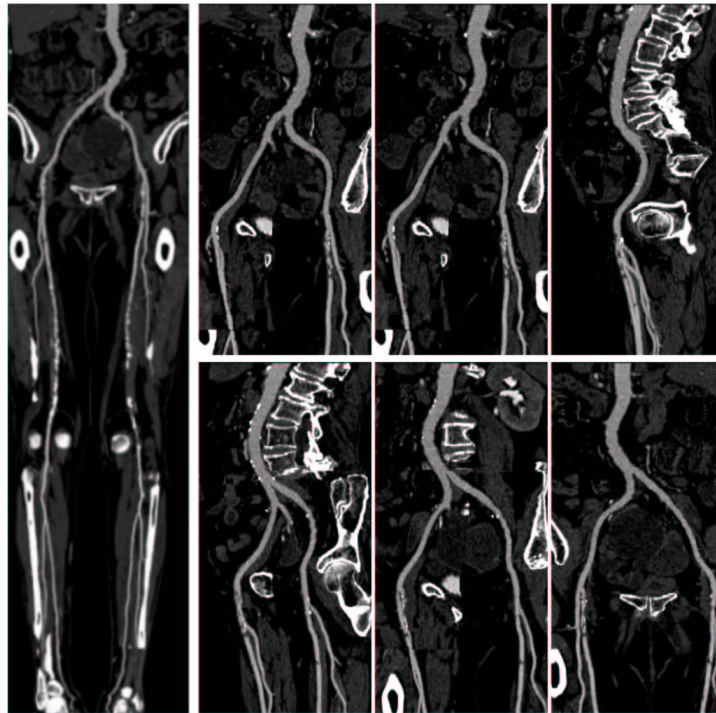


Figure 3.13: Overview of a projected multi-path CPR at 0° . Enlargement of the projected multi-path CPRs at 30° , 60° , 90° , 120° , 150° , 180° .

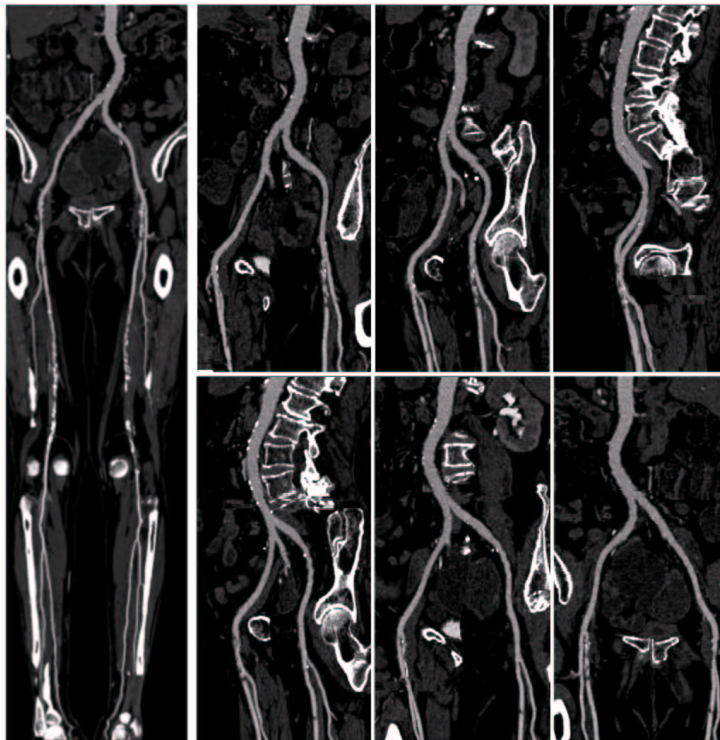


Figure 3.14: Overview of a stretched multi-path CPR at 0° . Enlargements of the stretched multi-path CPRs at 30° , 60° , 90° , 120° , 150° , 180° .

3.6 Conclusions and Discussion

In this paper methods for the generation of *Curved Planar Reformation* (CPR) images have been presented. This method allows the visualization of entire tubular structures with minimal modification of the original data. The main application of this visualization method is *Computed Tomography Angiography* (CTA). CPR provides the possibility to visualize the interior of vascular structures (i.e., the lumen of the vessel). Direct volume rendering approaches and surface shaded display methods only provide the possibility to inspect the surface of vascular structures. With volume rendering even mild vessel wall calcifications may obscure the true vessel lumen (flow channel), which is the clinically relevant information. In this case the diagnostically relevant information needs to be supplemented by browsing through the original cross-sectional images, which is impractical for large data sets. Diagnostic relevant information in this case is provided by axial slicing through the data, which is tedious for large data sets, or by CPR images.

Three different methods (i.e., projected, stretched, and straightened CPR) have been demonstrated. A comparison of the three methods with respect to spatial perception, isometry, and possible occlusions has shown that the stretched CPR is the preferred method for many applications.

Targeting the drawbacks of visualizing tubular structures using CPRs three enhancements to the basic methods have been introduced. The generalization of the re-sampled slice to a thick slab of voxels improves the image quality of thin structures. In daily practice the MIP re-sampling strategy was found out to be the most appropriate.

The rotating CPR significantly improves the quality of vessel investigation and we speculate that it substantially adds to diagnostic confidence. Interactivity is a main property of this improvement. The performance of this image based rendering technique mainly depends on the display size. The length of central axis has impact on the performance as each point has to be transformed. Finally the volume contributes to the rendering time due to the limited memory bandwidth. Yet all operations are linear thus the overall complexity is linear. The current implementation in Java on a PC workstation with an Intel PIII 1GHz main processor renders 9.8 frames per second of the real-world data set in a 557x523 image using the stretched CPR method for the path shown in Figure 3.6.

As fewer images have to be generated and as the spatial relationships of the vascular tree are well preserved, we believe that multi-path CPRs are not only very well suited for diagnostic purposes, but also for the documentation and for communicating the extent of diseases to the treating physician.

Chapter 4

Advanced Curved Planar Reformation: Flattening of Vascular Structures

This chapter is based on the following publications:

Kanitsar A., Wegenkittl R., Fleischmann D., Gröller M. E.: Advanced Curved Planar Reformation: Flattening of Vascular Structures. *In Proceedings of IEEE Visualization 2003*, pages 45-50, October 2003.

Kanitsar A., Wegenkittl R., Fleischmann D., Gröller M. E.: Advanced Curved Planar Reformation: Flattening of Vascular Structures. Technical Report TR-186-2-03-08, Institute of Computer Graphics and Algorithms, Vienna University of Technology. April 2003.

*Not only is there but one way of doing things rightly,
but there is only one way of seeing them,
and that is, seeing the whole of them.*
— John Ruskin

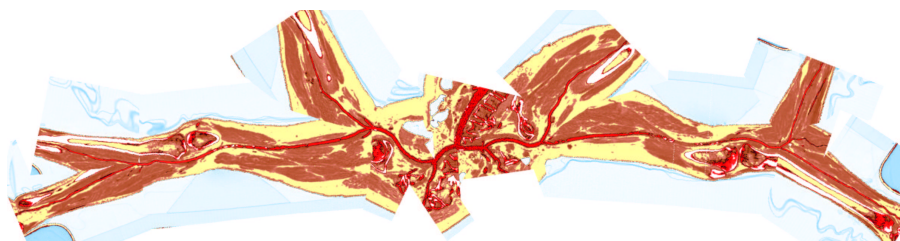


Figure 4.1: An untangled vascular tree of the peripheral arteries.

4.1 Introduction

Non-invasive imaging of the vascular system with computed tomography (CT) and magnetic resonance imaging (MRI) has become a well established alternative to invasive intraarterial angiography. CT and MRI provide high-resolution volumetric datasets of the human body. These data, however, may contain many objects of less or no diagnostic interest. This makes volume-rendering (i.e., Maximum Intensity Projection (MIP), ray casting, shaded surface display) without preprocessing often impossible or inaccurate.

CPR - Curved Planar Reformation is a way to visualize vascular structures with small diameter. High level information as the vessel's centerline is used to re-sample and visualize the data. By this technique the entire tubular structure is displayed within a single image. Vascular abnormalities (i.e., stenoses, occlusions, aneurysms, and vessel wall calcifications) are then investigated.

Current CPR techniques allow the investigation of the vessel lumen in a longitudinal section through the central axis of the vessel. However, vascular abnormalities might not be touched by this plane and therefore they do not appear in the generated image. One way to overcome this problem is to rotate the re-sampled plane around the central axis. This results in a set of images to be interpreted by the radiologist. A more comprehensive display of the entire vascular lumen in one representative image is highly desirable. A new visualization method was developed to overcome this limitation.

Another important aspect in *computed tomography angiography* (CTA) is the efficient visualization of treelike vascular structures using CPR display techniques. Multi-path CPR techniques based on a projective combination of vessel segments provide a spatially coherent display of the vascular anatomy. Depending on the intersecting plane, parts of the arteries might be superimposed by

other arteries. For a detailed inspection of the entire vascular tree different sections through the vessel's central axis have to be re-sampled. In order to have diagnostically valuable results the vessel lumen should be visible within each image. Thus a new technique for unobstructed displaying of an arterial tree is proposed.

Section 4.2 describes related work in this area. In Section 4.3 a new method for visualizing the interior of a vascular structure is presented. A technique for displaying the entire vascular tree without overlapping arteries is presented in Section 4.4. Possible improvements and conclusions are discussed in Section 4.5.

4.2 Related Work

The most important prerequisite for CPR visualization is an appropriate estimation of the vessel centerline. Latest CT technology, such as multiple detector-array CT, provide high resolution volumetric datasets. Due to the large size of these datasets (up to 1500 transverse cross-sectional images of the abdomen and entire legs), the manual definition of the vessel centerline is no longer an option. In this respect several algorithms [31, 61, 64] have been developed with different properties concerning reliability, speed and accuracy.

Avants and Williams presented a vessel tracking method consisting of two parts [3]. From user defined seed points a surface expansion is computed based on the eikonal partial differential equation. A minimal cost path is calculated from these regions. From this path a cross-sectional area/radius profile is generated.

He et al. [23] proposed a path extraction method based on a two-dimensional region-growing algorithm with a subsequent shortest path algorithm. The resulting path was refined using the multi-scale medial response. The vascular tree is flattened in a semi-automatic method called *Medial Axis Reformation*.

Some authors propose to take the central axis as an input for the generation of an abstract vessel model. Abstract vessel models allow fast rendering, as polygonal meshes of low complexity are generated [14]. Furthermore non-photorealistic rendering provides the possibility to emphasize global properties of the vascular tree [22].

In Section 3 three methods for CPR generation were compared: Projected CPR, stretched CPR, and straightened CPR. In addition three extensions to CPR have been proposed to overcome the most relevant clinical limitations: thick CPR, rotating CPR, and multi-path CPR. The latter provides a display of an entire vascular tree within one image. While superimposition of bones and arteries is prevented, the intersection of arteries itself is not avoided [30].

Further information about the clinical relevance of the CPR visualization technique can be found in [1, 33, 50].

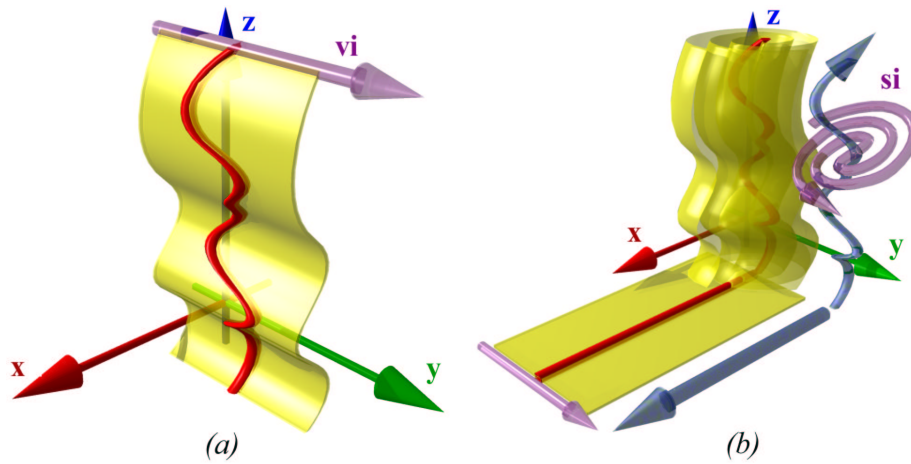


Figure 4.2: Traditional CPR (a), and helical CPR (b) generation.

4.3 Helical CPR

The basic idea of helical CPR visualization is to display the volumetric interior of a vessel within one image. To accomplish this, a re-sampling strategy different from existing CPR methods is introduced. CPR techniques display re-sampled data in close vicinity of a surface intersecting the volume. This surface is defined by the central axis of the vessel and a *vector-of-interest* (vi) (see Figure 4.2a). The latter might be defined in a local coordinate system of the central axis. In any case the data are re-sampled in a linear way defined by the vector vi . The vector-of-interest describes the re-sampling direction which is in some cases orthogonal to the viewing direction.

The helical CPR method is based on a non-linear re-sampling of the data. The vector-of-interest as generating element for the surface is replaced by a *spiral-of-interest* (si) (see Figure 4.2b). This results in a convoluted surface around the central axis. At a sufficiently small distance between each winding the vessel is intersected several times. Stenoses, calcifications, and occlusions are included in the computed surface. The helical surface is flattened and displayed.

4.3.1 Method Description

Similar to the straightened CPR a local coordinate system is used for re-sampling the data. Along the central axis of the vessel cross-sections are calculated at an appropriate sampling distance. Within each section a local 2D coordinate system is defined. The center of the cross-section represents the estimated center of the vessel lumen at the corresponding centerline position. Starting from this center point two interleaved spirals s_1 and s_2 are computed

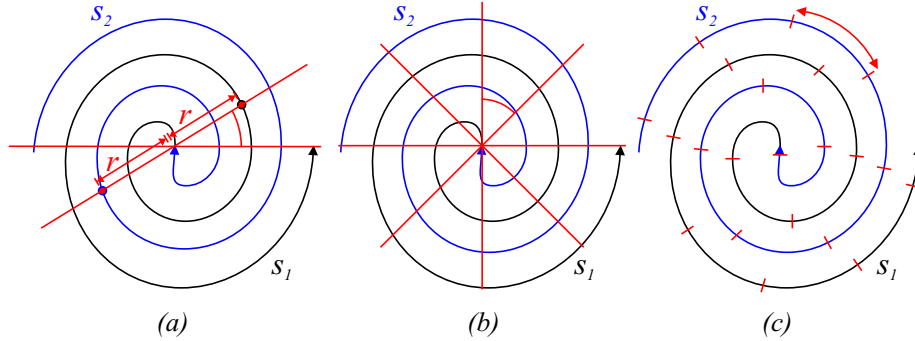


Figure 4.3: Spiral-of-interest s_i (a), constant angle sampling (b), constant arc-length sampling (c)

(see Figure 4.3a). In order to maintain a uniform sampling of the vessel cross-sections a spiral with constant inter-winding distance was selected. This requirement is satisfied by the Archimedean spiral which can be expressed in a simple equation using polar coordinates r and θ :

$$r = a\theta \quad (4.1)$$

The transformation of points on the curve into Cartesian coordinates is straightforward. Thus the computation of a point X_{s_1} on s_1 and a point X_{s_2} on s_2 is performed as follows:

$$X_{s_1} = a\theta \begin{pmatrix} \cos \theta \\ \sin \theta \end{pmatrix} \quad X_{s_2} = a\theta \begin{pmatrix} \cos \theta' \\ \sin \theta' \end{pmatrix} \quad \text{where } \theta' = \theta + \pi \quad (4.2)$$

For an appropriate sampling of the vessel lumen the parameter a was set to $1/\pi$. This assures a constant distance of one between the windings of the two interleaved spirals. The computed points X_{s_1} and X_{s_2} on the spiral are transformed back into volume space and re-sampled.

The center of each scanline in the final CPR image corresponds to the center of the vessel cross-section. Starting from this reference point the image space to the left is filled with data re-sampled by s_1 and to the right with data from s_2 . Thus the vessel central axis is centered in image space similar to the stretched CPR method.

4.3.2 Sampling Strategy

The current implementation of the helical CPR technique supports two sampling strategies for computing points from the spiral. In the case of *constant angle* sampling (see Figure 4.3b) the angle θ is increased by a constant angle ω for each point. If *constant arc-length* sampling is applied (see Figure 4.3c) for each sampling step a constant distance Δ on the arc-length of the spiral is covered.

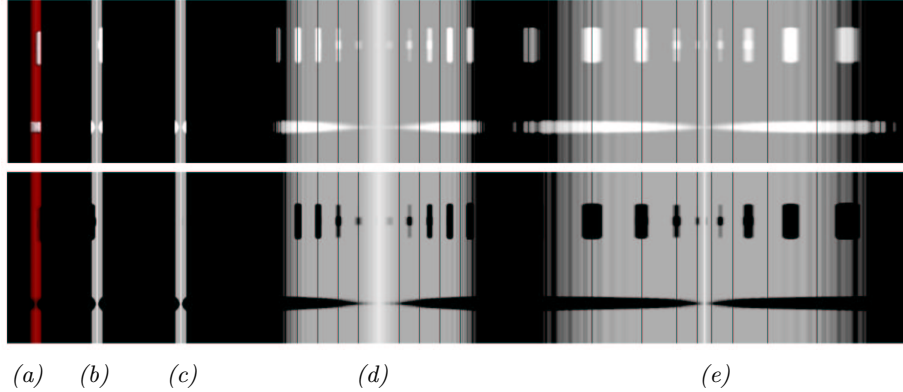


Figure 4.4: Phantom dataset: Direct volume rendering (a); Coronal (b) and sagittal (c) straightened CPR; helical CPR with constant angle (d) and constant arc-length (e).

Constant angle. For each point re-sampled from the spiral the generating angle θ is incremented by a fixed angle ω . Each winding is rendered into an equal sized area in the final image. Therefore the comparably dense sampled area in close vicinity of the vessel center is amplified in image space. The resulting fish-eye zooming effect is achieved at the cost of increased distortion.

Constant arc-length. Constant arc-length sampling means that adjacent sample points along the spirals are a constant length Δ apart. Given a fixed sampling distance Δ between two adjacent points on the spiral the increment ω of the angle θ is approximated. The increment ω is defined by the ratio of Δ and the circumference calculated from the most recent radius. As usually small sampling distances are used and the error introduced by this approximation is negligible. The extent of the vessel in the CPR image is directly proportional to the volume of the vessel lumen. Thus large vessels occupy a superproportional large part of the image space.

4.3.3 Phantom Dataset

The images generated by helical CPR visualization provide a quite unconventional display of vascular structures. Therefore a phantom dataset containing a set of typical vascular abnormalities was computed. By means of this dataset the typical patterns of each anatomical case are demonstrated (see Figure 4.4).

The simulated vessel of the phantom dataset contains a semi-circumferential vessel wall calcification, and a circumferential vessel wall calcification without luminal occlusion. An eccentric "soft-plaque" stenosis and a segmental concentric high-grade stenosis was also simulated, respectively (top-down order). Figure 4.4a shows a direct volume rendering display of this simulated vessel.

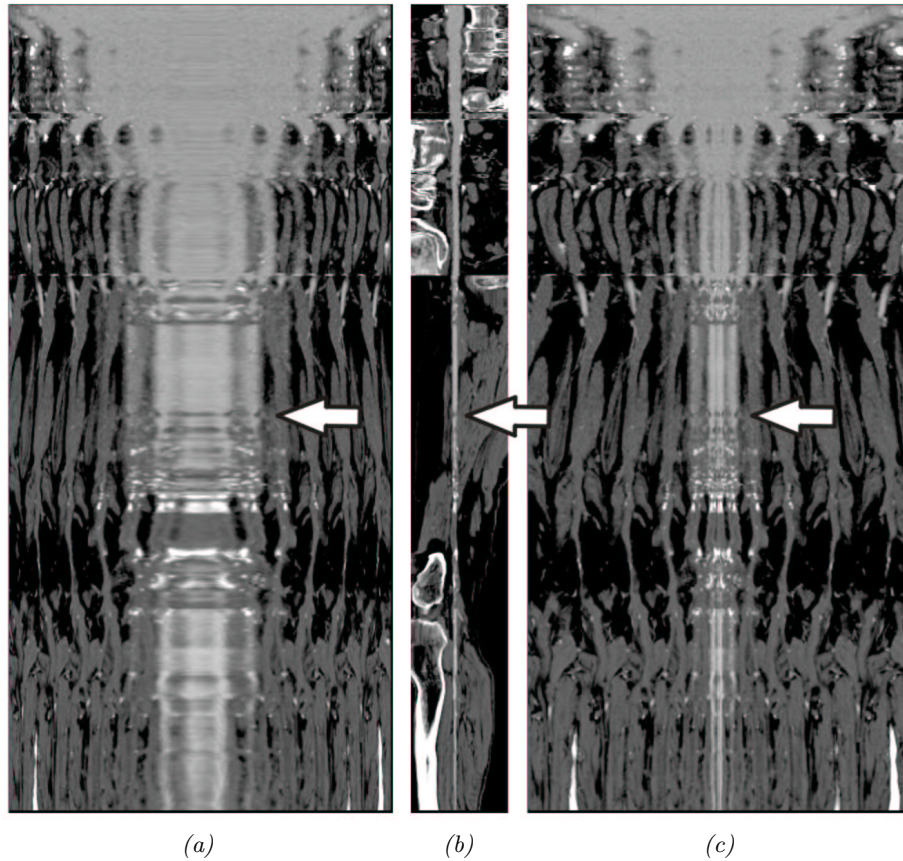


Figure 4.5: A helical CPR with constant angle sampling (a), a straightened CPR (b), and constant arc-length sampled helical CPR (c) of a real world dataset.

From this visualization method the flow channel within the circular vessel wall calcification can not be gauged. A coronal and sagittal straightened CPR is presented in Figure 4.4b and c. The partial vessel wall calcification as well as the eccentric stenosis are not visible in the sagittal straightened CPR. This demonstrates the need for different longitudinal sections. Figure 4.4d and e show the result of the helical CPR technique with constant arc-length and constant angle sampling. The vertical lines indicate the image space required for one winding. Partial vessel abnormalities tend to reoccur in a separated fashion several times in the image whenever the area is intersected by a winding. Vessel pathologies clearly stand out in the helical CPR images. The helical CPR "peels-off" the blood vessel. Thus the extent of abnormalities is enhanced.

4.3.4 Results

The application of a helical CPR technique on a real world dataset is presented in Figure 4.5. A constant angle and constant arc-length sampled helical CPR is compared to a straightened CPR image. In contrast to the straightened CPR the helical CPR shows the area of the vessel lumen instead of the diameter. The white arrow illustrates an example where the helical CPR outperforms a traditional CPR. The small flow-channel of the stenosis is not touched by the displayed longitudinal section of the straightened CPR and therefore not visible. However in both helical images this flow-channel is displayed. As eccentric lesions cause repetitive patterns in the image space, the attention of the observer is immediately drawn to those areas even if a lesion is not visible in a standard CPR display.

4.4 Untangled CPR

The aim of untangled CPR visualization is to display a vascular tree without overlapping arteries. This is independent from the spatial position of the intersecting plane. In order to accomplish this requirement the spatial relations of the projected vessels have to be relaxed. Branching points of the vessel tree are used as pivot points. Rotating the corresponding vessels around these pivot points in image space eliminates vessel overlaps. Keeping the introduced distortions small maintains fast perception and reduces the impact of re-sampling artifacts in the final image. Thus the applied transformations are restricted to the branching points (bifurcations) of the arterial tree. In addition to that this transformations should be appropriate in terms of changing the tree layout and appearance without violating the non-intersection criterion. The *non-intersection criterion* is defined in a way that two vessel hulls must not intersect at any time. A vessel hull is a wedge-shaped circle sector in 2D which encloses parts of a vessel tree. It is typically anchored at the bifurcation points.

The new CPR technique is based on the stretched CPR and the multi-path CPR enhancement introduced by Kanitsar et. al. [30] and described in Section 3. This method maintains the curvature of the vessel to a high extent and preserves isometry. The vessel's curvature is crucial in approximating a geometrically undistorted appearance of the vessel tree. Isometry on the other hand is important for vascular investigations. Stent planning and stenosis-grading estimation are possible in the final image.

The input of the algorithm is a tree graph representing the topology of the vascular structure. For each vessel segment the centerline of the vessel is stored as a set of adjacent points at an appropriate sampling distance. In practice it turned out that diameter estimations of vessels are not reliable enough in certain cases. Therefore for the purpose of generality the algorithm does not take diameter information into account. However, the adaptation to this additional information would be straightforward.

4.4.1 Method outline

The untangling CPR method consists of four main steps. As all untangling calculations are performed in image space the tree graph is first mapped to image space using a stretched CPR projection. In a consecutive step the transformation of each subtree with respect to the non-intersection criterion is performed. Afterwards the image space is partitioned in a way that each vessel obtains those parts of the image space which are closest in scanline direction. Finally the image is rendered.

Tree projection. The vascular tree is mapped to a projection plane coplanar to the viewing plane. For each two successive points on a vessel path the subsequent point is rotated around an axis defined by the previous point and the vector-of-interest. The rotation is carried out for each point starting from the root of the vascular tree. The result is a stretched vascular tree (see Section 3.5.3).

Untangling operation. From the projected tree graph in image space the necessary transformations for each node are calculated. This is done by recursively circumscribing the subtrees with vessel hulls. The first pass is bottom up maintaining only the correct transformation of the largest enclosing vessel hull. In a second pass the final transformation for each vessel hull segment is accumulated top down.

Image space partitioning. Before rendering the final image the extent of each vessel segment is cropped in a way that no overlapping image areas remain. This process determines the starting point and the end point of each scanline for rendering.

Rendering. Each vessel strip is rendered separately. Conceptually the vessel strip is first extracted from the dataset using a stretched CPR mapping. Afterwards the strip is transformed to the position defined by the untangling process. In a further step the strip is clipped according to the space partitioning information. Finally each cropped scanline is rendered into the image.

4.4.2 The vessel hull primitive

The *vessel hull* is the basic primitive for further intersection tests. It encloses the vessel's centerline in image space as shown in Figure 4.6. The centerline is given as a set of points $P = \{P_0..P_{n-1}\}$. A vessel hull is a circle sector. The root of a vascular subtree defines the center point H_{center} . A matrix $\mathfrak{R}_{H_{center}}$ associated with each center point describes a rotational transformation of the subsequent tree. The points H'_{right} and H'_{left} result from a conservative estimation of the leftmost and rightmost extent of the enclosing subtree seen from the center point.

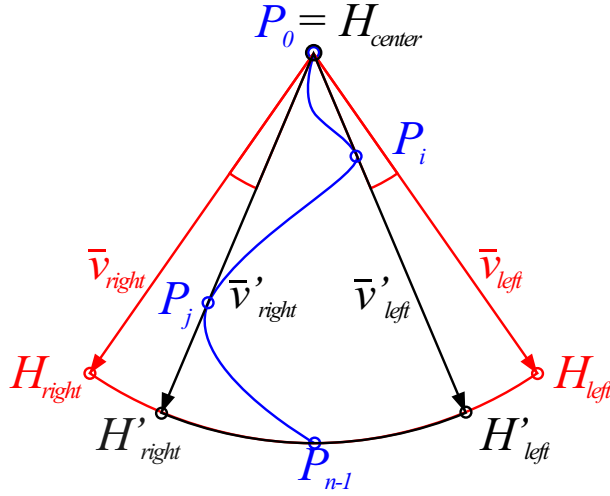


Figure 4.6: The vessel hull primitive

The vessel hull encloses just the centerline of the vessel, but not the vessel itself, thus two neighboring vessels touching each other is not prevented by this primitive. To overcome this situation the vessel hull is enlarged by a small angle ϵ as depicted in Figure 4.6. Depending on the size of the inspected vessels ϵ may be adjusted by the user on the fly. However an $\epsilon \leq 2^\circ$ was found to be appropriate for most tested datasets. If the vessel diameter is known at the extremal points P_i and P_j then ϵ can be easily calculated more accurately. The points comprising the ϵ -tolerance are referred to as H_{right} and H_{left} .

Each vessel hull primitive is described as a tuple of $V = \{H_{center}, H_{left}, H_{right}, \Re_{H_{center}}\}$ where $\vec{v}_{left} = \overrightarrow{H_{center}H_{left}}$ and $\vec{v}_{right} = \overrightarrow{H_{center}H_{right}}$.

4.4.3 Putting things together

A rule based approach is applied for combining vessel hulls from various parts of the vascular tree (see Figure 4.8). The projected vessel tree is approximated by an enclosing hierarchy of vessel hulls. This hierarchy is constructed bottom up. Combining two vessel hulls at a branching point involves a rotation around the common pivot point H_{center} . This results in a new larger hull which bounds the entire subtree. Constructing the vessel hull hierarchy involves several cases which are discussed in the following. A vessel hull created from the vessel centerline is based on *case 1*. Neighboring vessel hulls are combined according to *case 2*. An enclosing vessel hull from two consecutive vessel hulls is created in *case 3*. The assembling process is done bottom up. This results in a binary tree of vessel hulls where each node is represented by a vessel hull circumscribing all subjacent vessel hulls.

Case 1:

$$\begin{aligned}
H_{center} &\leftarrow P_0 \\
\vec{v}_{right} &\leftarrow P_j - H_{center}, \{P_j | P_j, \ell \in P \wedge \forall \ell (\ell \text{ left of } \overrightarrow{H_{center}P_j})\} \\
\vec{v}_{left} &\leftarrow P_i - H_{center}, \{P_i | P_i, \ell \in P \wedge \forall \ell (\ell \text{ right of } \overrightarrow{H_{center}P_i})\} \\
rad &\leftarrow |P_{n-1} - P_0| \\
H_{right} &\leftarrow H_{center} + rad \cdot (\Re_{\epsilon} \star \vec{v}_{right} / |\vec{v}_{right}|) \\
H_{left} &\leftarrow H_{center} + rad \cdot (\Re_{-\epsilon} \star \vec{v}_{left} / |\vec{v}_{left}|)
\end{aligned}$$

Case 2:

$$\begin{aligned}
H_{center} &\leftarrow H_{center}^1 \\
(V^l, V^r) &\leftarrow \text{if (changeOrder) then } (V^2, V^1) \text{ else } (V^1, V^2) \\
\Re_{H_{center}^r} &\leftarrow \text{RotationMatrix}(H_{center}, -0.5 \max(\angle(\vec{v}_{left}^r, \vec{v}_{right}^l), 0)) \\
\Re_{H_{center}^l} &\leftarrow \text{RotationMatrix}(H_{center}, +0.5 \max(\angle(\vec{v}_{left}^r, \vec{v}_{right}^l), 0)) \\
\vec{v}_{right} &\leftarrow \vec{v}_{right}^r \\
\vec{v}_{left} &\leftarrow \vec{v}_{left}^l \\
rad &\leftarrow \max(rad^l, rad^r) \\
H_{right} &\leftarrow H_{center} + rad \cdot (\Re_{H_{right}} \star \vec{v}_{right} / |\vec{v}_{right}|) \\
H_{left} &\leftarrow H_{center} + rad \cdot (\Re_{H_{left}} \star \vec{v}_{left} / |\vec{v}_{left}|)
\end{aligned}$$

Case 3:

$$\begin{aligned}
H_{center} &\leftarrow H_{center}^1 \\
\vec{v}_{right} &\leftarrow \text{if } (H_{right}^2 \text{ left of } \overrightarrow{H_{center}H_{right}^1}) \\
&\quad \text{then } H_{right}^1 - H_{center} \text{ else } H_{right}^2 - H_{center} \\
\vec{v}_{left} &\leftarrow \text{if } (H_{left}^2 \text{ right of } \overrightarrow{H_{center}H_{left}^1}) \\
&\quad \text{then } H_{left}^1 - H_{center} \text{ else } H_{left}^2 - H_{center} \\
rad &\leftarrow \max(rad^l, |H_{center} - H_{right}^2|, |H_{center} - H_{left}^2|) \\
H_{right} &\leftarrow H_{center} + rad \cdot \vec{v}_{right} / |\vec{v}_{right}| \\
H_{left} &\leftarrow H_{center} + rad \cdot \vec{v}_{left} / |\vec{v}_{left}|
\end{aligned}$$

Figure 4.7: Assembling of vessel hulls.

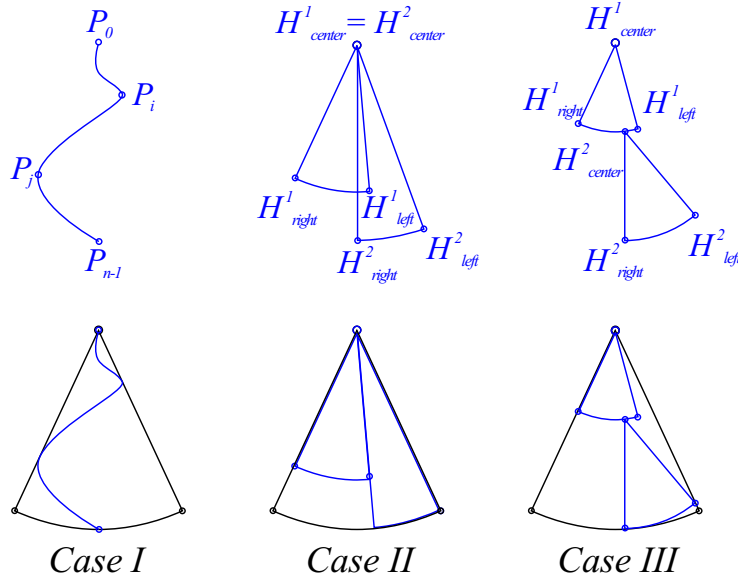


Figure 4.8: The cases for combining vessel hulls.

Case 1. The center point H_{center} is defined by the first point P_0 of the vessel segment. The first point on the convex hull of the vessel segment in clockwise orientation is denominated as point P_i and in counterclockwise direction as point P_j . Because of the stretched CPR mapping from volume to image space, point P_{n-1} is the point with maximum distance from P_0 . Thus the radius of the vessel hull is computed as $|P_{n-1} - P_0|$. The vectors \vec{v}_{left} and \vec{v}_{right} represent the directions from H_{center} to P_i and P_j respectively. These vectors are scaled according to the radius of the vessel hull. The tolerance angle ϵ is incorporated by a transformation with \mathfrak{R}_ϵ and $\mathfrak{R}_{-\epsilon}$. Finally H_{right} and H_{left} are computed.

Case 2. For the case of two adjacent vessel hull primitives (V^1 and V^2) (see Figure 4.8) the ordering of the subtrees has to be determined first. According to this decision the left vessel hull with respect to $H_{center} = H^1_{center} = H^2_{center}$ is denominated as V^l and the right one as V^r . If the vessel hull primitives overlap, an untangling angle γ is computed from \vec{v}_{left}^r and \vec{v}_{right}^l (see Figure 4.9). From this angle the rotational matrices $\mathfrak{R}_{H_{center}^r}$ and $\mathfrak{R}_{H_{center}^l}$ are calculated. These matrices define a transformation of the vessel hull primitives V^r and V^l in a way that the primitives do not overlap anymore. More precisely they describe the rotations of $\gamma/2$ and $-\gamma/2$ respectively. This implies a transformation of the associated vascular subtree (see Figure 4.9a). If the vessel hull primitives do not overlap the matrices are simply the identity matrices.

The vectors \vec{v}_{left} and \vec{v}_{right} of the combined vessel hull are computed from the transformed vectors \vec{v}_{left}^l and \vec{v}_{right}^r . The radius of the enclosing vessel

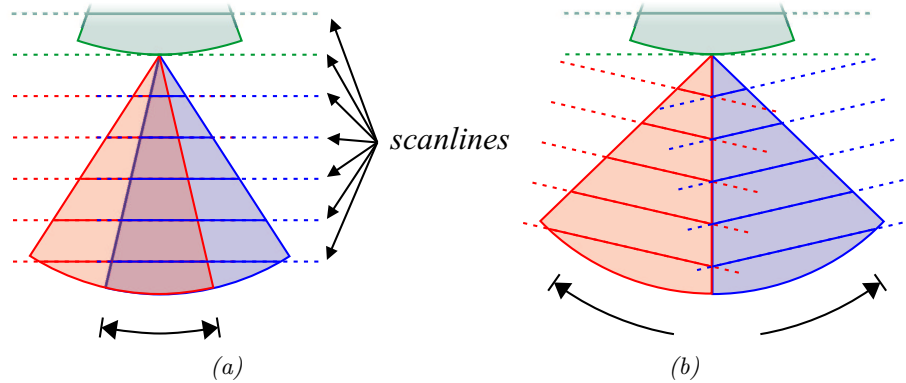


Figure 4.9: Image space partitioning

hull is defined by the maximal radius of V^1 and V^2 . From this information H_{left} and H_{right} is computed. The newly generated vessel hull encloses the non-overlapping underlying vessel hulls.

Case 3. The combination of two successive vessel hulls is straightforward. V^1 is considered to be the predecessor of V^2 as depicted in Figure 4.8. H_{center}^1 is taken as the new center point H_{center} of the enclosing vessel hull. The direction to the rightmost point of H_{right}^1 and H_{right}^2 with respect to H_{center} is considered to be \vec{v}_{right} . Vector \vec{v}_{left} is calculated likewise. The radius of the new vessel hull V is defined by the maximum distance from H_{center} to H_{right}^1 , H_{left}^1 , H_{right}^2 , and H_{left}^2 .

Case 3 is similar to the 2^{nd} case. However no additional transformation is introduced during this step since undersampled areas would occur under these circumstances (see Figure 4.10).

Any treelike vascular structure can be processed using this set of rules. One bifurcation for instance is subdivided into three *cases 1*, one *case 2* and, one *case 3*. The recursion follows a bottom up approach. First each vessel segment distal from one of the bottom most bifurcation is enclosed by a vessel hull using *case 1*. This step results in two adjacent vessel hulls connected at the branching point. According to *case 2* these vessel hulls are combined and possible overlapping areas are resolved. The preceding vessel segment in respect to the bifurcation is covered by a vessel hull following the rules of *case 1*. In a succeeding step the two vessel hulls connected at the bifurcation are combined using *case 3*.

The recursive algorithm finishes with a hierarchy of enclosing vessel hulls where the root hull contains the entire vessel tree. A detailed description of each assembling case in abstract notation is given in Figure 4.7.

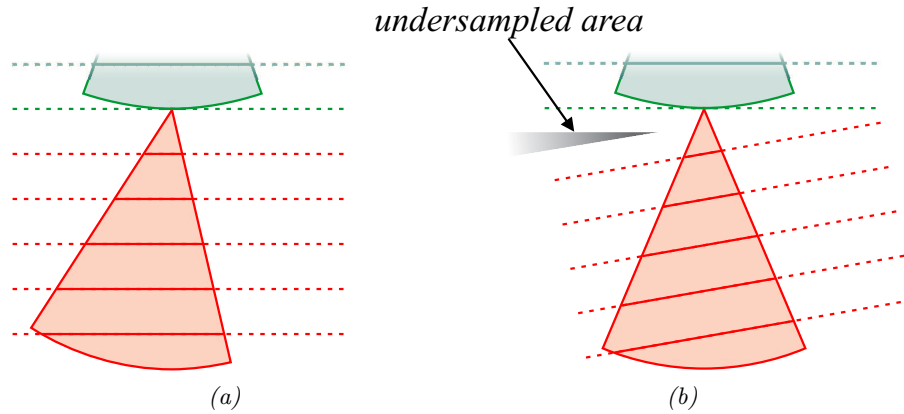


Figure 4.10: Undersampled area

4.4.4 Layout definition

The decision of the vessel hull ordering in *case 2* has a significant impact on the layout of the displayed vascular tree. Two different approaches have been investigated (see Figure 4.11). One possibility is a left-to-right ordering based on the spatial relations of the vascular tree according to the currently used viewing direction. In this case the ordering is based on the spatial location of the vessel hulls according to the current viewing direction. This approach is referred to as *adaptive layout*. In contrast to that a *fixed layout* was investigated, too. The fixed layout is independent from the viewing direction. The ordering of the vessel segments is defined once and remain the same for all viewing angles. In the present prototype implementation the vessel ordering of the coronal display is maintained for all viewing directions. For clinical routine applications a standardized ordering might be a reasonable solution. According to this standardization the leftmost artery for peripheral CTA examinations might be the left deep femoral artery (*profunda femoris*) followed by the left anterior tibial artery and so on.

The advantage of an adaptive tree layout is a more efficient utilization of image space. Less distortion is introduced by the untangling operation compared to a fixed layout. The introduced distortion measured by the sum of untangling angles γ over a 360° rotation of a peripheral CTA dataset is depicted in Figure 4.12. However, in the case of an adaptive tree layout discontinuities occur whenever the order of the vessels changes. Thus the inspection of a sequence of images becomes more difficult as the identification of each vascular segment becomes more difficult. Labelling the vessel segments eases this limitation for examinations carried out on a set of images.

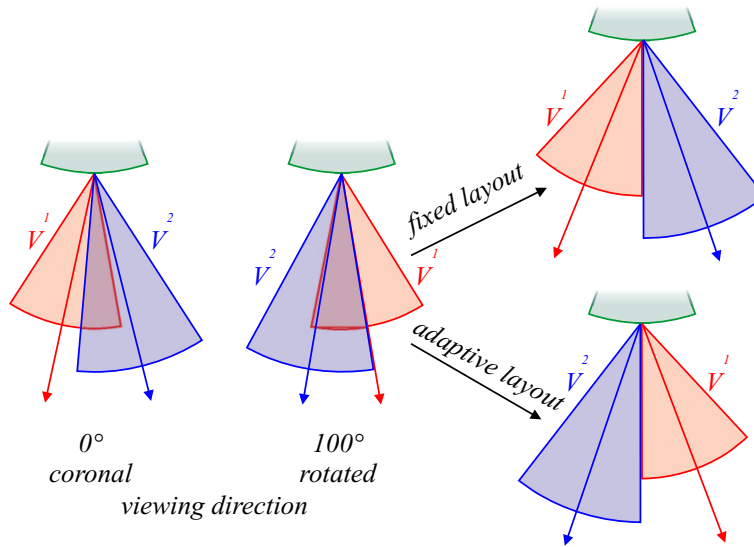


Figure 4.11: Different layout definition

4.4.5 Image space partitioning

Before rendering the final image the image space has to be partitioned into fragments for each vascular structure. This step is necessary because arteries are possibly obscured by bones if multiple layers are rendered into a single image area [30].

A principle drawing direction is associated with each vessel segment. Each point of the projected vessel centerline maintains a scanline deduced from this principal drawing direction. These scanlines are transformed according to the rotational matrix $\mathfrak{R}_{H_{center}}$ (see Figure 4.9). The scanlines represent those parts of the image into which the corresponding re-sampled are rendered. Because of the applied transformations the scanlines need not be aligned to the pixel rows of the image.

In order to avoid overlapping areas an appropriate start and endpoint for each scanline has to be determined. For this reason a special sort of distance map is created every time an image is rendered. This distance map is defined by the projected centerlines of the vessel tree and its scanlines. In contrast to the traditional distance map the distance metric is not defined by an Euclidean distance but by a distance along scanlines. The result of this operation is a fragmented image space where each vessel segment is assigned a maximal image area.

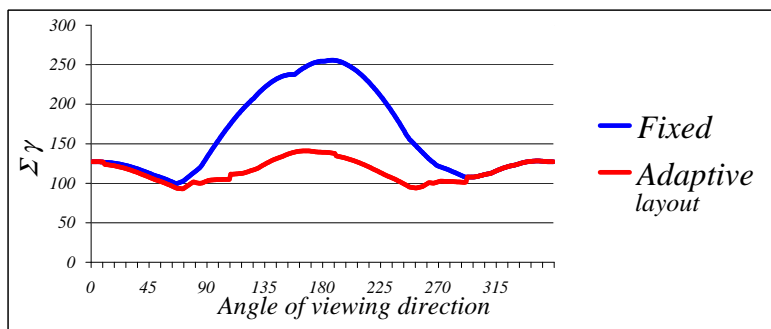


Figure 4.12: Comparison of introduced distortion: fixed versus adaptive layout.

4.4.6 Results

A comparison of a stretched multi-path CPR and an untangled CPR is presented in Figure 4.13. In an anterior view the results of the compared methods are rather similar, because there are only few overlapping arteries. In the case of a lateral view the multi-path CPR display provides hardly any diagnostically relevant information. Many superimposed arteries obscure each other. In comparison to that the untangled CPR still provides an unobstructed view of the entire vascular tree. Each vessel segment is displayed in diagnostic quality. For instance the stenosis, heavy calcification, and a long occlusion in the left superficial femoral artery is clearly visible. For both untangled CPRs a fixed layout was used.

Figure 4.14 presents a sequence of untangled CPR images from an abdominal CT-angiographic dataset. A fixed layout was used. A 1D transfer function was applied to the re-sampled data approximating the tissue color of the anatomical structures. The abdominal aorta is the main vessel in the upper half of the image. It is branching into the left and right iliac (pelvic) arteries where left and right in the image is interchanged due to the patient orientation. The pelvic artery branches into the thicker external pelvic artery and the thinner inner pelvic artery. Areas of arterial wall calcification are shown in the distal abdominal aorta (225°) and in the left internal pelvic artery (270°).

Even though the examination is intended to be done on a small set of pre-computed images, the performance of the algorithm is acceptable for applications in the clinical workflow. The displayed untangled CPR image in Figure 4.13 was calculated from a real world dataset with a scanned resolution of 512x512x988 voxels and an original image size of 1164x1097 pixel. The average rendering time per image of the current Java based implementation on a PC workstation with an Intel PIII 1GHz main processor took 2.3 seconds. Figure 4.1 presents an untangled CPR of this dataset using manual layout demonstrating the flexibility of this method.



Figure 4.13: A peripheral CTA dataset rendered from a coronal and a sagittal view using stretched multi-path CPR (a, c) and untangled CPR with fixed layout (b, d) respectively.

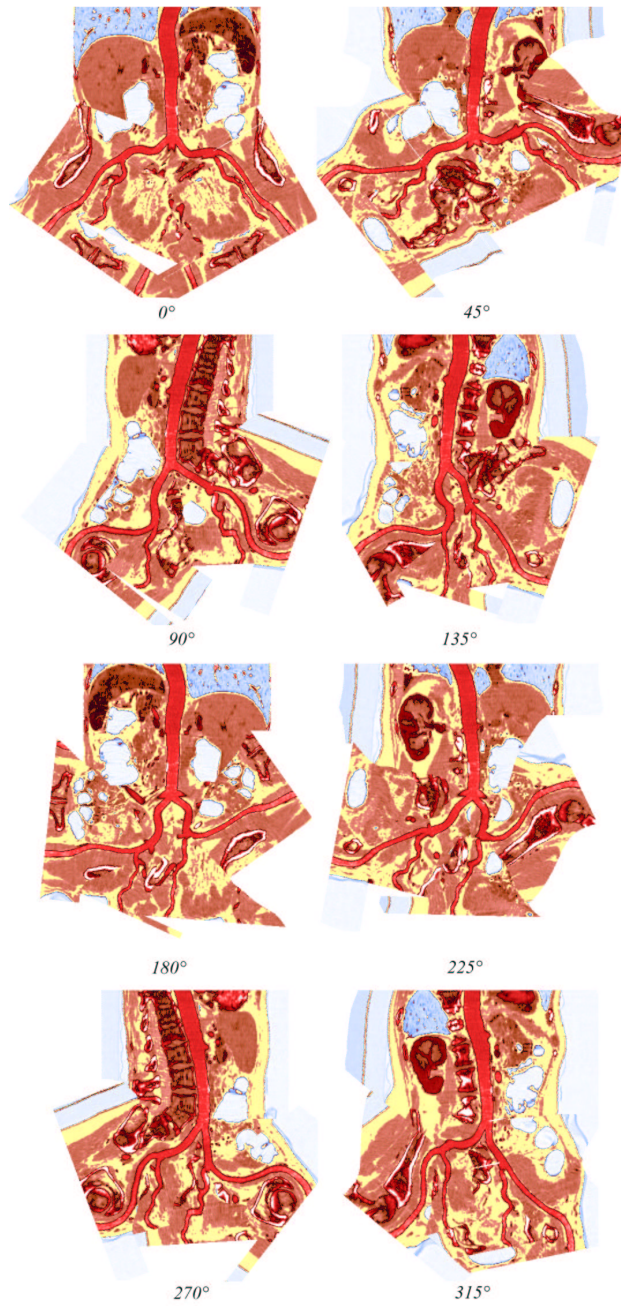


Figure 4.14: A colored sequence of untangled CPR images from different viewing directions.

4.5 Conclusions and Discussion

Two methods for efficient vessel visualization were proposed. In both methods the spatial coherence of the investigated objects is relaxed to a certain degree. With the helical CPR the dataset is re-sampled in a spiral manner making the entire vessel visible. Small distortions of the vascular tree prevent self-intersections in the case of the untangled CPR.

The helical CPR technique is a new way to display the volume of vascular structures. The motivation for this visualization technique was not an imitation of the natural appearance of the object but the revelation of diseased vessel segments. Helical CPR visualizes the interior of a vessel in a single image. Re-sampling a spiral around the vessel central axis does not involve any compositing of samples. Therefore no features of the vessel are hidden by other structures as long as the vessel area is sampled densely enough. An explorative study has shown that the detection of vessel abnormalities is possible from such visualizations which literally peel-off the vessel volume. A particularly attractive future application of this technique is visualization of coronary artery diseases from recently developed electrocardiographically gated CT.

The untangled CPR has significant advantages over existing multi-path CPR techniques. This new technique produces an unobscured display of a vascular tree, independent of the viewing direction. Small rotations around the branching points of a vessel tree eliminate occlusions. Therefore the size of the introduced distortion is kept small.

Even though the usage of image space is not optimal, the main requirement for an unobscured display of vessels from any viewing direction is fulfilled. In addition, untangled CPR preserves isometry which is an important requirement for vascular lesion assessment. The potential for clinical application of this technique is obvious: A more efficient way to assess any complex arterial trees for the presence and extent of vascular disease. Clinical validity and applicability to other vascular territories are currently investigated.

Chapter 5

Computed Tomography as a Tool for Mastering Complex Real World Objects with Applications in Computer Graphics

This chapter is based on the following publications:

Kanitsar A., Theussl T., Mroz L., Sramek M., Vilanova Bartroli A., Csébfalvi B., Hladuvka J., Guthe S., Knapp M., Wegenkittl R., Felkel P., Roettger S., Fleischmann D., Purgathofer W., Gröller M. E.: Christmas Tree Case Study: Computed Tomography as a Tool for Mastering Complex Real World Objects with Applications in Computer Graphics. *In Proceedings of IEEE Visualization 2002*, pages 489-492, October 2002. (**best case study award**)

Kanitsar, A., Fleischmann, D., Theußl, T., Mroz, L., Sramek, M., Gröller, M. E.: Demonstration of different segmentation and visualization techniques by means of a complex real world object exemplified by a Christmas tree (Abstract), *European Congress of Radiology 2003* (ECR 2003), C-0965, Vienna.

Kanitsar A., Theussl T., Mroz L., Sramek M., Vilanova Bartroli A., Csébfalvi B., Hladuvka J., Guthe S., Knapp M., Wegenkittl R., Felkel P., Fleischmann D., Purgathofer W., Gröller M. E.: Christmas Tree Case Study: Computed Tomography as a Tool for Mastering Complex Real World Objects with Applications in Computer Graphics. Technical Report TR-186-2-02-07, Institute of Computer Graphics and Algorithms, Vienna University of Technology. 2002.

*The most exciting phrase to hear in science,
the one that heralds new discoveries,
is not 'Eureka!' (I found it!) but 'That's funny ...'
— Isaac Asimov (1920 – 1992)*

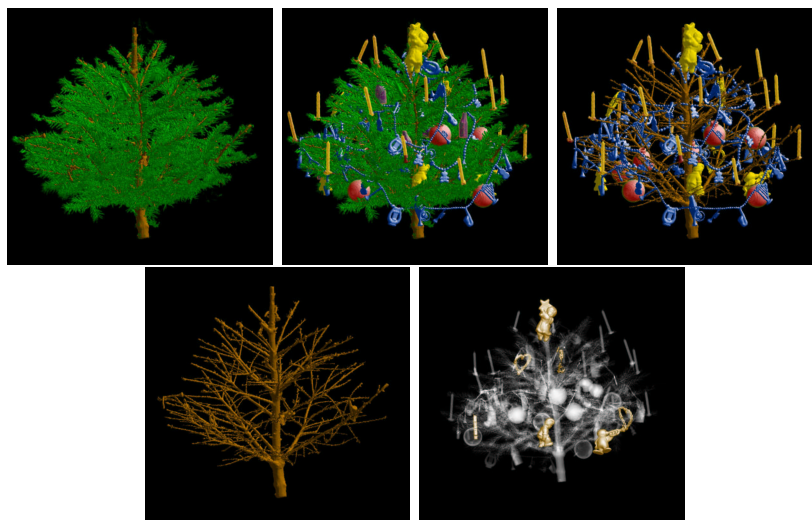


Figure 5.1: A short story: Before Christmas – the 25th – left for holidays – the sad end – Christmas tree in heaven.

5.1 Introduction

In computer art, one is often faced with the task to digitize real world objects for further processing with various computer graphics tools. Commonly used methods like range scanning suffer from certain limitations since only information on the visible surfaces of objects is provided. Non-convex surfaces, an inherent property of complex objects, often cause difficulties or even cannot be handled at all. Similar arguments hold for taking a set of photographs from different viewpoints to be used for image based rendering.

With procedural modeling of existing physical objects it is difficult to come up with an accurate description of the real world object. Furthermore it requires a special effort to get a physically correct model. The more complex the model is the more difficult the modeling task becomes.

Generating datasets (i.e., modeling the objects) by scanning real world objects using CT modalities is independent of model complexity and physical correctness is automatically achieved. Different structures within the dataset can be segmented and the interior can be examined as CT provides volumetric descriptions. On the other hand, CT scanners are rather expensive and not easily

accessible. In this Chapter the experiences of using CT to model a decorated Christmas tree are described, a very complex object with many different structures and small details.

This Chapter describes how a CT modality can be used to acquire complex models. In addition to that a demonstration of various visualization algorithms on this complex dataset is presented. In Section 5.2 related work in this area is presented. The data acquisition process is described in Section 5.3. Different visualization algorithms are evaluated on this dataset in Section 5.4. The topic is concluded in Section 5.5.

5.2 Related Work

Computed tomography has been used for non-destructive investigations of trees [21]. In order to do this, mobile CTs have been built which extract single slices. This way diseases of trees are detected with adequate precision.

State-of-the-art interactive modeling tools today are either polygon or patch oriented (Maya, Truespace). However, manipulation of the underlying data structures (polygonal meshes, NURBS) is often not versatile enough to fulfill the artist’s demands. Therefore, in the early stages of the design often clay models are created, which are subsequently digitized by means of range scanners [44].

There is of course a lot of literature on laser range scanning of objects. Particularly interesting for the visualization community is the work by Levoy et al. [37], who describe their efforts to digitize large objects at high resolution with mobile laser range scanning hardware. However, for objects with a high degree of complexity this approach is not applicable. This is because concavities and holes cause undesired artifacts. These artifacts have to be corrected manually in an additional post-processing step.

5.3 Dataset Acquisition

To obtain a realistic model of a Christmas tree, we decided to use CT as the main drawback of this technique – the exposure to radiation – was of no relevance. The following section describes the generation process and preprocessing of the dataset.

Model Preparation:

Firstly, special care had to be taken in the preparation of the real model to achieve a high dataset quality. Especially, no metal was allowed to be used, as this would result in artifacts. Therefore the sweets were unwrapped and metal hooks replaced (see Figure 5.2). Due to the limited diameter of the CT gantry, the size of the tree must not exceed 50 cm. Furthermore the proportions of the Christmas tree decoration and the small conifer should match those of a real Christmas tree. Therefore special items, as small candles for birthday cakes, were used.



Figure 5.2: A picture of the Christmas tree.

Scanning Process:

The CT acquisition protocol had to be specifically designed as neither presets nor protocols are available for small trees. The Christmas-tree model was scanned with a Siemens Somatom Plus 4 Volume Zoom Multislice-CT scanner at the general hospital in Vienna. A tube voltage of 140kV and a tube current of 100mAs was used during the 40s scan. The collimation was 4 x 1mm, the table increment was 3mm/360° gantry rotation. Transverse sections with a nominal slice width of 1.25mm were reconstructed at 0.5mm intervals using a medium/sharp (B40) reconstruction kernel. A dataset of 512 x 512 x 998 voxels was reconstructed from a field of view of 476mm x 476mm x 499mm.

Preprocessing:

Due to low noise and good spatial resolution of the dataset no further preprocessing and enhancement was necessary. Limitations of some rendering tools required separate 8 bit voxel-valued datasets.

The resulting data were originally stored in DICOM format, which is the standard format in medical imaging. For scientific and experimental purposes more handy file formats are desirable. Therefore, the dataset was converted (and is publicly available therein) to the .dat and f3d formats [63, 56]. The first six bytes of the .dat format represent the dataset dimension. Each following pair of bytes represent one voxel. The f3d format is more general and stores all the necessary data attributes in an easy to read header, followed by a preview image and the compressed 3D data itself.

Segmentation of tomographic datasets is, depending on the goals, either very simple or very complicated. The simple task in our case was classification of the foreground voxels (the tree itself with decorations) with respect to the background. This task was accomplished easily by thresholding. The hard segmentation task was to separate various tissues of the tree (trunk and needles) and decorations. For this purpose we used two segmentation tools, ISEG [54] and the segmentation functionality of JVision (a medical 3D workstation from TIANI MedGraph [39]). ISEG is a general purpose interactive system for segmentation of 3D datasets based on the assumption of spatial object homogeneity. Such objects can be identified by thresholding. Several objects can be selected even if their density ranges overlap. Therefore, tools are provided to separate such objects. The available features include connected component labeling, morphological operations like erosion, dilation, and smoothing, and logical operations like voxel-wise AND, OR, XOR. 15 different objects were labeled, some of them representing several instances of similar but spatially disconnected decorations (e.g., candles or balls). A similar functionality is available for segmentation using JVision. Separating objects with similar value ranges and close spatial locations is often difficult to handle with just threshold based and morphological methods. Therefore, a local water-shed method [13] was applied to split and divide masks containing multiple objects.

5.4 Visualization algorithms

In the following the results of different volume visualization methods are presented.

Shaded Surface Display:

Figure 5.3 shows polygon rendering using OpenGL hardware acceleration. The iso-surfaces at a value of -944 HU (Hounsfield Units) were extracted from the data set using an extended marching cubes algorithm. The internal structure of the decoration is represented with opaque surfaces.

Object labels and masks, which were the result of the segmentation step were further used for high quality rendering by means of ray tracing. Smooth object surfaces were obtained directly from the label volume by a first-order interpolation and thresholding [55], while the normals, necessary for realistic surface shading, were estimated directly from the original CT data by central differences and trilinear interpolation (Figure 5.4). The Chessboard distance ray traversal technique [57] was used to speed up the rendering.

Direct Volume Rendering:

In Figure 5.5 software raycasting is presented using a sharp transfer function which emphasizes an iso-surface at -954 HU.

Interactive direct volume rendering running at 5 to 10 frames per second, on a Pentium 4 based system using a GeForce4 Ti4600 graphics card is used in Figure 5.6. This approach is based on real-time decompression of a wavelet encoded multiresolution hierarchy and multiresolution volume rendering [20].

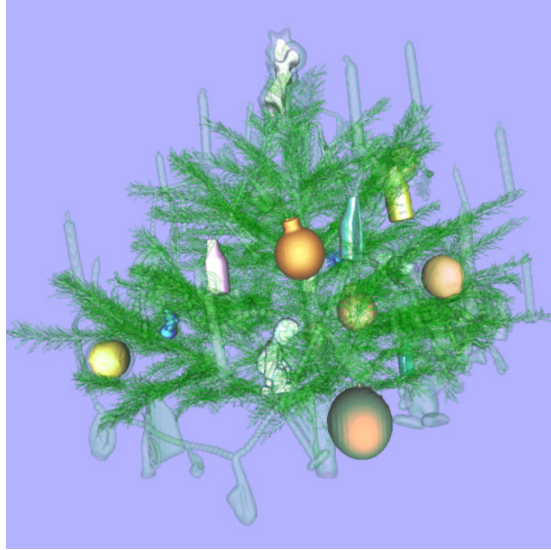


Figure 5.3: OpenGL polygon rendering based on marching cubes surface extraction.



Figure 5.4: Ray tracing of the segmented tree.

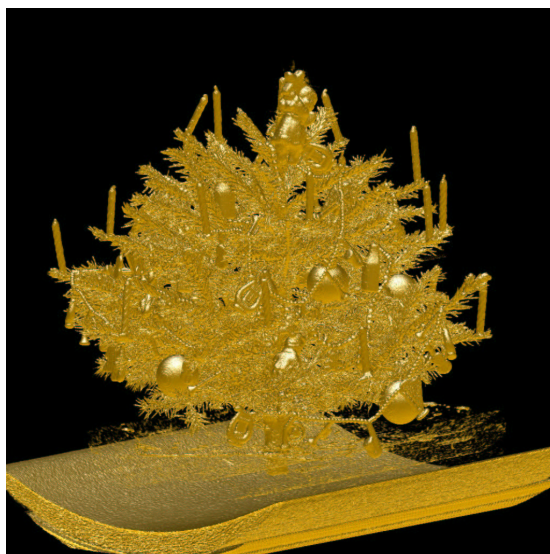


Figure 5.5: Direct volume rendering with ray casting.

The images are rendered using lossless compression at a ratio of about 3.9:1.

Figure 5.7 demonstrates volume rendering using a view-dependent hierarchical octree representation and a screen space error of less than one pixel. Pre-integration was used to render the data with exactly projected cells.

Figure 5.1 shows images of the Christmas tree rendered using the RTVR library [43]. About 3-4 frames per second on a PIII/1.2GHz machine (full spatial resolution of the dataset, 512x512 image). RTVR allows to combine different compositing modes for different objects like surface rendering for the angels and summation (X-ray) for the remaining objects in the 5th image of Figure 5.1. As RTVR is a pure Java solution the tree can be viewed interactively using an RTVR applet [63].

Figure 5.9 shows non-photorealistic direct volume rendering using the "Bubble Model" [10]. Iso-surfaces are rendered as thin semi-transparent membranes similarly to blown soap bubbles. The approach is a fast previewing technique for volumetric data which does not require a time consuming transfer function specification to visualize internal structures. Originally developed for medical data the method also works for the scanned data set in quickly illustrating the most important features.

Arboroscopy:

Virtual endoscopy is used to inspect tubular objects of volumetric data sets. Applied to our data set, the term arboroscopy most illustratively describes this technique. A seven-fold branching is shown in Figure 5.10. As branches of such high degree rarely exist in common endoscopic applications, this dataset

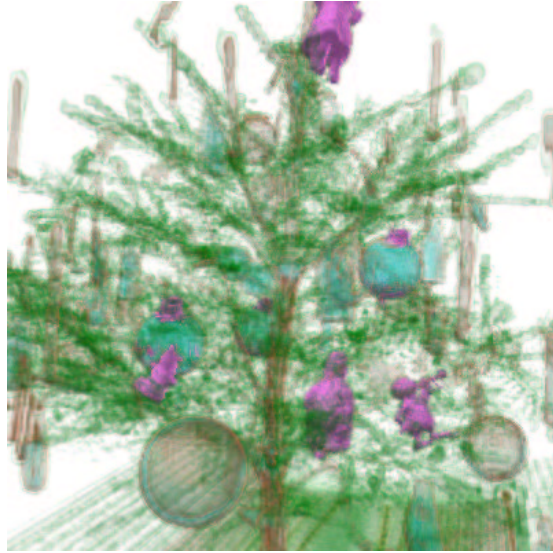


Figure 5.6: Interactive wavelet encoded multiresolution volume rendering.



Figure 5.7: Viewdependent simplification with error threshold of 1 pixel. The tetrahedral mesh is rendered with pre-integrated cell projection.

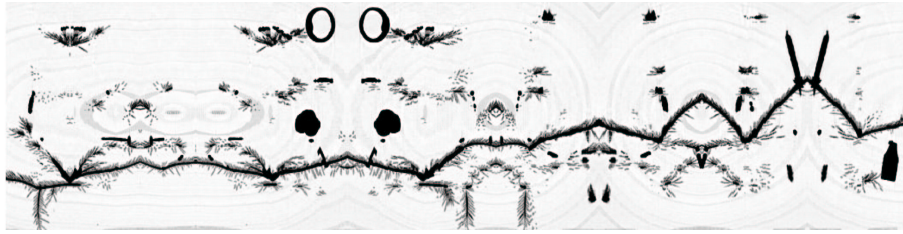


Figure 5.8: A Curved Planar Reformation of the XMas-Tree dataset.

provides an interesting worst-case test scenario.

Curved Planar Reformation (CPR):

Curved Planar Reformation is typically used to inspect vascular structures as described in Section 2. The re-sampled plane in Figure 5.8 is generated from the central axis of a branch of the tree. Thus the stability and correctness of CPR algorithms can be investigated exemplarily on this special data set.

5.5 Conclusions

A straightforward technique for modeling of complex shapes by means of tomographic scanning has been presented. The limits of its applicability are given by the scanner properties, which define the outer and inner scale of the representable object. One can scan objects with dimensions up to about 500 mm with small details at about 1 mm or even less. Some materials (i.e., metal) cause artifacts and therefore should be, if possible, avoided. Color information is lost during the scan process. Up to now CT modalities are expensive and restricted in accessibility.

On the other hand this model acquisition method provides important properties. The data acquisition is independent from the object complexity and both surfaces and object interiors are represented. Different types of material are distinguishable according to the material dependent attenuation. Computed Tomography produces high resolution data sets. Even small features, as the needles of the presented data set, are still properly sampled.

Finally, a contribution of this Chapter is to provide the visualization community with a high resolution data set with some interesting properties. It includes rather large and smooth objects like the figure on top of the tree as well as a lot of fine details like the needles. It is usable as a test data set for several applications which we showed by applying various visualization algorithms. The Christmas tree data set is publicly available from the web site [63].

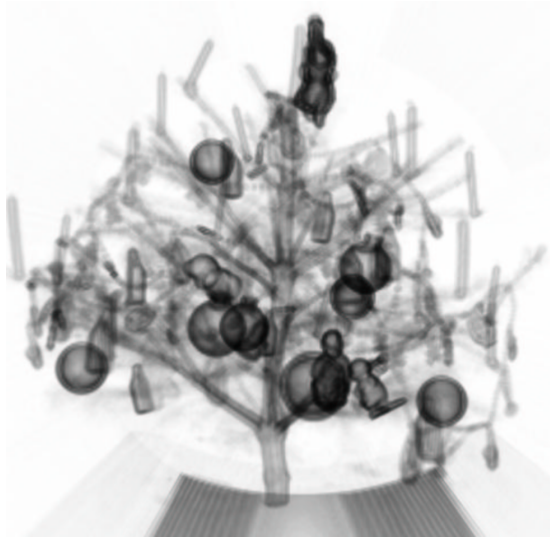


Figure 5.9: Non-photorealistic rendering using the "Bubble Model".

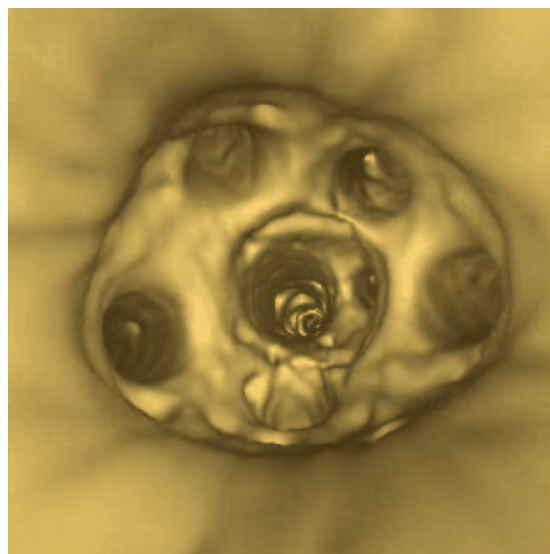


Figure 5.10: View of a seven-fold branch in a virtual arboroscopy.

Chapter 6

Conclusions

*And now, the end is near;
And so I face the final curtain.
— Frank Sinatra (1915 – 1998)*

The main topic of this thesis is curved planar reformation (CPR) for vessel visualization. A robust method for extracting the vessel central axis is introduced. Four different methods for exploring vascular segments are proposed: Projected CPR, stretched CPR, straightened CPR, and helical CPR. For the display of vascular trees three methods are developed: Multi-path projected CPR, multi-path stretched CPR, and untangled CPR. Algorithmic details are elaborated and advantages and disadvantages are discussed. In addition application relevant properties are summarized.

Table 6.1 summarizes the introduced Methods: Projected CPR (*Proj.*), stretched CPR (*Stre.*), straightened CPR (*Stra.*), and helical CPR (*Helical.*), multi-path projected CPR (*M-Proj.*), multi-path stretched CPR (*M-Stre.*), and untangled CPR (*Untang.*). The methods are grouped according to whether displaying a whole vessel tree is possible or not (*Vessel tree*). The criterion *Spatial Perception* indicates how radiologists judge the spatial expressiveness, i.e., the mapping of positions within the CPR to locations in the volumetric dataset without additional aid. Whether the method preserves true distances in close vicinity of the computed centerline is depicted by the field *Isometry*. The possible occurrence of bones superimposing the tracked vessel is expressed by *Occlusions (bone)*. The criteria *Occlusions (artery)* shows whether arteries may cross in image space and consequently overlap each other. Finally *Rotation needed* indicates if multiple viewing directions are needed in order to investigate the entire vessel lumen.

An image-based comparison of the introduced methods is given in Figures 6.2 to 6.8. The comparison is based on the vascular tree extracted from the dataset shown in Figure 6.1. In addition to that the application of multi-path CPR methods on the Christmas-Tree dataset is presented in Figure 6.9.

	Proj.	Stre.	Stra.	Helical	M-Proj.	M-Stre.	Untang.
Vessel tree	no	no	no	no	yes	yes	yes
Spatial Perception	high	med	low	low	high	med	med
Isometry	no	yes	yes	yes	no	yes	yes
Occlusions by bones	poss.	no	no	no	poss.	no	no
Occlusions by arteries	poss.	no	no	no	poss.	poss.	no
Rotation needed	yes	yes	yes	no	yes	yes	yes

Table 6.1: Comparison of CPR methods.



Figure 6.1: The example dataset: Extracted vascular tree including the aorta and left iliac artery and right iliac artery.

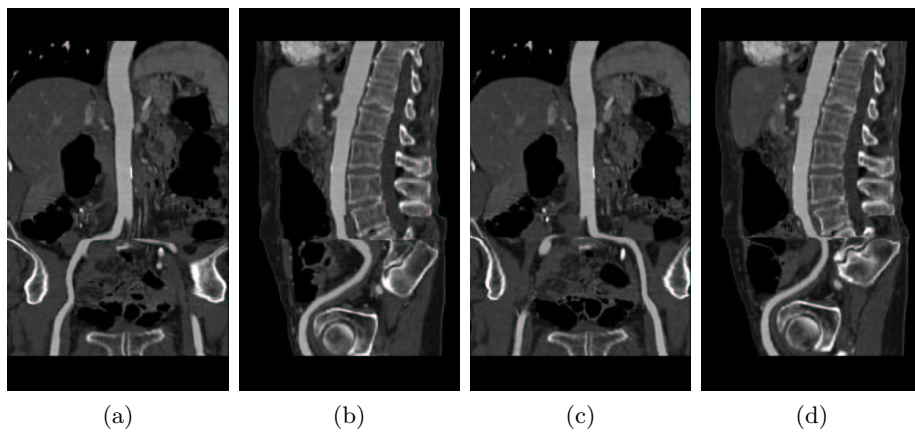


Figure 6.2: Projected CPR: Right iliac artery coronal (a) sagittal (b); left iliac artery coronal (c) sagittal (d).

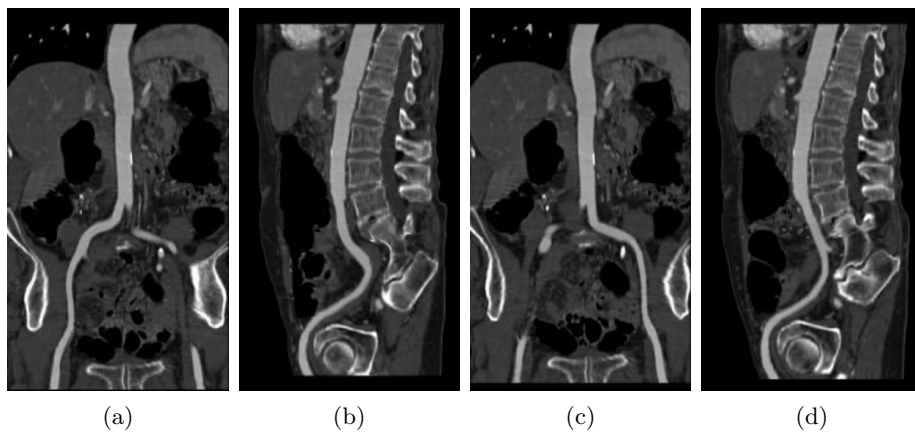


Figure 6.3: Stretched CPR: Right iliac artery coronal (a) sagittal (b); left iliac artery coronal (c) sagittal (d).

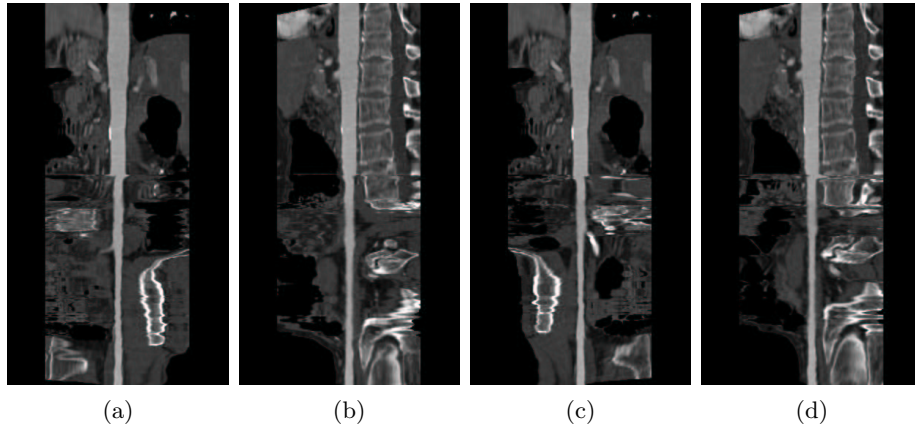


Figure 6.4: Straightened CPR: Right iliac artery coronal (a) sagittal (b); left iliac artery coronal (c) sagittal (d).

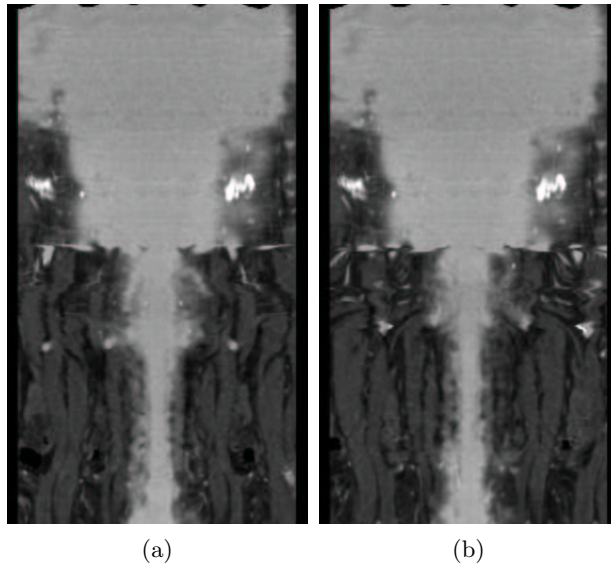


Figure 6.5: Helical CPR: Right iliac artery (a) and left iliac artery (b).

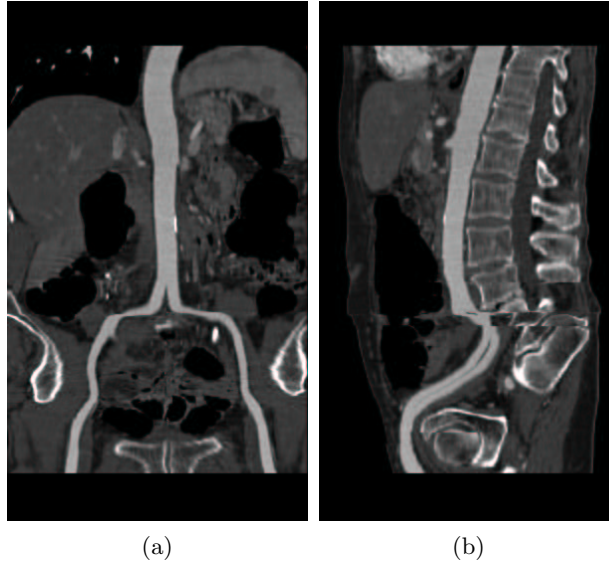


Figure 6.6: Multi-path projected CPR: coronal view (a) and sagittal view (b).

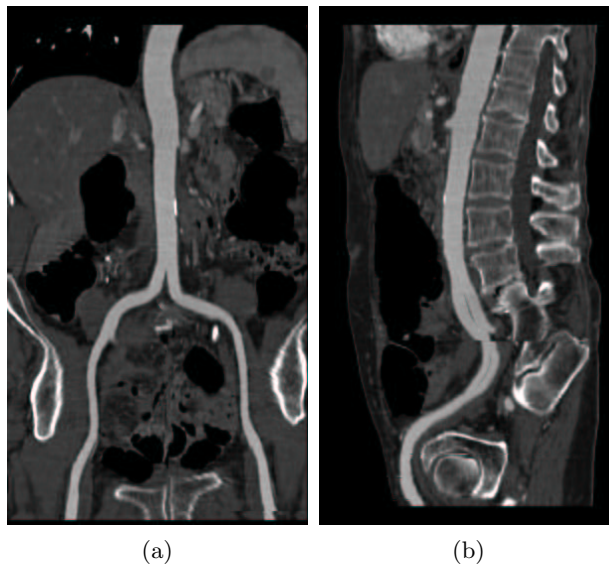


Figure 6.7: Multi-path stretched CPR: coronal view (a) and sagittal view (b).

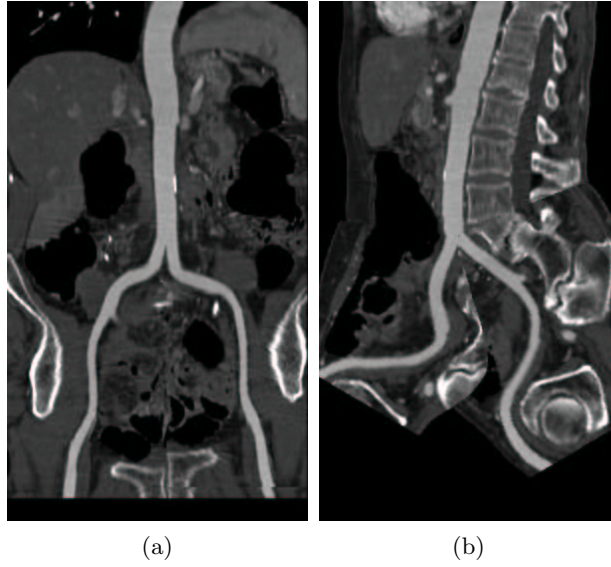


Figure 6.8: Untangled CPR: coronal view (a) and sagittal view (b).

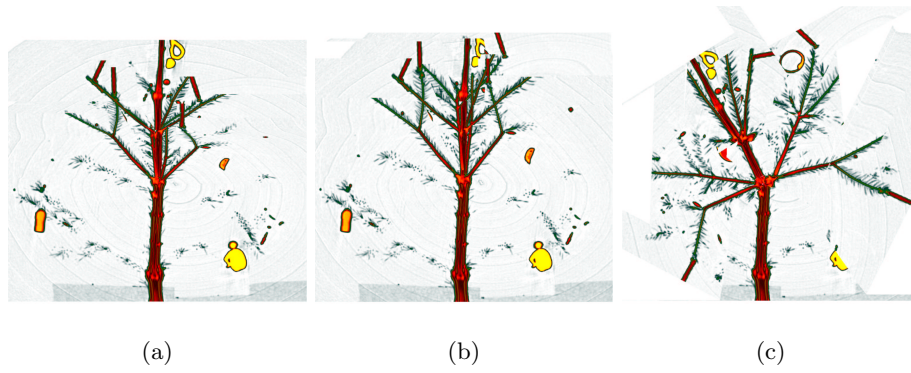


Figure 6.9: CPR of the Christmas-Tree dataset: Multi-path projected CPR (a), multi-path stretched CPR (b), and untangled CPR (c).

Chapter 7

Acknowledgements

First I want to thank **Meister Edi Gröller**. I believe that he believed in me before I believed in me and encouraged me to go into scientific work. I want to thank him for fruitful discussions and for sharing his immense knowledge with me. Second I thank **Rainer Wegenkittl** for all the great ideas I could incorporate into my work and for being an understanding executive. Especially I want to thank **Dominik Fleischmann** who introduced me in the topic of CTA and patiently instructed me to the medical aspects of this area. His excellent medical expertise had a significant influence on the success of all publications.

I want to thank all members of the Visualization Group – in particular **Tom Theussl** – for the scientific support. Especially I want to thank the members of the ADAPT team **Ivan Viola**, **Michi Knapp**, **Sören Grimm**, and **Stefan Bruckner** (in order of appearance) for the excellent work. At this point I also want to thank **Werner Purgathofer** for providing the environment to carry out the project.

Furthermore I want to thank **Franz Tiani** and **Martin Tiani** for supporting my research activities. In this respect I want to thank all members of the TIANI crew, especially **Lukas Mroz**, **Petr Felkel**, and **Mario Bruckschwaiger**.

I want to thank all co-authors not mentioned yet for the productive cooperations. In addition to that I express my thanks to the Viennese scientific community for stimulating discussions. Furthermore I want to thank all my friends who accompanied me through my present lifetime.

Last but not least I want to thank my family **Peter**, **Johanna**, and **Martin Kanitsar** for supporting me during all the years. Without them all this would have never been possible.

The work has been supported by the ADAPT project (FFF-804544). ADAPT is supported by *Tiani Medgraph*, Vienna (<http://www.tiani.com>), and the *Forschungsförderungsfonds für die gewerbliche Wirtschaft*, Austria.

Bibliography

- [1] S. Achenbach, W. Moshage, D. Ropers, and K. Bachmann. Curved Multiplanar Reconstructions for the Evaluation of Contrast-Enhanced Electron-Beam CT of the Coronary Arteries. In *Am. J. Roentgenol.*, pages 895–899, 1998.
- [2] K. Addis, K. Hopper, T. Iyriboz, Y. Liu, S. Wise, C. Kasales, J. Blebea, and D. Mauger. CT Angiography: In Vitro Comparison of Five Reconstruction Methods. In *Am. J. Roentgenol.*, pages 1171–1176, 2001.
- [3] B. Avants and J. Williams. An Adaptive Minimal Path Generation Technique for Vessel Tracking in CTA/CE-MRA Volume Images. In *MICCAI 2001*, pages 707–716, 2000.
- [4] D. Balériaux. Neuroradiology: Past, Present and Future. *Medica Mundi*, 40(3):156–170, 2002.
- [5] W. Barrett and E. Mortensen. Interactive Live-Wire Boundary Extraction. *Medical Image Analysis*, 1(4):331–341, 1997.
- [6] S. Baum and M. J. Pentecost. *Abrams’ Angiography: Vascular and Interventional Radiology*. Little, Brown Medical Division, 1997.
- [7] K. Bühler, P. Felkel, and A. La Cruz. Geometric Methods for Vessel Visualization and Quantification - A Survey. Technical Report TR-VRVis-2002-035, VRVis Research Center, Vienna, Austria, 2002.
- [8] E. Bullitt and S. Aylward. Volume Rendering of Segmented Tubular Objects. In *MICCAI 2001*, pages 161–168, 2001.
- [9] A. Cormack. Representation of a Function by its Line Integrals, with Some Radiological Applications. *J. Appl. Physics*, 34:2722–2727, 1963.
- [10] B. Cséfalvi and E. Gröller. Interactive Volume Rendering Based on a “Bubble Model”. In *GI 2001*, pages 209–216, 2001.
- [11] M. E. DeBakey. *The New Living Heart*. Adams Media Corporation, 1997.

- [12] A. Falcao and J. Udupa. An Ultra-Fast User-Steered Image Segmentation Paradigm: Live Wire on the Fly. *IEEE Transactions on Medical Imaging*, 19(1), 2000.
- [13] P. Felkel, M. Bruckschwaiger, and R. Wegenkittl. Implementation and complexity of the watershed-from-markers algorithm computed as a minimal cost forest. In *Eurographics 2001*, volume 20 of *Computer Graphics Forum*, pages 26–35, Manchester, United Kingdom, 2001.
- [14] P. Felkel, A. Fuhrmann, A. Kanitsar, and R. Wegenkittl. Surface Reconstruction of the Branching Vessels for Augmented Reality Aided Surgery. In *BIOSIGNAL 2002*, pages 252–254, June 2002.
- [15] F. G. Fowkes, E. Housley, E. H. Cawood, C. C. Macintyre, C. V. Ruckley, and R. J. Prescott. Edinburgh Artery Study: Prevalence of Asymptomatic and Symptomatic Peripheral Arterial Disease in the General Population. *Int J Epidemiol*, 20:384–392, 1991.
- [16] A. Frangi, W. Niessen, and M. Viergever. Three-Dimensional Modeling for Functional Analysis of Cardiac Images: A Review. *IEEE Transactions on Medical Imaging*, 20(1):2–25, 2001.
- [17] A. Frangi, W. Niessen, K. Vincken, and M. Viergever. Multiscale Vessel Enhancement Filtering. In *Lecture Notes in Computer Science*, volume 1496, pages 130–137, 1998.
- [18] O. Glasser. *Wilhelm Conrad Röntgen und die Geschichte der Röntgenstrahlen*. Springer, 3rd edition, 1995.
- [19] A. A. Goshtasby, M. Sonka, and J. Udupa. Analysis of Volumetric Images. *Computer Vision and Image Understanding: CVIU*, 77(2):79–83, 2000.
- [20] S. Guthe and W. Strasser. Real-time Decompression and Visualization of Animated Volume Data. In *IEEE Visualization 2001*, pages 349–356. ACM, 2001.
- [21] A. Habermehl and H. W. Ridder. Applications of Computerized Tomography in Forest and Tree Sciences. In *International Symposium on Computerized Tomography for Industrial Applications*, 1994.
- [22] H. Hahn, B. Preim, D. Selle, and H. O. Peitgen. Visualization and Interaction Techniques for the Exploration of Vascular Structures. In *IEEE Visualization 2001*, pages 395–402. ACM, October 2001.
- [23] S. He, R. Dai, B. Lu, C. Cao, H. Bai, and B. Jing. Medial Axis Reformation: A New Visualization Method for CT Angiography. *Academic Radiology*, 8(8):726–733, 2001.
- [24] R. Heitzman. Thoracic Radiology: The Past 50 Years. *Radiology*, 214:309 – 313, 2000.

- [25] C. B. Holman and F. E. Bullard. Application of Closed Circuit Television in Diagnostic Roentgenology. In *Staff Meetings of the Mayo Clinic*, volume 38, page 67, Mayo Foundation for Medical Education and Research, Rochester, Minnesota, USA, 1963.
- [26] G. Hounsfield. Computerised Transverse Axial Scanning (Tomography) Part I. Description of System. *Br. J. Radiol.*, 46:1016–1022, 1973.
- [27] G. Hounsfield. Computed Medical Imaging. *Nobel Lectures in Physiology or Medicine*, 1:568–586, 1979.
- [28] W. A. Kalender. *Computed Tomography*. Publicis MCD Verlag, 2000.
- [29] A. Kanitsar. Advanced Visualization Techniques for Vessel Investigation. Master’s thesis, Vienna University of Technology, Institute of Computergraphics and Algorithm, March 2001.
- [30] A. Kanitsar, D. Fleischmann, R. Wegenkittl, P. Felkel, and M. E. Gröller. CPR - Curved Planar Reformation. In *IEEE Visualization 2002*, pages 37–44, October 2002.
- [31] A. Kanitsar, R. Wegenkittl, P. Felkel, D. Fleischmann, D. Sandner, and E. Gröller. Computed Tomography Angiography: A Case Study of Peripheral Vessel Investigation. In *IEEE Visualization 2001*, pages 477–480, October 2001.
- [32] A. Kanitsar, R. Wegenkittl, P. Felkel, D. Sandner, E. Gröller, and D. Fleischmann. Automated Vessel Detection at lower Extremity Multislice CTA, March 2001. Oral presentation at ECR 2001.
- [33] A. Köchl, A. Kanitsar, F. Lomoschitz, E. Gröller, and D. Fleischmann. Comprehensive Assessment of Peripheral Arteries using Multi-path Curved Planar Reformation of CTA Datasets. In *Europ. Rad.*, volume 13, pages 268–269, 2003.
- [34] F. Klok. Two Moving Coordinate Frames for Sweeping along a 3D Trajectory. In *Computer Aided Geometry Design*, pages 3:217–229, 1986.
- [35] R. A. Kruger, C. A. Mistretta, J. Lancaster, T. L. Houk, M. Goodsitt, C. G. Shaw, S. J. Riederer, J. Hicks, J. Sackett, A. B. Crummy, and D. Flemming. A Digital Video Image Processor for Real-time X-ray Subtraction Imaging. *Optical Engineering*, 17(6):652–657, 1978.
- [36] D. Laidlaw, K. Fleischer, and A. Barr. Partial Volume Segmentation with Voxel Histograms. In Isaac N Bankman, editor, *Handbook of Medical Imaging, Processing, and Analysis*, pages 195–211. Academic Press, 2000.
- [37] M. Levoy, K. Pulli, B. Curless, S. Rusinkiewicz, D. Koller, L. Pereira, M. Ginzton, S. Anderson, J. Davis, J. Ginsberg, J. Shade, and D. Fulk. The Digital Michelangelo Project: 3D Scanning of Large Statues. In *Siggraph 2000, Computer Graphics Proceedings*, pages 131–144. ACM, 2000.

- [38] T. McInerney and D. Terzopoulos. T-snakes: Topology Adaptive Snakes. *Medical Image Analysis*, 4(2):73–91, 2000.
- [39] TIANI Medgraph. JVision/Spacevision Diagnostic Workstation, 2002. <http://www.tiani.com/>.
- [40] E. Meijering. *Image Enhancement in Digital X-ray Angiography*. Printed by Ponsen & Looijen, 2000.
- [41] E. Meijering, W. Niessen, and M. Viergever. Retrospective Motion Correction in Digital Subtraction Angiography: A Review. *IEEE Transactions on Medical Imaging*, 18(1):2–21, January 1999.
- [42] I. Mori. Computerized Tomographic Apparatus Utilizing a Radiation Source. United States Patent Number 4630202; Dec. 16, 1986.
- [43] L. Mroz and H. Hauser. RTVR – a flexible Java Library for Interactive Volume Rendering. In *IEEE Visualization 2001*, pages 279–286. ACM, 2001.
- [44] R. N. Perry and S. F. Frisken. Kizamu: A System For Sculpting Digital Images. In Eugene Fiume, editor, *Siggraph 2001, Computer Graphics Proceedings*, Annual Conference Series, pages 47–56. ACM, 2001.
- [45] B. G. Ziedses Des Plantes. *Planigraphie en Subtractie. Röntgenographische Differentiatimethoden*. Thesis, Kemink en Zoon, Utrecht, 1934.
- [46] J. Radon. Über die Bestimmung von Funktionen durch ihre Integralwerte längs gewisser Mannigfaltigkeiten. *Berichte Sächsische Akademie der Wissenschaften, Leipzig, Math.-Phys. Kl.*, 69:262–277, 1917.
- [47] W. C. Röntgen. Über eine Neue Art von Strahlen. *Sitzungsberichte der Physikalisch-medizinischen Gesellschaft zu Würzburg*, 137:132–141, 1895.
- [48] R. A. Robb, E. A. Hoffman, L. J. Sinak, L. D. Harris, and E. L. Ritman. High-speed Three-dimensional X-ray Computed Tomography: The Dynamic Spatial Reconstructor. *Proc. IEEE*, 71(3):308–319, 1983.
- [49] J. Rogowska. Overview and Fundamentals of Medical Image Segmentation. In Isaac N Bankman, editor, *Handbook of Medical Imaging, Processing, and Analysis*, pages 69–86. Academic Press, 2000.
- [50] G. D. Rubin, A. Schmidt, L. Logan, and M. Sofilos. Multi-Detector Row CT Angiography of Lower Extremity Arterial Inflow and Runoff: Initial Experience. In *Radiology 2001*, pages 146–158, 2001.
- [51] G. D. Rubin, A. J. Schmidt, L. J. Logan, C. Olcott, C. K. Zarins, and S. Napel. Multidetector-row CT-Angiography of Lower Extremity Occlusive Disease: A New Application for CT Scanning. *Radiology*, 210:588, 1999.

- [52] Y. Sato, S. Nakajima, N. Shiraga, H. Atsumi, S. Yoshida, T. Koller, G. Gerig, and R. Kikinis. Three-Dimensional Multiscale Line Filter for Segmentation and Visualization of Curvilinear Structures in Medical Images. *Medical Image Analysis*, 2(2):143–168, 1998.
- [53] Y. Sato, C. F. Westin, A. Bhalerao, S. Nakajima, N. Shiraga, S. Tamura, and R. Kikinis. Tissue Classification Based on 3D Local Intensity Structures for Volume Rendering. *IEEE Transactions on Visualization and Computer Graphics*, 6(2):160–180, June 2000.
- [54] M. Šrámek. Interactive Segmentation of Tissues for Medical Imaging. In Václav Hlaváč and Tomáš Pajdla, editors, *Czech Pattern Recognition Workshop '93*, pages 164–171, Temešvár u Písku, Czech Republic, 1993.
- [55] M. Šrámek. Fast Surface Rendering from Raster Data by Voxel Traversal Using Chessboard Distance. In *IEEE Visualization'94*, pages 188–195. ACM, 1994.
- [56] M. Šrámek and L. I. Dimitrov. f3d — A File Format and Tools for Storage and Manipulation of Volumetric Data Sets. In *1st International Symposium on 3D Data Processing, Visualization and Transmission*, pages 368–371, Padova, Italy, 2002. IEEE CS.
- [57] M. Šrámek and A. Kaufman. Fast Ray-tracing of Rectilinear Volume Data Using Distance Transforms. *Transactions on Visualization and Computer Graphics*, 6(3):236–252, 2000.
- [58] L. H. Staib, X. Zeng, R. T. Schultz, and J. S. Duncan. Shape Constraints in Deformable Models. In Isaac N Bankman, editor, *Handbook of Medical Imaging, Processing, and Analysis*, pages 147–157. Academic Press, 2000.
- [59] R. Van Tiggelen. Historical Article. In Search for the Third Dimension: from Radiostereoscopy to Three-dimensional Imaging. *Belgian Journal of Radiology*, 85(5), 2002.
- [60] A. Vilanova, A. König, and E. Gröller. VirEn: A Virtual Endoscopy System. *MACHINE GRAPHICS & VISION*, 8(3):469–487, 1999.
- [61] O. Wink, W. Niessen, and M. Viergever. Fast Delineation and Visualization of Vessels in 3-d Angiographic Images. *IEEE Transactions on Medical Imaging*, 19(4):337–346, 2000.
- [62] S. M. Wolpert. Neuroradiology Classics. *American Journal of Neuroradiology*, 20(9):1752–1753, 1999.
- [63] XMT. Christmas Tree Web Page, 2001. <http://ringlotte.cg.tuwien.ac.at/datasets/XMasTree/XMasTree.html>.
- [64] C. Zahlten, H. Juergens, and H. O. Peitgen. Reconstruction of Branching Blood Vessels from CT-Data. In *Eurographics Workshop on Visualization in Scientific Computing*, pages 161–168, 1994.

Appendix A

Curriculum Vitae

Armin Markus Kanitsar

Curriculum Vitae

Armin Kanitsar was born on September 4th, 1976 in Graz as first child of Peter Kanitsar and Johanna Kanitsar (maiden name Holler). He spent his childhood together with his younger brother Martin Kanitsar in Fürstenfeld (Austria).

- Sep. 1983 Primary school education at Volksschule Parkstraße, Fuerstenfeld for two years. Continued at Volksschule Schillerplatz, –
- Sep. 1987 Fürstenfeld due to re-organization.
- Sep. 1987 –
- Secondary school at Bundes Realgymnasium Fürstenfeld.
- Sep. 1991
- Sep. 1991 High school (sixth form) at Bundes Realgymnasium Fürstenfeld –
- with main focus on computer science and mathematics.
- May. 1995
- Jun. 1995 Final exam with distinction.
- Oct. 1995 Fulfilled the general conscription within the scope of a one year –
- voluntarily army officer training course. Successfully completed
- Oct. 1996 the course and promotion to Sergeant.
- Oct. 1996 Start of the diploma study Computer Science at the Vienna University of Technology.
- Mai. 2000 **Best Paper Award** at the Central European Seminar on Computer Graphics for a publication based on the research project ALVIS. (<http://www.cg.tuwien.ac.at/studentwork/CESCG-2000/awards.html>).
- Jun. 2000 Successfully completed the project 'Faked Mouse' - Implementation of an operating system independent PC remote control. (<http://www.cg.tuwien.ac.at/~armin/FMouse.htm>)
- Sep. 2000 Successfully completed the project 'TTP/A - Prosthesis'. A field bus application for flexible hand prosthesis control.

- Mar. 2001 Completed the diploma study below minimum duration of study and graduation to a Dipl.-Ing. (equal to a Master-degree) with distinction.
- Since
Mar. 2001 Research associate at the Institute of Computer Graphics and Algorithms, Vienna University of Technology.
- Since
Mar. 2001 Member of the development department for 3D visualization and post-processing at TIANI Medgraph AG.
- May. 2001 Promotion to a Lieutenant at the Theresianischen Militäarakademie (military academy) with personal congratulations by the Austrian President Dr. Thomas Klestil.
- Since
Dec. 2001 Projectmanager of the research project ADAPT - Advanced Diagnosis, Analysis & Planning Tools, funded by the FFF.
- Aug. 2002 **Cover Selection Award** winner for the cover of the proceedings of the IEEE Visualization 2002 Conference in Boston, MA with a figure from the publication: CPR - Curved Planar Reformation.
- Nov. 2002 **Best Case Study Award** winner at the IEEE Visualization 2002 Conference in Boston, MA for the publication: Christmas Tree Case Study: Computed Tomography as a Tool for Mastering Complex Real World Objects with Applications in Computer Graphics.
- Aug. 2003 **Cover Selection Award** winner for the cover of the proceedings of the IEEE Visualization 2003 Conference in Seattle, WA with a figure from the publication: Advanced Curved Planar Reformation: Flattening of Vascular Structures.

Projects

- Jul. 1999 ALVIS Project on mathematical correct surface extraction and visualization from large datasets for the purpose of non-destructive material investigation of aluminium foam.
-
- Apr. 2000 Faked Mouse Project on the implementation of an operating system independent hardware and software solution for a PC
- Jan. 2000 – remote control based on commodity devices.
- Jun. 2000 TTP/A - Prosthesis Application of the TTP/A Protocol for the implementation of a real-time bus system connecting actors and sensor of hand prosthesis.
-
- Sep. 2000 AngioVis (former BBA) Development of new diagnosis supporting methods for vessel tracking, vessel detection, and vessel visualization.
- Sep. 2000 –
- Dec. 2001 ADAPT Advanced Diagnosis, Analysis & Planning Tools in Medicine - research and development of computer aided methods for medical applications.
-

Publication List

- Neu00AL Neubauer A., **Kanitsar A.**: ALVIS - Meeting the tremendous requirements arising with the visualization of aluminum foam samples investigated by high resolution industrial CT-modalities, Central European Seminar on Computer Graphics (CESCG2000), Budmerice, Slovakia, pp. 229–242, März 1. - 3., 2000.
- Obe00Ap Obermaisser R., **Kanitsar A.**: Application of TTP/A for the Otto Bock Axon Bus, Research report 27/2000, Technische Universität Wien, Institut für Technische Informatik, 2000.
- Kan01Au **Kanitsar A.**, Wegenkittl R., Felkel P., Sandner D., Gröller E., Fleischmann D.: Automated Vessel Detection at Lower Extremity Multislice CTA (Abstract), European Congress of Radiology, 2001, (ECR 2001) Supplement 1 to Vol. 11, page 236, Vienna.
- Kan01Th **Kanitsar A.**: Advanced Visualization Techniques for Vessel Investigation, Master's thesis, Vienna University of Technology, Institute of Computergraphics and Algorithm, März, 2001.
- Kan01Po **Kanitsar A.**, Wegenkittl R., Felkel P., Fleischmann D., Sandner D., Gröller E.: Postprocessing and Visualization of Peripheral CTA Data in Clinical Environments, Central European Seminar on Computer Graphics (CESCG'2001), Budmerice, Slovakia, April 23.-25., 2001.
- Fel01Ve Felkel P., Wegenkittl R., **Kanitsar A.**: Vessel Tracking in Peripheral CTA Datasets – An Overview. In R. Durikovic and S. Czanner (editors). Spring conference on Computer Graphics (SCCG'2001), Proceedings, pages 232-239, IEEE Computer Society (Held in April 25-28, 2001, Budmerice, Slovakia).
- Kan01Pe **Kanitsar A.**, Wegenkittl R., Felkel P., Fleischmann D., Sandner D., Gröller E.: Peripheral Vessel Investigation for Routine Clinical Use. In Proceedings of IEEE Visualization 2001, pages 477–480, October 2001.
- Fel02Su Felkel P., Fuhrmann A. L., **Kanitsar A.**, Wegenkittl R.: Surface Reconstruction of the Branching Vessels for Augmented Reality Aided Surgery. In J. Jan and J. Kozumplik and I. Provaznik (eds). BIOSIGNAL 2002, The 16th international EURASIP conference, volume 16, pages 252-254, Brno, Czech Republic, June 26 - 28, 2002.
- Kan02Xm **Kanitsar A.**, Theussl T., Mroz L., Sramek M., Vilanova Bartroli A., Csébfalvi B., Hladuvka J., Guthe S., Knapp M., Wegenkittl R., Felkel P., Roettger S., Fleischmann D., Purgathofer W., Gröller M. E.: Christmas Tree Case Study: Computed Tomography as a Tool for Mastering Complex Real World Objects with Applications in Computer Graphics. In Proceedings of IEEE Visualization 2002, pages 489–492, October 2002. (best case study award)

- Kan02CP **Kanitsar A.**, Fleischmann D., Wegenkittl R., Felkel P., Gröller M. E.: CPR - Curved Planar Reformation. In Proceedings of IEEE Visualization 2002, pages 37–44, October 2002.
- Cse02Sm Csébfalvi B., Neumann L., **Kanitsar A.**, Gröller E.: Smooth Shape-Based Interpolation using the Conjugate Gradient Method. In G. Greiner, H. Niemann, T. Ertl, B. Girod, H.-P. Seidl, (eds.), Vision, Modeling, and Visualization 2002 (VMV 2002), pages 123–130, November 2002.
- Fle02Mu Fleischmann D., **Kanitsar A.**: 3D computer assisted vascular lesion evaluation and treatment planning: CT angiography. C.I.R.S.E., 2002.
- Kan03Au **Kanitsar A.**, Fleischmann D., Wegenkittl R., Felkel, P., Gröller M. E.: Multi-Path Curved Planar Reformation: Visualization of a Vascular Tree (Abstract), European Congress of Radiology 2003 (ECR 2003), B-0204, Vienna.
- Kan03De **Kanitsar A.**, Fleischmann D., Theußl T., Mroz L., Sramek M., Gröller M. E.: Demonstration of different segmentation and visualization techniques by means of a complex real world object exemplified by a Christmas tree (Abstract), European Congress of Radiology 2003, (ECR 2003), C-0965, Vienna.
- Koe03Co Koechl A., **Kanitsar A.**, Lomoschitz F., Gröller M. E., Fleischmann D.: Comprehensive assessment of peripheral arteries using multi-path curved planar reformation of CTA datasets (Abstract), European Congress of Radiology, 2003, (ECR 2003), B-0635., Vienna.
- Kan03Ad **Kanitsar A.**, Wegenkittl R., Fleischmann D., Gröller M. E.: Advanced Curved Planar Reformation: Flattening of Vascular Structures. In Proceedings of IEEE Visualization 2003, 43–50, October 2003.
- Vio03Ha Viola I., **Kanitsar A.**, Gröller M. E.: Hardware-Based Nonlinear Filtering and Segmentation using High-Level Shading Languages. In Proceedings of IEEE Visualization 2003, pages 309–316, October 2003.
- Gri04Re Grimm S., Bruckner S., **Kanitsar A.**, Gröller E.: A Refined Data Addressing and Processing Scheme to Accelerate Volume Raycasting. To appear in Computers & Graphics.
- Kna04Se Knapp M., **Kanitsar A.**, Gröller E.: Semi-Automatic Topology Independent Contour-Based 2 1/2 D Segmentation Using Live-Wire. To appear in Proceedings of Winter School of Computer Graphics 2004, WSCG 2004.